

**XEROGRAPHIC PROPERTIES OF
CHLORINE-DOPED AMORPHOUS SELENIUM**

BY

WANG, YAN

***A thesis submitted to
the Faculty of Graduate Studies and Research
in partial fulfillment of the requirements for the degree of
Master of Engineering***

**Department of Electrical Engineering
McGill University
Montreal, Canada
March, 1994**

ABSTRACT

A study has been made of the xerographic properties of amorphous selenium doped with chlorine at concentrations below 100 parts per million (ppm) by weight. The sample consisted, in each case, of an aluminum plate with a thin deposited r.f. sputtered aluminum oxide film, on which a 50 micrometer layer of amorphous selenium was deposited by evaporation, with a substrate temperature of 50 °C. It was found that the chlorine decreased the acceptance voltage following corona charging, increased the dark decay rate and decreased the residual voltage after illumination discharge. The changes were such as to be beneficial xerographically for small additions of chlorine to the selenium in the ppm range. Analysis of the time derivative of the dark decay voltage indicated that depletion discharge was the dominant process in the decrease of dark decay voltage with time and a modified relation was introduced to describe the increase of bulk space charge density with time, arising from thermal excitation of holes from deep discrete centres in the photoreceptor. This analysis indicated a decrease of the release time of the holes with increase of chlorine content, whereas an observed decrease of single cycle and cycled-up residual voltages with increased chlorine indicated an increase of hole capture time from their relevant trapping centres. Capacitance and incremental resistance measurements on the aluminum oxide blocking layers indicated higher resistance in films deposited by r.f. sputtering than by d.c. reactive sputtering on aluminum substrates. However, no difference in xerographic performance could be detected between the two sputtering methods. Oxide layers were also deposited on nickel and gold substrates by r.f. sputtering.

RÉSUMÉ

Une étude a été réalisée sur les propriétés du sélénium amorphe dopé au chlore à des concentrations inférieures à 100 ppm en poids. Dans chaque cas, les échantillons consistaient en une plaque d'aluminium recouverte d'une mince couche d'oxyde d'aluminium déposée par pulvérisation h.f., elle-même recouverte d'une couche de 50 micromètres de sélénium amorphe déposée par évaporation, le tout sur un substrat à 50°C. On a constaté que l'ajout de chlore réduisait la tension admissible après application d'une charge à l'aide d'un corotron, augmentait la décharge d'obscurité et réduisait la tension résiduelle après une décharge d'illumination. Les modifications se sont révélées bénéfiques sur le plan xérogaphique pour de petits ajouts de chlore (de l'ordre d'une ou deux ppm) au sélénium. L'analyse de la dérivée de la tension d'obscurité selon le temps révèle que la décharge de déplétion est le processus qui intervient le plus dans la réduction de la tension d'obscurité selon le temps; une relation modifiée a été introduite afin de décrire l'augmentation de la densité de charge d'espace «bulk» selon le temps. Cette augmentation résulte de l'excitation thermique des trous à partir des centres discrets profonds du photorécepteur. L'analyse révèle une réduction du temps de libération des trous proportionnelle à l'augmentation de la teneur en chlore; en revanche, la réduction, selon l'augmentation de la teneur en chlore, des tensions résiduelles après un seul cycle et après plusieurs cycles («cycled-up») montre qu'il y a augmentation du temps de capture des trous à partir de

leurs centres-pièges pertinents. Les mesures de la capacité et de la résistance interne sur les couches d'arrêt d'oxyde d'aluminium révèlent que la résistance est plus élevée dans les couches déposées par pulvérisation h.f. réactive que dans celles déposées par pulvérisation réactive en c.c. sur des substrats d'aluminium. Toutefois, on n'a pu détecter aucune différence entre les deux méthodes pour ce qui est du rendement xérogaphique. Des couches d'oxyde ont également été déposées par pulvérisation h.f. sur des substrats de nickel et d'or.

ACKNOWLEDGEMENTS

The author wishes to express his sincere gratitude to his supervisor, professor C.F. Champness, for his guidance, assistance and patience throughout this study.

Acknowledgments are also given to Dr. I. Shih for his help, to Mr. Kezia Cheng and Guy Rodrigue for their assistance with the maintenance of the equipment, to Mr. Ziad Shukri and Mr. Colin Xu for their helpful discussions.

The author also extends his thanks the Natural Sciences and Engineering Research Council of Canada, for partial financial support, to Noranda Technology Centre, Pointe Claire, for the supply of the selenium, to Noranda Copper Smelting and Refining, CCR Refinery, for the analysis of the chlorine concentration.

The author would specially like to give his thanks to his wife for her continuous understanding.

TABLE OF CONTENTS

ABSTRACT	i
RESUME	ii
ACKNOWLEDGEMENT	iv
1 INTRODUCTION	1
2 THEORETICAL CONSIDERATIONS	5
2.1 Introduction	5
2.2 Dark Decay by Bulk Charge Depletion Discharge	6
(a) Physical Description	6
(b) Depletion Discharge Model	8
(i) Formulation of Model	8
(ii) Simple Power Law Charge Density Time Dependence	12
(iii) Modified Charge Density Time Dependence	14
(iv) dV/dt -Voltage Variation	17
2.3 Residual Voltage	18
3 PREPARATION OF SAMPLES	22
3.1 Introduction	22
3.2 Substrate Cleaning and Etching	23
3.3 Oxide Blocking Layer Deposition	23
(a) d.c. Sputtering Method	24
(b) r.f. Sputtering Method	24
3.4 Selenium Deposition	25
3.5 Surface Treatment of Samples	26
3.6 Deposition of Metal for Capacitance Measurement	27
3.7 Preparation of Chlorine-doped Selenium	27

4 MEASUREMENT TECHNIQUES	39
4.1 Introduction	39
4.2 Definitions of the Xerographic Parameters Measured	39
4.3 Measurement Apparatus for Xerographic Parameters	41
4.4 Xerographic Parameter Determination with Saturated Charging	43
4.5 Light Fatigue Measurement	45
4.6 Single Pass Charging for Determination of Dark Decay Voltage Slopes	45
4.7 Calibration of Measurement System	46
4.8 Measurement of C_p and P_p of Oxide	47
4.9 Selenium Film Thickness Measurement	48
4.10 Control System for Semiautomatic Measurement	48
(a) Communication between host device and indexer	49
(b) Command string set to control the rotation of turntable	50
(c) Test of control system	51
5 XEROGRAPHIC RESULTS OF CHLORINE-DOPED SELENIUM	63
5.1 Introduction	63
5.2 Result of Single Cycle Xerographic Measurements	63
(a) Acceptance voltage	63
(b) Dark decay rate	64
(c) Residual voltage	64
5.3 Results of Cycled Xerographic Measurements	65
(a) Residual voltage	66
(b) Dark decay rate	67
5.4 Results of Strong Initial Illumination	67
5.5 Discussion	68

6 DARK DECAY TIME GRADIENT MEASUREMENTS	83
6.1 Introduction	83
6.2 Effect of Chlorine Content	84
6.3 Effect of Initial Voltage	85
6.4 Effect of Absence of Oxide Blocking Layer	85
6.5 Analysis of Results	86
(a) Plots of dV/dt versus t	86
(i) Effect of chlorine	86
(ii) Effect of V_1	87
(b) Plots of t_d versus $2V_d$	88
6.6 Discussion	88
7 RESULTS OF MEASUREMENTS ON OXIDE LAYER	105
7.1 Introduction	105
7.2 Oxide Deposition Rate	105
7.3 Xerographic Comparison of d.c. and r.f. Sputtering Oxide	106
7.4 Capacitance and Resistance Results with r.f. Sputtered Oxide	107
7.5 Voltage Breakdown of Oxide Layers	108
7.6 Discussion	109
8 GENERAL CONCLUSIONS AND FURTHER DISCUSSION	127
8.1 Conclusions and discussion	127
8.2 Future work	132
REFERENCES	134

Chapter 1

INTRODUCTION

Selenium-based photoreceptors have been much used in xerographic applications, such as in office photocopiers, laser printers and X-ray xerography. In the future, it appears that they will continue to be used in xeroradiography. A comprehensive review of the xerographic properties of chalcogenide photoreceptors has been given by Kasap [1]. The chalcogenide photoreceptors involved in xerographic applications are often Se-As and Se-Te alloys, doped with small quantities of other materials, such as halogens, monovalent and other elements to control their xerographic properties. To understand the action of these additions, it is helpful and simpler to study their effect in the prototype photoreceptor material amorphous selenium, rather than in the alloys in the first instance. Accordingly, a large part of the work in this thesis is devoted to xerographic measurements on amorphous selenium doped with small amounts of chlorine. Other parts of the work are on the deposition of the aluminum oxide blocking layer between the metal substrate and the selenium layer in xerographic test structures.

The first thesis research on the xerographic properties of amorphous selenium in this laboratory was carried out by Qi-Hua Zhang [2], who studied particularly different methods of preparing the aluminum oxide blocking layers. The present writer has

continued this work by improving the xerographic test apparatus, making it semiautomatic, partly computer-controlled and, more importantly, by improving the measurement accuracy. In addition, a more precise and a more detailed study on chlorine-doped selenium has been carried out and better quality r.f. sputtered aluminum oxide layers have been used for the blocking layer. Furthermore, a new theoretical analysis of dark decay arising from the depletion discharge model has been explored.

While xerographic studies have already been made on amorphous selenium doped with chlorine, such as the work of Abkowitz, Jansen and Melnyk [3], there appears to be no detailed published work at lower concentrations of chlorine, below 100 parts per million by weight (ppm). This is important because it is at these levels that the chlorine appears to have its greatest effect on xerographic properties. Accordingly, the present thesis consists, for the most part, of an investigation of the xerographic properties of amorphous selenium doped with up to 100 wt ppm of chlorine. A typical xerographic sample studied consists usually of an aluminum substrate covered with a thin film of r.f. sputtered aluminum oxide, on which a 50 micrometer layer of selenium was deposited by evaporation from a selenium source containing ppm quantities of chlorine. The xerographic measurements made on these samples, with positive initial charging, were: acceptance voltage, dark decay rate and residual voltage. A special study was made of the variation of the dark decay voltage and its derivative with time. In addition to this, measurements of capacitance and resistance were made on the aluminum oxide blocking layer deposited on three different metal substrates.

The basic principles of xerography, as applied to the photocopying process, have been described frequently in the literature [4], [5], [6], [7]. However, a brief description of the process, referring to Fig 1.1, is as follows.

(a) The photoreceptor surface is first charged from a high voltage corona discharge, (b) then the charged surface is illuminated with the image from the document to be copied, (c) the image is next developed by applying a powder mixture of toner and carrier to the surface, whereby it only sticks to charged regions with excess powder removed, (d) following this, the powder pattern is transferred to an oppositely charged sheet of paper and then (e) the paper, with the attached powder, is heated to bake the ink of the toner into the paper and finally (f) the residual powder is removed from the photoreceptor surface, ready for the next photocopy.

The structure of the thesis is as follows. The essentials of the theory of depletion discharge are presented in chapter 2, along with a newly proposed expression for the space charge density increase during dark decay. Chapter 3 describes the making of the samples and chapter 4 the method used to carry out the measurements. The xerographic results on chlorine-doped selenium are presented in chapter 5 and the results of the time derivative determinations of the dark voltage with time are given in chapter 6. The results of capacitance and resistance measurements on the aluminum oxide blocking layers are presented in chapter 7 and conclusions and discussion are finally given in chapter 8.

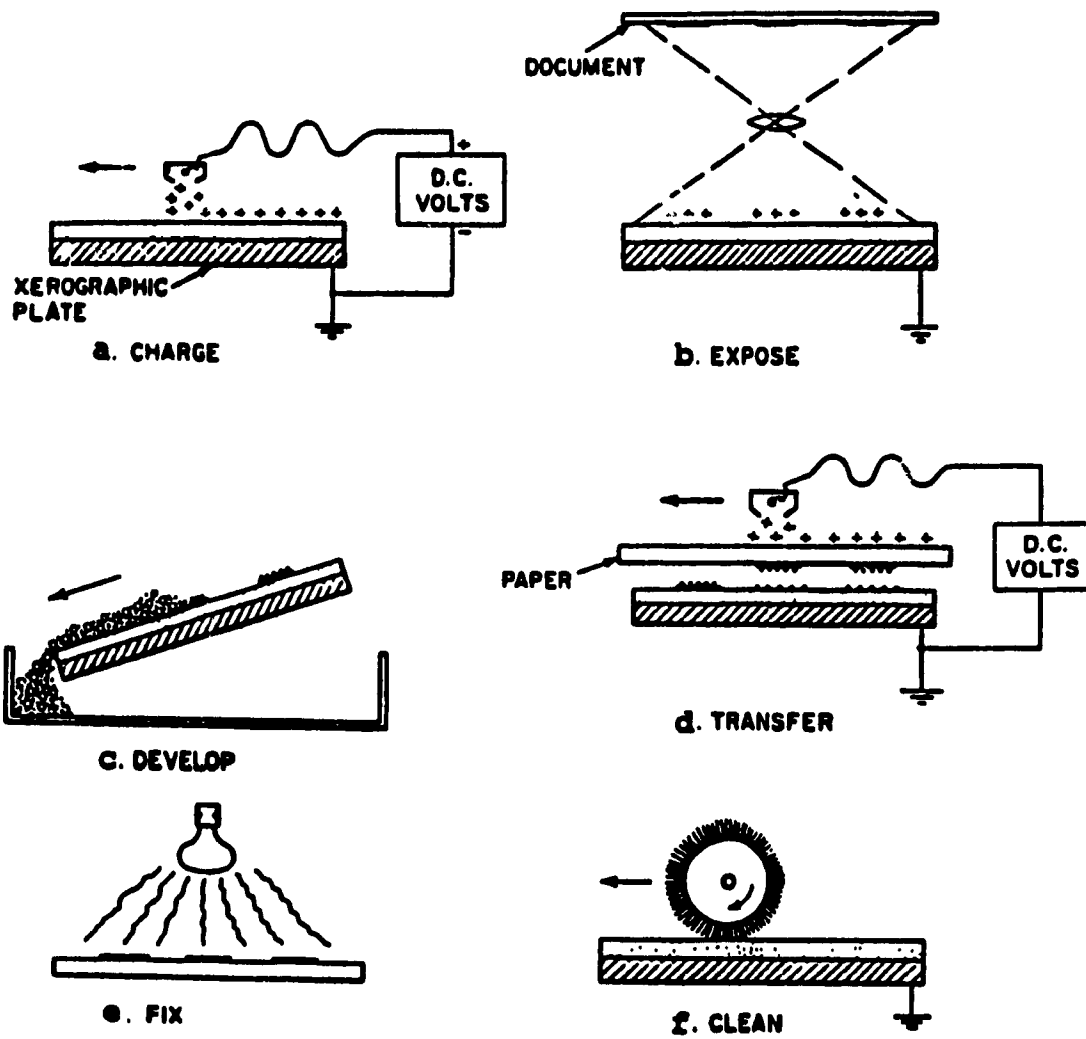


Fig 1.1 Basic steps in xerographic photocopying.
 (from Schaffert [5])

Chapter 2

THEORETICAL CONSIDERATIONS

2.1 Introduction

As briefly described in chapter 1, the essential xerographic process consists of charging the surface of the photoreceptor from a corona discharge, maintaining the charge for a sufficient period and then discharging it under illumination. During the period in darkness, the surface voltage arising from the surface charge, decreases slowly with time, a process known as dark decay. During the illumination period, by contrast, the surface voltage decreases rapidly to a smaller but finite value called the residual voltage. This voltage decrease, under illumination, called photoinduced decay, was not studied in detail experimentally in this thesis, other than some measurements of residual voltage. Hence its theory is not presented here, since excellent treatments of photoinduced decay exist in the literature, such as Kasap [8]. However, the Warter relation [9] will be used, despite its limitations for the residual voltages measured. Dark decay, on the other hand, is an important part of the present thesis and hence, one mechanism, depletion discharge, will be treated in this chapter. Kasap [10] has identified 8 different mechanisms which can cause the surface voltage to decrease in darkness. Perhaps the three most important for amorphous selenium are charge injection from the surface, charge injection from the substrate and thermal bulk generation of

carriers of one sign and depletion. The last mechanism has been extensively treated in the literature [11] [12], but it will be presented here again because it seems to be the dominant mechanism in chlorine-doped amorphous selenium [11]. It appears also to be the dominant dark decay process in As_2Se_3 [13], in Se-Te alloys [12] and in amorphous selenium doped with iodine, arsenic, potassium or rubidium [14], in addition to chlorine. The special manifestation of depletion discharge appears to be a kink in a plot of dV/dt against t , where V is the surface voltage with respect to the substrate and t is the time after the initial charging voltage V_1 . This kink, which is more easily seen on a double logarithmic plot, was apparently first reported in detail by Ing and Neyhart in 1972 [15] in As_2Se_3 films. They found that it was more pronounced in samples which were thicker, with measurements at lower V_1 values and at higher temperatures. For example, Fig 2.1 shows their results on a 65 micrometer thick As_2Se_3 film at 45 °C for various electric fields. They recognized the contribution of bulk hole generation but considered only the interpretation of the pre-kink variation of their $dV/dt-t$ plots. For the portion after the kink, they stated "*The phenomenon of the second branch is complicated and its understanding is not essential...*". Later, both portions of the variation were considered, for example, by Abkowitz et al [3].

2.2 Dark Decay by Bulk Charge Depletion Discharge

(a) Physical Description

Consider a photoreceptor film of thickness L deposited on a

metal substrate, as shown in Fig 2.2. Suppose the surface of the photoreceptor receives a positive charge of σ per cm^2 at a time $t=0$, yielding a potential at the surface with respect to the substrate of V_1 . Suppose the charged film is in darkness. If the mobility of the electrons is very much smaller than that of the holes (μ), as is the case for amorphous selenium, only holes may be considered as mobile carriers. It may be noted, in parenthesis, that μ is the effective mobility and not the microscopic mobility, which would prevail only if the material were free of shallow traps. Arising from the initial electric field V_1/L in the selenium, the residual holes are swept out to the substrate with a transit time of $t_t=L/(\mu V_1/L)=L^2/(\mu V_1)$. Thus, for $L=50\mu\text{m}$, $V_1=1000$ volts and $\mu=0.1 \text{ cm}^2\text{volt}^{-1}\text{sec}^{-1}$, t_t would be $0.25 \mu\text{sec}$. Following this sweep-out, negative charge exists mostly in the substrate plus a small amount of bulk space charge in the receptor, with the total negative charge per cm^2 equal to the positive charge σ on the receptor surface. At this time, just after t_t , the surface potential is still V_1 . Suppose that direct injection of negative charge as electrons, from outside into the top and bottom surfaces can be neglected.

Now the deep-lying discrete centres, which supplied the original low concentration of holes in the selenium, will continue to generate more holes but at a slow rate because of the large energy needed to reach the mobility edge of the valence band. However, every new conducting hole will be swept out by the electric field in the photoreceptor, so that there cannot be an equilibrium process of refilling of the centres. Consequently, as

each fixed centre loses its hole, it acquires a negative charge. Hence, as time proceeds, there is a progressive buildup of negative space charge, of density ρ , within the receptor. Since the net positive charge in the film (surface positive charge minus bulk negative charge) decreases, the dark voltage V across the film will also decrease. While the shape of the voltage decrease with time depends on the specific rate of increase of ρ , it will be shown that there is an abrupt change in the voltage slope dV/dt at the time when the negative bulk space charge just equals the surface charge σ .

(b) Depletion Discharge model

(i) Formulation of model

It is assumed in this treatment that the initial surface charging is positive and that there is no loss of surface charge with time i.e. $d\sigma/dt=0$.

From Gauss's theorem, the electric field \mathcal{E} during the dark decay at a position z , measured downwards from the receptor surface (Fig 2.2) is given by:

$$\epsilon_0 \epsilon_r \mathcal{E} = \sigma - \int_0^z \rho(z) dz \quad , \quad (2.1)$$

where $\rho(z)$ is the negative space charge density at z , ϵ_r is the relative dielectric constant of the photoreceptor material and ϵ_0 is the permittivity of a vacuum.

The electrostatic potential difference between z and z_0 is given by

$$\psi(z) - \psi(z_0) = - \int_{z_0}^z \mathcal{E} \cdot dz$$

and if z_0 is taken as the distance at which $\mathcal{E}=0$, ie $\mathcal{E}(z_0)=0$, then the surface voltage V , taken as equal to the potential at $z=0$ ie $V=\psi(0)$, is given by:

$$V = - \int_{z_0}^0 \mathcal{E} \cdot dz = \int_0^{z_0} \mathcal{E} \cdot dz \quad (2.2)$$

Substituting for \mathcal{E} from equation (2.1) gives:

$$V = \frac{1}{\epsilon_0 \epsilon_r} \int_0^{z_0} \left[\sigma - \int_0^z \rho \cdot dz \right] \cdot dz \quad (2.3)$$

The total negative charge per unit area Q within the receptor layer of thickness L is

$$Q = \int_0^L \rho(z) \cdot dz$$

As $\rho(z)$ increases with time from the slow release of holes from the deep centres, Q increases. In the early stage, $Q < \sigma$, so that $\mathcal{E}=0$ at the interface with the substrate ie at $z_0=L$. As $\rho(z)$ grows, there will eventually come a situation when Q just equals σ ,

so that all the negative space charge is just spread across the thickness L , with zero charge in the substrate. Suppose this time is t_d . For times greater than t_d , $\rho(z)$ grows even further and the negative space charge layer of width z_o , will now extend over a distance less than L i.e. $z_o < L$. Eventually, all the deep centres will be ionized and an equilibrium will be established with a final fixed space charge width, which will be denoted as z_{oo} .

If $\rho(z)$ is independent of electric field and the receptor material is homogeneous, it may be taken as independent of z , so that $\rho(z) = \rho$. In this case, it follows from equation (2.3) that

$$V = \frac{1}{\epsilon_o \epsilon_r} \left(\sigma z_o - \frac{\rho z_o^2}{2} \right) \quad . \quad (2.4)$$

During time zone 1 when $t < t_d$, $Q < \sigma$, $z_o = L$ and $Q = \rho L$, so that equation (2.4) yields:

$$V = \frac{1}{\epsilon_o \epsilon_r} \left(\sigma L - \rho \frac{L^2}{2} \right) = \frac{L}{\epsilon_o \epsilon_r} \left(\sigma - \rho \frac{L}{2} \right) \quad . \quad (2.5)$$

During time zone 2 when $t > t_d$, $Q = \sigma$, $z_o \leq L$ and $\rho z_o = \sigma$, equation (2.4) yields:

$$V = \frac{1}{\epsilon_o \epsilon_r} \left(\sigma z_o - \frac{\rho z_o^2}{2} \right) = \frac{1}{\epsilon_o \epsilon_r} \left(\frac{\sigma^2}{\rho} - \frac{\sigma^2}{2\rho} \right) = \frac{\sigma^2}{2\epsilon_o \epsilon_r \rho} \quad . \quad (2.6)$$

From equation (2.5) in zone 1, differentiation gives

$$\left(\frac{dV}{dt}\right)_1 = -\frac{L^2}{2\epsilon_0\epsilon_r} \frac{d\rho}{dt} \quad , \quad (2.7)$$

with $d\sigma/dt=0$.

From equation (2.6) in zone 2, differentiation yields

$$\left(\frac{dV}{dt}\right)_2 = -\frac{\sigma^2}{2\epsilon_0\epsilon_r\rho^2} \frac{d\rho}{dt} \quad , \quad (2.8)$$

with $d\sigma/dt=0$.

At $t=0$, even just after sweep-out at $t>t_t$, ρ may be taken as zero. Thus, from equation (2.4) with $\rho=0$ and $z_0=L$, it follows that the initial voltage is

$$V_1 = \frac{\sigma L}{\epsilon_0\epsilon_r} \quad . \quad (2.9)$$

At $t=t_d$, $z_0=L$ and $\sigma=\rho L$, so that from equation (2.4) the voltage V_d is

$$V_d = \frac{\sigma L}{2\epsilon_0\epsilon_r} \quad . \quad (2.10)$$

Thus, it follows that $V_d/V_1=1/2$, that is the voltage at $t=t_d$ is half of the initial voltage. If $d\sigma/dt<0$, equation (2.10) should be replaced by

$$V_d = \frac{\sigma_d L}{2\epsilon_o \epsilon_r} \quad , \quad (2.10a)$$

so that $V_d/V_1 = \sigma_d/2\sigma_o$, where σ_o and σ_d are the values of σ at times 0 and t_d respectively. In this case, the ratio would be less than 1/2.

(ii) Simple Power Law Charge Density Time Dependence

In the treatment of Melnyk [13] and of Abkowitz et al [3] [11] [16], the ionization of the deep discrete centres in the photoreceptor was considered to result in the charge density increasing with time according to a relation of the form

$$\rho = at^p \quad , \quad (2.11)$$

where a and p are time-independent parameters, with $p \leq 1$.

For deep states in the mobility gap with an energy distribution of the form

$$N = N_o e^{\frac{-|E-E_o|}{W}} \quad , \quad (2.12)$$

it was shown [17] that $p = kT/W$, where E is the energy above the mobility valence edge, E_o is the energy of the peak of the distribution and W is a measure of its energy width. The total density of states over all the entire distribution, by integration, is $2N_o W$.

If $\rho(t)$, of the form of equation (2.11), is introduced into equations (2.7) and (2.8) the results are

$$\left(\frac{dV}{dt}\right)_1 = -\frac{L^2}{2\epsilon_o\epsilon_r} a p t^{p-1} \quad , \quad (2.13)$$

for $t < t_d$, and

$$\left(\frac{dV}{dt}\right)_2 = -\frac{\sigma^2}{2a\epsilon_o\epsilon_r} p t^{-p-1} \quad , \quad (2.14)$$

for $t \geq t_d$, which with $\sigma = V_1 \epsilon_o \epsilon_r / L$ from equation (2.9), gives

$$\left(\frac{dV}{dt}\right)_2 = -\frac{\epsilon_o \epsilon_r \left(\frac{V_1}{L}\right)^2}{2a} p t^{-p-1} \quad . \quad (2.15)$$

It is thus seen that at $t = t_d$, dV/dt changes from a t^{p-1} dependence to a t^{-p-1} dependence, representing a break-point in a plot of dV/dt versus t , which is more clearly apparent on double logarithmic scales. Furthermore, equation (2.15) predicts that the slope in zone 2 is inversely proportional to the square of the film thickness for a fixed initial voltage. Note that a p value greater than unity would mean that the dark voltage initially would rise with time.

At $t = t_d$, $\sigma_d = \rho_d L$, so that from equation (2.10a) with equation (2.11), it follows that t_d is given by

$$t_d = \left(\frac{\epsilon_o \epsilon_r 2V_d}{aL^2}\right)^{\frac{1}{p}} \quad , \quad (2.16)$$

and since $2V_d = V_1 (\sigma_d / \sigma_o)$

$$t_d = \left(\frac{\epsilon_o \epsilon_r}{aL^2} V_1 \frac{\sigma_d}{\sigma_o} \right)^{\frac{1}{p}} \quad (2.17)$$

(iii) Modified Charge Density Time Dependence

While the power law dependence of equation (2.11) appears to be satisfactory for relative short dark decay periods, especially for $t < t_d$, it cannot apply for times when complete ionization of the discrete centres is approached. Eventually, when t exceeds the release time τ_r of the deep traps, the negative space charge layer will decrease to a stable depletion width of z_{oo} , with a time independent charge density ρ_o . Accordingly, a more appropriate form for ρ would appear to be:

$$\rho = \rho_o \left(1 - e^{-\left(\frac{t}{\tau}\right)^p} \right) \quad (2.18)$$

where τ is a time constant, related to the trap release time τ_r . With this expression, ρ approaches its fixed value of ρ_o , when $t \gg \tau$. However, when $t \ll \tau$, ρ tends to the value

$$\rho = \rho_o \left\{ 1 - \left[1 - \left(\frac{t}{\tau} \right)^p \right] \right\} = \rho_o \left(\frac{t}{\tau} \right)^p \quad (2.19)$$

which has the same form as equation (2.11) with $a = \rho_o / \tau^p$

Using equation (2.18) in equation (2.7) for $t < t_d$ yields

$$\left(\frac{dV}{dt}\right)_1 = - \frac{L^2 \rho_o P}{2 \epsilon_o \epsilon_r \tau^p} t^{p-1} e^{-\left(\frac{t}{\tau}\right)^p} \quad , \quad (2.20)$$

which reduces to equation (2.13) for $t \ll \tau$.

If the quantity $\rho_o L^2 / \epsilon_o \epsilon_r$ is denoted by V_x , equation (2.20) can be written as

$$\left(\frac{dV}{dt}\right)_1 = - \frac{V_x}{2 \tau} P \left(\frac{t}{\tau}\right)^{p-1} e^{-\left(\frac{t}{\tau}\right)^p} \quad . \quad (2.20a)$$

For $t \geq t_d$ from equations (2.8) and (2.18), it follows that

$$\left(\frac{dV}{dt}\right)_2 = - \frac{\sigma^2 P \left(\frac{t}{\tau}\right)^{p-1} e^{-\left(\frac{t}{\tau}\right)^p}}{2 \epsilon_o \epsilon_r \tau \rho_o [1 - e^{-\left(\frac{t}{\tau}\right)^p}]^2} \quad , \quad (2.21)$$

using $\sigma = V_1 \epsilon_o \epsilon_r / L$ and $V_x = \rho_o L^2 / \epsilon_o \epsilon_r$, gives

$$\left(\frac{dV}{dt}\right)_2 = - \frac{V_1^2}{2 V_x} \frac{P}{\tau} \left(\frac{t}{\tau}\right)^{p-1} \frac{e^{-\left(\frac{t}{\tau}\right)^p}}{[1 - e^{-\left(\frac{t}{\tau}\right)^p}]^2} \quad , \quad (2.21a)$$

which reduces to equation (2.15) for $t_d \leq t \ll \tau$, a condition which might be difficult to fulfil.

If a loss of surface charge σ is considered, the values of

$(dV/dt)_1$ and $(dV/dt)_2$ will be changed. For simplicity, a linear relationship is assumed of the form:

$$\sigma = \sigma_0(1 - Kt) \quad , \quad (2.22)$$

where K is a constant with dimensions of $(\text{time})^{-1}$. Then equations (2.20a) and (2.21a) with equations (2.5) and (2.6) will be changed to

$$\left(\frac{dV}{dt}\right)_1 = -\frac{V_x}{2\tau} p \left(\frac{t}{\tau}\right)^{p-1} e^{-\left(\frac{t}{\tau}\right)^p} - V_x K \quad , \quad (2.20b)$$

$$\left(\frac{dV}{dt}\right)_2 = -\frac{V_x^2}{2V_x} \frac{p \left(\frac{t}{\tau}\right)^{p-1} e^{-\left(\frac{t}{\tau}\right)^p}}{\left[1 - e^{-\left(\frac{t}{\tau}\right)^p}\right]^2} - \frac{V_x^2}{V_x} K \frac{1 - Kt}{\left[1 - e^{-\left(\frac{t}{\tau}\right)^p}\right]} \quad . \quad (2.21b)$$

At $t=t_d$, $\sigma_d = \rho_d L$ with equations (2.10a) and (2.18) gives

$$\left(\frac{t_d}{\tau}\right)^p = \ln \left[\left(1 - \frac{2\epsilon_0 \epsilon_r V_d}{\rho_0 L^2} \right)^{-1} \right] = \ln \left[\left(1 - \frac{2V_d}{V_x} \right)^{-1} \right] \quad ,$$

so that

$$\ln \left(\frac{t_d}{\tau} \right) = \frac{1}{p} \ln \left\{ \ln \left[\left(1 - \frac{2V_d}{V_x} \right)^{-1} \right] \right\} \quad . \quad (2.23)$$

This indicates that a plot of t_d/τ against $-\ln(1-2V_d/V_x)$ on double logarithmic scales, should give a straight line with a slope of $1/p$.

Since $2V_d = V_1 \sigma_d / \sigma_0$, equation (2.23) can be re-written as

$$\ln \left(\frac{t_d}{\tau} \right) = \frac{1}{p} \ln \left\{ \ln \left[\left(1 - \frac{V_1}{V_x} \frac{\sigma_d}{\sigma_0} \right)^{-1} \right] \right\} \quad (2.24)$$

which, if $d\sigma/dt=0$, reduces to

$$\ln \left(\frac{t_d}{\tau} \right) = \frac{1}{p} \ln \left\{ \ln \left[\left(1 - \frac{V_1}{V_d} \right)^{-1} \right] \right\} \quad (2.24a)$$

(iv) dV/dt Voltage Variation

As well as the relation between dV/dt and t , it is also of interest to see the relation between dV/dt and V .

With the ρ dependence of equation (2.11), equations (2.5) and (2.13) for zone 1 yield the result

$$\left(\frac{dV}{dt} \right)_1 = - \frac{L^2 a p}{2 \epsilon_0 \epsilon_r} \left[\frac{2}{aL} \left(\sigma - \frac{\epsilon_0 \epsilon_r V}{L} \right) \right]^{1-\frac{1}{p}} \quad (2.25)$$

and since $\sigma = \epsilon_0 \epsilon_r V_1 / L$ at $t=0$, then for $d\sigma/dt=0$, equation (2.25) may be re-written as

$$\left(\frac{dV}{dt} \right)_1 = -p \left(\frac{aL^2}{2 \epsilon_0 \epsilon_r} \right)^{\frac{1}{p}} (V_1 - V)^{1-\frac{1}{p}} \quad (2.25a)$$

The slope would thus be constant if $p=1$.

In zone 2, with the same ρ dependence of equation (2.11), equations (2.6) and (2.14) yield

$$\left(\frac{dV}{dt}\right)_2 = -p \left(\frac{2a\epsilon_o\epsilon_f}{\sigma^2}\right)^{\frac{1}{p}} V^{1+\frac{1}{p}} \quad (2.26)$$

For $d\sigma/dt=0$, equation (2.26) may be re-written as

$$\left(\frac{dV}{dt}\right)_2 = -p \left(\frac{2aL^2}{\epsilon_o\epsilon_f V_1^2}\right)^{\frac{1}{p}} V^{1+\frac{1}{p}} \quad (2.26a)$$

or

$$\left(\frac{dV}{dt}\right)_2 = -\frac{p}{\tau} \left(\frac{2V_x}{V_1^2}\right)^{\frac{1}{p}} V^{1+\frac{1}{p}} \quad (2.26b)$$

Thus, if $p=1$, the slope would have a quadratic dependence on voltage.

For the ρ dependence of equation (2.18), the equations for $(dV/dt)_1$ and $(dV/dt)_2$ in terms of V , corresponding to equations (2.25) and (2.26), are rather complex and are therefore not stated here. Hence, for computation purposes, it is simpler to find numerical solutions from equations (2.18), (2.5) and (2.20) for $t < t_d$ and from equations (2.18), (2.6) and (2.21) for $t > t_d$.

2.3 Residual Voltage

When the pre-charged surface of the photoreceptor, having a

surface voltage V_0 , is illuminated with short wavelength light, the voltage rapidly decreases to the residual voltage V_r . Kasap [8] has given a full treatment of this photoinduced discharge process and has shown that, in practical circumstances, the residual voltage can be approximated by:

$$V_r = \frac{L^2}{2\mu\tau_c} \quad , \quad (2.27)$$

which is known as the Warter relation [9]. Here μ is the hole mobility (if the surface charge was positive) and τ_c is the hole capture time of traps in the photoreceptor.

A simplistic justification for the Warter relation is as follows. The illumination creates a thin conducting layer of electron-hole pairs, which permits the positive surface charge to be swept across the receptor in the transit time of $t_t = L^2/(\mu V_0)$ in the field V_0/L (assuming $t \ll t_d$). However, only a fraction of this charge will be trapped by the trapping centres in the photoreceptor, since t_t is much smaller than the capture time τ_c of the traps. If this fraction is taken as t_t/τ_c , then the trapped charge density remaining can be taken to be

$$(t_t/\tau_c) \times (\text{surface charge spread over } L) = (t_t/\tau_c) (\sigma/L).$$

By double integration of Poisson's equation, this leads a voltage across the receptor layer of

$$V_r = \left(\frac{t_t \sigma}{\tau_c L} \right) \left(\frac{L^2}{2 \epsilon_0 \epsilon_r} \right)$$

which, with substitution for t_t and $V_0/L = \sigma / (\epsilon_0 \epsilon_r)$, yields the Warter relation:

$$V_r = \left(L^2 \frac{\sigma}{\mu V_0 \tau_c L} \right) \left(\frac{L^2}{2 \epsilon_0 \epsilon_r} \right) = \frac{L^2}{\mu \tau_c} \cdot \frac{L^2}{2 \epsilon_0 \epsilon_r} = \frac{L^2}{2 \mu \tau_c}$$

Close examination of this justification shows many weaknesses, one of which is that the sweeping field is not constant during the discharge process. Never-the-less, the Warter relation is a simple, approximate and useful result.

After many cycles of charging and illumination, all the trapping centres, with a volume density N_t , will be fully charged, yielding a uniform charge density of eN_t , where e is the electronic charge. Double integration of Poisson's equation, then gives the voltage across the layer, known as the cycled-up residual voltage, of [17]

$$V_{r\infty} = \frac{eN_t L^2}{2 \epsilon_0 \epsilon_r} \quad (2.28)$$

Finally, in this chapter, it is important to point out that there are three important time periods relevant to the present work. These are: the transit time t_t , the trapping time τ_c and the trap release time τ_r for holes, where normally $t_t \ll \tau_c \ll \tau_r$. The traps involved here are deep and distinct from the shallow traps, which control the usually measured microscopic mobility μ .

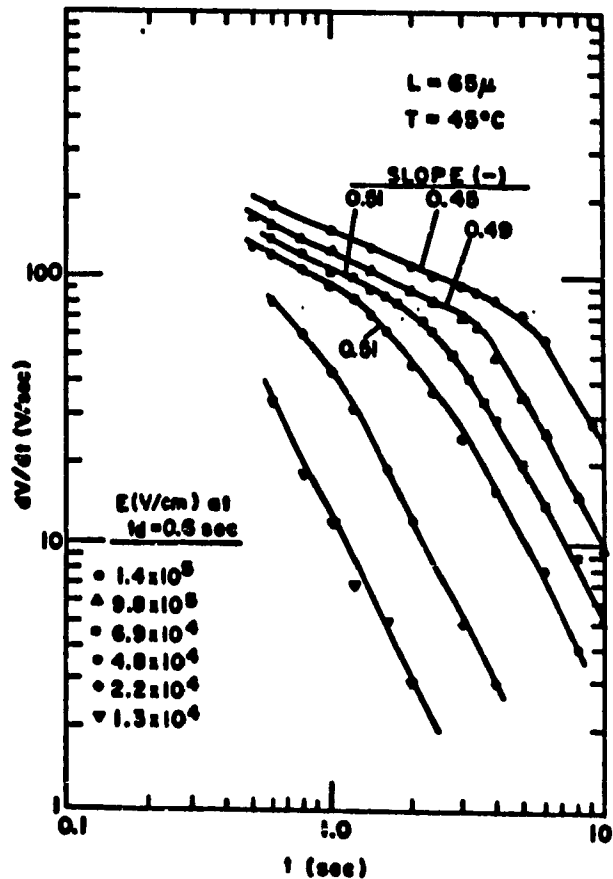


Fig 2.1 Double logarithmic plot of dV/dt versus time t for a 65 micrometer thick As_2Se_3 film at $45\text{ }^\circ\text{C}$. (from Ing and Neyhart [15])

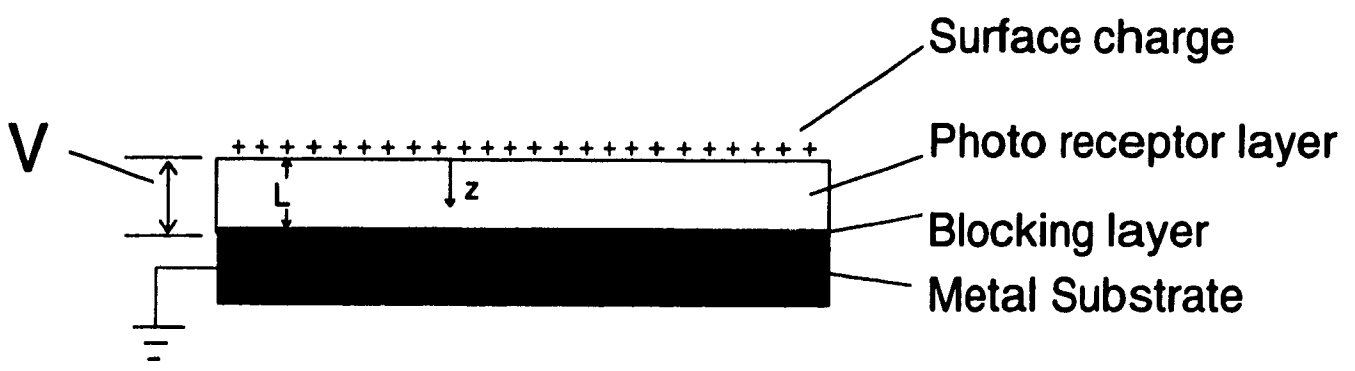


Fig 2.2 Schematic of photoreceptor structure.

Chapter 3.

PREPARATION OF SAMPLES

3.1. Introduction

The basic fabrication of the selenium xerographic test structures (often called samples), was briefly described in chapter . In this chapter, however, more details of the sample fabrication process are given. The undoped high purity selenium was kindly supplied by the Noranda Technology Centre, Pointe Claire. For the xerographic measurements in chapters 5 and 6, selenium doped with chlorine was used, while for the measurements on samples employing variations in the aluminum oxide blocking layer in chapter 7, undoped selenium, as supplied, was employed. In the latter work, special non-xerographic test samples were fabricated in the form of metal-oxide-indium structures (Fig 3.1a) for measurements of oxide thickness via capacitance, where the metal base was usually aluminum. These are referred to as capacitance samples. The steps involved in the fabrication of the xerographic samples (Fig 3.1b) were: cleaning the aluminum substrate, depositing the oxide blocking layer and depositing the selenium. These steps and the process of preparing the chlorine-doped selenium source material are now described. Table 3-1 lists details of the fabrication of all the samples, xerographic and capacitance samples, relevant to the present thesis.

3.2 Substrate Cleaning and Etching

A plate of aluminum, 0.035 inch in thickness, 2 x 2 inches in lateral dimensions and polished to a mirror finish on one surface, was used as the base electrode and substrate for all the xerographic samples and some of the capacitance samples. This plate was cut from an aluminum sheet 20 x 20 inches, as supplied by the Noranda Technology Centre and, as received, had a transparent plastic cover over the polished surface. For many of the capacitance samples, an aluminum substrate film, evaporated on glass, was also used.

Each aluminum plate was ultrasonically cleaned by successive immersion in propanol, acetone and deionized water for 10 minutes each. An etching treatment was then applied to it, which was reported to be beneficial for xerographic action [18]. This consisted of immersion of the plate in chromic/phosphoric acid (20 g CrO₃ plus 35 ml 85% H₃PO₄ per litre) at 95 °C for 10 minutes, after which it was rinsed with deionized water and alcohol and dried in air. The evaporated aluminum films on glass for the capacitance samples were not cleaned or etched but transferred immediately to the oxide sputtering chamber.

3.3 Oxide Blocking Layer Deposition.

The aluminum oxide blocking layer, with a thickness between about 100 to 2000 Å, was deposited by either d.c. reactive

sputtering from an aluminum target in low pressure air or by r.f. sputtering from an Al_2O_3 target in argon. These methods are now described in detail:

(a) d.c. Sputtering Method

Following the substrate cleaning and etching of the aluminum plate, the sample was introduced into a 12-inch vacuum system (Edwards model E306A coating system) for the d.c. oxide sputtering (Fig 3.2). The plate was fixed 40 or 60 mm vertically above an aluminum target. The target consisted of a disc, 5 cm in diameter, 4 mm thick of high purity aluminum (99.999%). With the bell jar in place, the pressure was reduced to 10^{-6} torr, following which air was allowed to flow into the system continuously via the needle valve; the pressure was brought up to a value of 50 millitorr, controlled by the diffusion pump high vacuum valve and the inlet needle valve. The pressure was measured with a Pirani type vacuum gauge (Edwards model 8/2). With the pressure maintained at this value, a negative d.c. voltage of 800-1000 volts was applied to the target (cathode) to yield a constant sputtering current of 10 mA, which was continued for different times ranging from 20 to 120 minutes, depending on the oxide thickness required. After switching off the sputtering current, the system was pumped down to lower pressure, left for more than 3 hours to allow sufficient cooling and then the sample was removed from the chamber.

(b) R.F. Sputtering Method

The blocking oxide layer in many of the later prepared samples

was done using r.f. sputtering. In this method, the aluminum plate was introduced into a 12-inch vacuum system (different from that used for d.c. sputtering), supplied with radio frequency power from a 500W Varian RF-500MB generator with matching network (Fig 3.3), and a magnetron cathode (U.S. Gun II). The substrate for oxide deposition was located 60 or 80 mm vertically above the target, which consisted of a disc, 2 inches in diameter and 3.5 mm thick, of high purity sintered Al_2O_3 (99.99%). With the bell jar in place, the pressure was pumped down first to 10^{-6} torr, following which, high purity argon (99.99%) was allowed to flow into the system and the pressure raised to 2 millitorr. It was maintained at this value using the inlet needle valve and the diffusion pump high vacuum valve. At this pressure, r.f power at 60 watts was applied between the grounded sample and the target for different periods ranging from 7 to 60 minutes, depending on the oxide thickness required. At the end of the deposition, the sputtering power was switched off and the system was pumped down to 10^{-6} torr again and left for more than 3 hours to allow sufficient cooling. Then the sample was removed from the chamber in readiness for the next process.

3.4 Selenium Deposition

Immediately after the sputtering process, the plate, with the oxide film on it, was mounted in another 12-inch vacuum coater (Edwards model E12E) and positioned on a heated graphite block about 60 mm above a source of selenium (Fig 3.4). This source consisted of selenium pellets in a stainless steel cylinder, held in a quartz cup and heated with a surrounding tungsten coil (Fig 3.5).

With the bell jar in place, the system was pumped down to a pressure of 10^{-6} torr and the substrate temperature was brought up to 50 °C as indicated by a thermocouple (type J) located in the heated sample holder. Next, a current of 35 to 45 amps was passed through the tungsten source coil to obtain a source temperature of 245 °C, as indicated by another type J thermocouple located in the stainless steel boat. After bubbles of dissolved gases from the liquid selenium had ceased (after about 5 minutes), the shutter in front of the substrate was moved away, allowing the evaporation of the selenium to start. The evaporation was continued for about 60 minutes, after which the shutter was moved back in front of the source. The source current was maintained at the same value, however, as that during deposition until all the selenium in the boat was exhausted. This was done to ensure that, for the next selenium deposition, only fresh selenium was used. After the source and substrate currents were switched off, the system was allowed to cool until the temperature was lower than 80 °C (after about 3 hours). Then the sample was removed.

3.5 Surface Treatment of Samples

After the deposition of the selenium, the fabrication of the xerographic test sample was essentially complete. However, in the earlier part of the study, it was found that the xerographic dark decay rate was often greatly reduced by treating the selenium surface with a cleaning process. Later smaller dark decay rates were obtained without the cleaning but it was done anyway to ensure uniformity of treatment. The treatment consisted simply of spraying the selenium surface with propanol (Class 1B) from a bottle with a

squirt-nozzle for a few seconds and allowing the surface to dry in air for three minutes.

3.6 Deposition of Metal for Capacitance Measurement

For the non-xerographic oxidized aluminum plates used for capacitance measurements, indium was deposited in localized areas by vacuum evaporation. This was done by mounting the plate within a 12-inch vacuum coater (Cooke system CV-301FR) some 40 mm above the source of high purity indium (99.999%) in a tantalum boat cut from tantalum foil. Next, a specially-made stainless steel metal mask was clamped over the oxidized surface. This mask contained circular holes of varying diameter (Fig 3.6) for deposition of the indium discs of different area. Usually about 5 pellets of indium were placed in the boat. With an initial pressure of about 10^{-6} torr, evaporation of the indium was carried out for 20 minutes as controlled with a metal shutter. The source current through the tantalum boat during the process was 30 amps.

3.7 Preparation of Chlorine-doped Selenium

For the xerographic measurements to be reported in chapters 5 and 6, samples were used employing selenium doped with 6 different nominal levels of chlorine, namely: undoped, 3, 6, 10, 20, 66 and 100 ppm. The undoped, 66, and 100 ppm samples were obtained directly from selenium batches supplied to us by Noranda Copper Smelting and Refining, CCR Refinery. However, the nominal 3, 10 and 20 ppm selenium sources were prepared in the laboratory using the

following steps:

- 1) W_1 grams of pure and W_2 grams of pre-doped selenium pellets were mixed together and inserted in a quartz ampoule, which had been previously cleaned with acetone and propanol.
- 2) The open end of the ampoule was next connected to a vacuum pumping system (Edwards high vacuum 100M-E2M8), and pumped down to 10^{-7} torr and kept at this pressure for 12 hours or more without heating. After this, it was vacuum-sealed with an oxy-hydrogen flame.
- 3) The ampoule was then placed in an electric oven, (Thermolyne type 10500), and the temperature increased to 800 °C and maintained at this value for 24 hours. During this period, the ampoule was shaken periodically to ensure homogeneity.
- 4) After the 24 hour period, the ampoule was taken out of the oven and allowed to cool down to room temperature. The ampoule was then broken open to remove the solid selenium piece, which was next divided into several smaller pieces. The top and the bottom parts were discarded because it was suspected that these regions could have deviations from the average chlorine concentration. Only the middle pieces were retained as the materials for the evaporation sources and for analysis.

If D is the nominal chlorine concentration in the 100 ppm pre-doped pellets, the nominal concentration in the prepared selenium therefore was taken to be $DW_2 / (W_1 + W_2)$. These values are indicated in

the first row of Table 3-2 below as the 3, 10, and 20 ppm nominal values.

Table 3-2 Chlorine concentrations in selenium sources

Nominal Cl concentration (ppm)	0 ⁽¹⁾	3 ⁽²⁾	10 ⁽²⁾	20 ⁽²⁾	66 ⁽¹⁾	100 ⁽¹⁾
Determined Cl concentration (ppm)	0.7	1.2	1.4	6.0	65	95

(1) Nominal chlorine content in pellets as supplied.

(2) Nominal chlorine in laboratory-doped selenium.

Chemical analysis of the prepared selenium samples was kindly carried out by Noranda Copper Smelting and Refining, CCR Refinery. The method used was stated to be as follows: First dissolution (6 hours) of the selenium in nitric acid with subsequent filtration was carried out. The AgCl precipitate was next dissolved in ammonia and the silver content was then determined by flame atomic absorption. The values obtained are listed in the second row of Table 3-2. Inspection shows good agreement for the nominally undoped, 66 and 100 ppm samples but for the laboratory-prepared samples, the concentrations are lower than the nominal values. This is probably due to some loss of the chlorine on the walls of the ampoule and into the top or bottom parts of the charge in the ampoule or to possible error in estimating the chlorine content from chemical analysis.

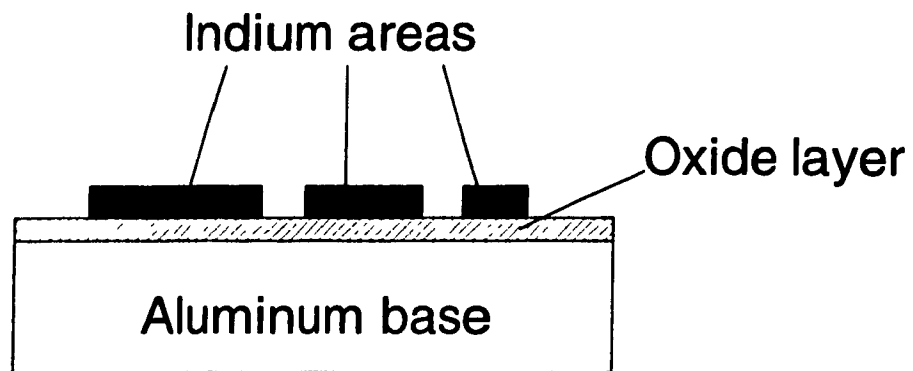


Fig 3.1a Diagram of structure of Al-oxide-In sample used for oxide thickness measurements.

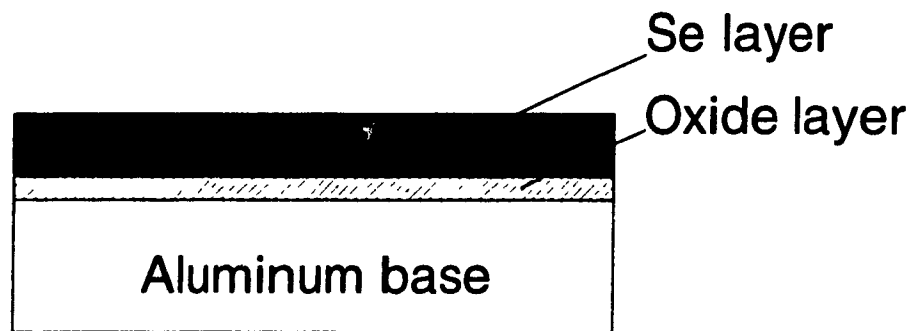


Fig 3.1b Diagram of structure of Al-oxide-Se sample used for xerographic measurements.

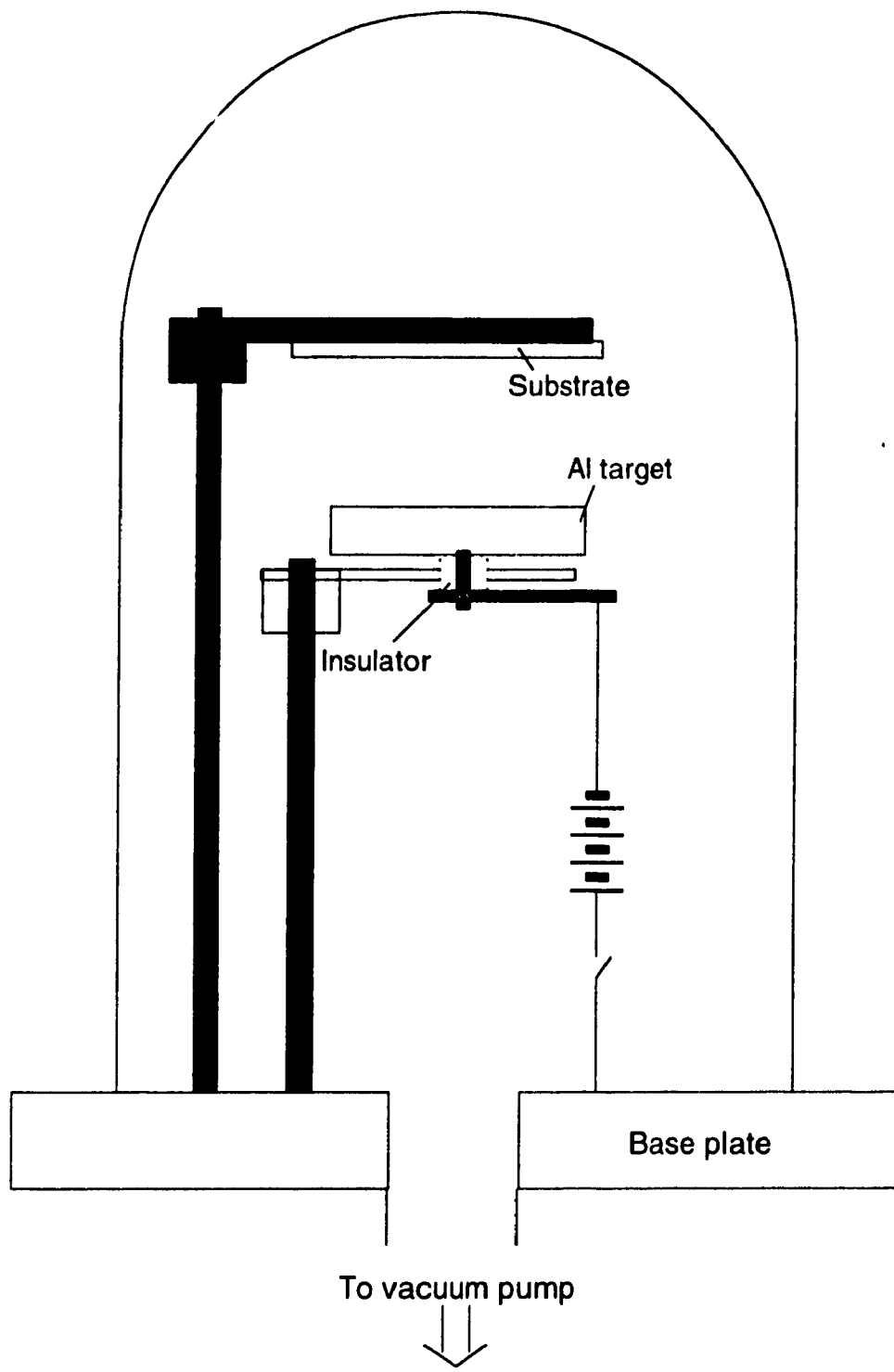


Fig 3.2 Schematic diagram of d.c. reactive sputtering system used to deposit the aluminum oxide blocking layer.

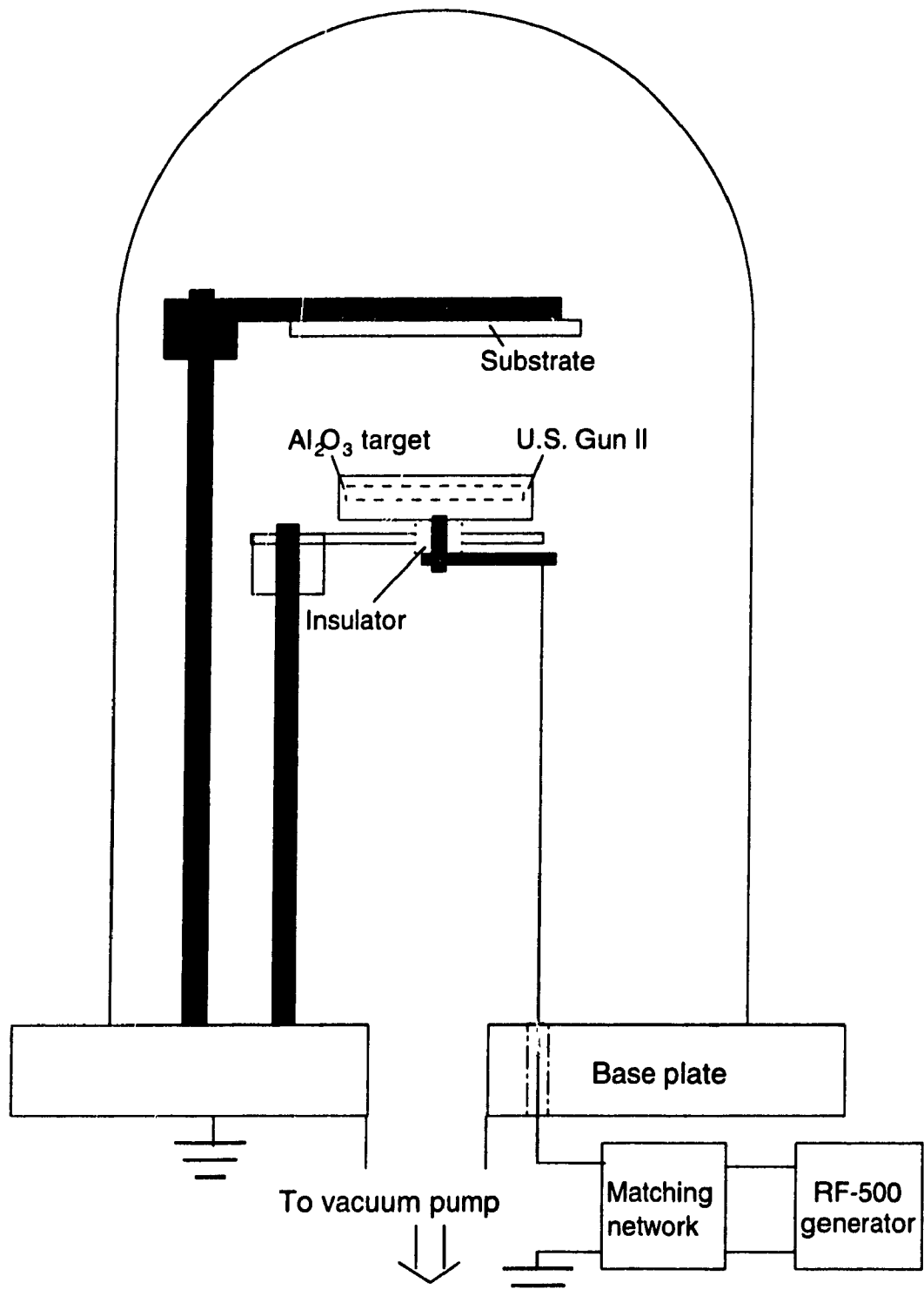


Fig 3.3 Schematic diagram of r.f. sputtering system used to deposit the aluminum oxide blocking layer.

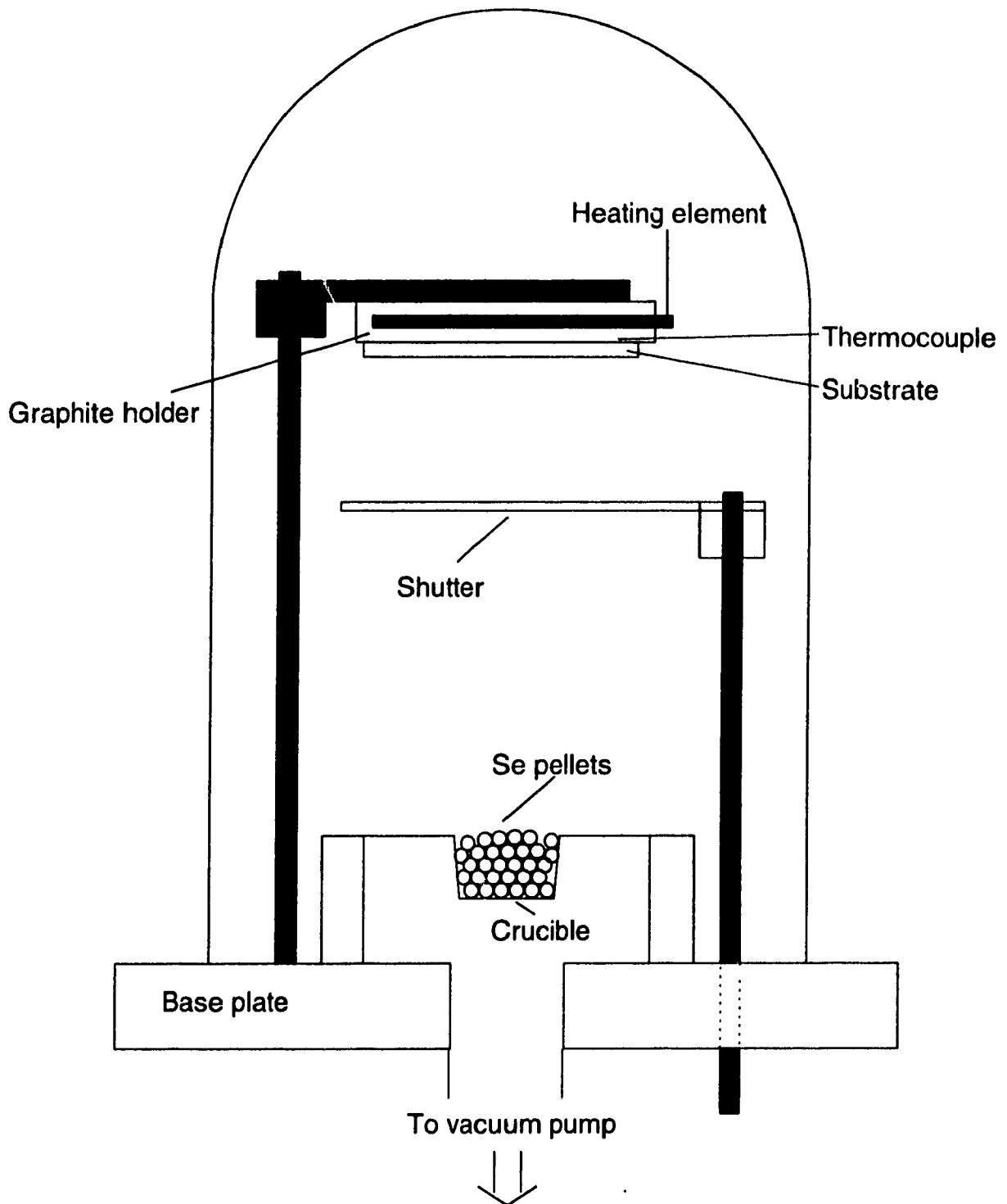


Fig 3.4 Schematic diagram of evaporation system used to deposit the amorphous selenium layer.

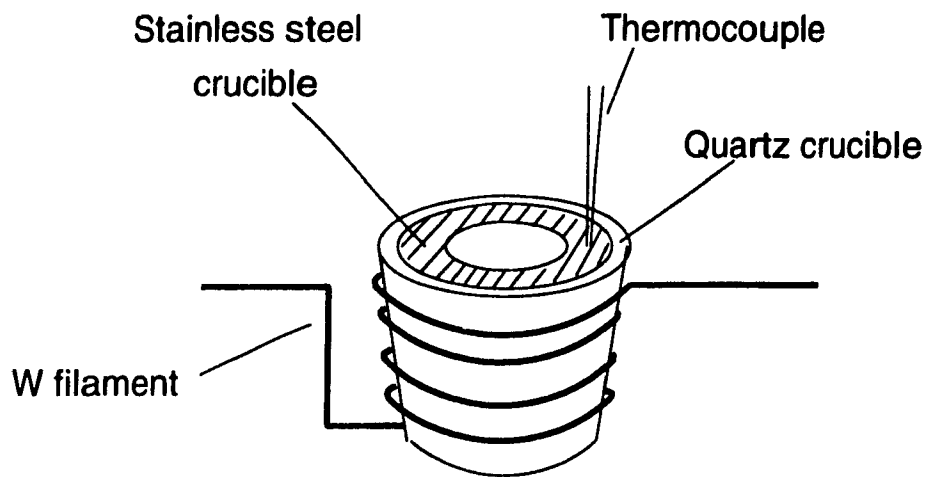


Fig 3.5 Schematic diagram of the stainless steel crucible used for selenium evaporation.

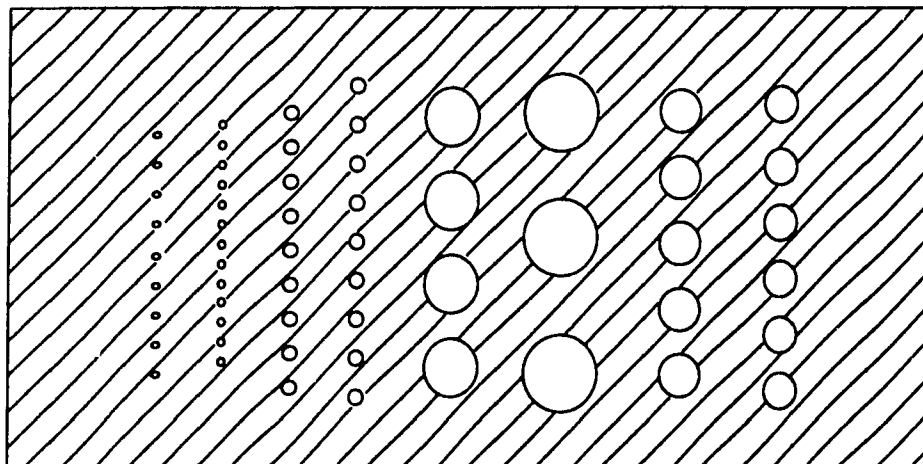


Fig 3.6 Aluminum mask for indium electrode evaporation on to oxide film.

**Table 3-1
Fabrication of Measurement Samples**

Sample Number	Structure	Oxide			Selenium			Remarks	
		¹ Sputt. Method	Sputt Time (min)	Thickness ² (Å)	Thickness ³ (μm)	Cl concentration (ppm)			
						Nominal ⁴	Determined ⁵		
C1	Al-Ox-In	d.c.	80	415	---	---	---	Samples for xerographic & capacitance measurement with different thickness of oxide made with d.c. sputtering method	
X1	Al-Ox-Se		80	not measureable	45	0	0.7		
C2	Al-Ox-In		60	Failed	---	---	---		
X2	Al-Ox-Se		60	not measureable	50	0.	0.7		
X3	Al-Se	---	---	---	50	0	0.7		
C4	Al-Ox-In	d.c.	120	730	---	---	---		
X4	Al-Ox-Se		120	not measureable	48	0	0.7		
X5	Glass-Al-Ox-Se		50	510	50	0	0.7		
X6	Al-Ox-Se		20	220	45	0	0.7		
C7	Glass-Al-Ox-In	r.f.	22	1070	---	---	---		R.F sputt. with a new Al ₂ O ₃ target. Target-sample separation 60mm
C8			10	393	---	---	---		
C9			7	370	---	---	---		
C10			20	374	---	---	---	Separation changed to 80mm	
C11			40	Failed	---	---	---		
C12			30	450	---	---	---		

**Table 3-1 (continued)
Fabrication of Measurement Samples**

Sample Number	Structure	Oxide			Selenium			Remarks
		1 Sputt. Method	Sputt. Time (min)	Thickness ² (Å)	Thickness ³ (μ m)	Cl concentration (ppm)		
						Nominal ⁴	Determined ⁵	
C13	Glass-Al-Ox-In	r. f.	45	813	---	---	---	Samples for measurement of oxide on Al.
C14			7	141	---	---	---	
C15			60	1050	---	---	---	
C16	Glass-Ni-Ox-In		60	981	---	---	---	Samples for measurement of oxide on Ni.
C17			37	509	---	---	---	
C18			20	434	---	---	---	
C19	Glass-Au-Ox-In		60	955	---	---	---	Samples for measurement of oxide on Au
C20			20	325	---	---	---	
X21	Al-Ox-Se		60	not measurable	50	0	0.7	Samples for xerographic measurement
X22		60	58		0	0.7		
X23		30	48		0	0.7		
X24		30	50		0	0.7		
X25		30	48		0	0.7		
X26		30	48		0	0.7		
X27		30	50		10	1.6	Samples used to study the xerographic properties of samples with different chlorine content	
X28		30	48		10	1.6		

**Table 3-1 (continued)
Fabrication of Measurement Samples**

Sample Number	Structure	Oxide			Selenium			Remarks	
		1 Sputt. Method	Sputt. Time (min)	Thickness ² (Å)	Thickness ³ (μm)	Cl concentration (ppm)			
						Nominal ⁴	Determined ⁵		
X29	Al-Ox-Se	r. f.	30	not measurable	45	20	6.0	Samples used to study the xerographic properties of samples with different chlorine content	
X30			30		50	66	65		
X31			30		55	66	65		
X32			30		52	20	6.0		
X33			30		55	100	95		
X34			30		50	100	95		
X35			30		52	3	1.4		
X36			30		48	3	1.4		
X37			20		48	100	---		Prepared from 0.3% As- doped Se
X38			20		55	0	0.7		Samples used to compare the xerographic properties of samples with oxide layers obtained with different methods
X39		d. c.	40		52	0	0.7		
X40		r. f.	20		52	0	0.7		
X41		d. c.	40		50	0	0.7		
X42		r. f.	20		52	66	65		

**Table 3-1 (continued)
Fabrication of Measurement Samples**

Sample Number	Structure	Oxide			Selenium			Remarks
		Sputt Method ¹	Sputt. Time (min)	Thickness ² (Å)	Thickness ³ (μm)	Cl concentration (ppm)		
						Nominal ⁴	Determined ⁵	
X43	Al-Ox-Se	d.c.	40	not measurable	48	66	65	Samples for xerographic measurement
X44		r.f.	20		50	66	65	
X45		d.c.	40		48	66	65	
X46	Al-Se	---	---	no oxide	54	66	65	
X47		---	---		52	0	0.7	

1. Either d.c. sputtering from Al target at air pressure of 50 and 100 millitorr or r.f. sputtering from Al₂O₃ target in argon at pressure at 2 millitorr.

2. Thickness measured from capacitance at frequency of 1 kHz.

3. Thickness measured chip observed under microscope.

4. Nominal composition is that of the mixture used to form the material for evaporation.

5. Determined composition is that determined chemically at Noranda Copper Smelting and Refining, CCR Refinery.

Chapter 4.

MEASUREMENT TECHNIQUES

4.1 Introduction

This chapter describes the experimental techniques used for the measurements on the samples. For the Al-oxide-Se xerographic samples, measurements were made of acceptance voltage, dark decay rate, residual voltage and cycled up residual voltage. These xerographic properties, as used, will be defined in this chapter. The specific apparatus for the measurements is described, along with its calibration and operation with both manual and semiautomatic control. The procedure for saturated charging and single pass charging is also described. To obtain the blocking layer oxide thickness, capacitance measurements were made on the special samples without the selenium layer. Oxide conductances were also measured on the samples, to obtain information on oxide quality.

4.2 Definitions of the Xerographic Parameters Measured

Fig 4.1 shows a schematic of the surface potential variation with time on a selenium plate after charging and illumination. The definitions of the xerographic parameters as measured in this thesis are given as follows:

Acceptance voltage, V_A , is the potential at the selenium surface, with respect to the metal substrate, immediately after charging positively or negatively from a corona discharge. This term implies saturation of the charge, for a fixed voltage applied to the corotron. Another term, initial voltage V_1 , will be explained later on.

Dark decay rate is the percentage decrease of voltage from the acceptance voltage (following charging) on the selenium surface in darkness after a specific period of time. The time used in the present work was 2 minutes. Thus from Fig 4.1, the dark decay rate is given by $(V_A - V_2) / V_A$.

Residual voltage is the voltage on the selenium surface recorded in darkness during a period of about 30 seconds after illumination for 10 seconds, when preceded by charging and delay in darkness of two minutes.

Cycled-up dark decay rate is the average value of the dark decay rate after 30 cycles of regular charging and discharging plus a further 300 cycles of fast charging and discharging treatment.

Cycled-up residual voltage is the average value of the residual voltage after 30 cycles of regular charging and discharging plus a regime of 300 cycles of fast charging and discharging.

4.3 Measurement Apparatus for Xerographic Parameters

The apparatus used for measuring the above defined xerographic parameters is shown schematically in Fig 4.2. It consisted of an aluminum rotatable disc, a fixed aluminum table, positioned over the turntable and an aluminum base on which both the disc and the table were mounted. On the turntable, there was a brass holder to support the Al-oxide-Se sample for xerographic measurements. On the fixed table, there was a corotron(A) for charging the sample from a corona discharge. There was also a measuring probe(B), consisting of a brass disc, 1.5 cm in diameter, attached to the end of a threaded brass rod and insulated from the table using Teflon. In another position on the table, there was an 8-watt tungsten lamp(C) for illumination of the sample under test after a certain period of dark decay. There was also a 40W tungsten lamp(D) at a further position, which was used to erase the residual charge.

The system for measuring the potential V_p on the selenium film as a function of time is shown schematically in Fig 4.3. The potential V_m itself was measured with a Keithley model 617 electrometer (having an input impedance of $>200\text{ T}\Omega$ in parallel with 20 pF of capacitance), using a supplied co-axial cable. The output from the electrometer was connected to a Hewlett-Packard model 7015B X-Y recorder using its time base. The voltage V_{ps} for the corotron was supplied from a Sorenson model 1020-30 d.c. power supply, capable of supplying up to 25 kV.

In the measurement position, the separation d between the probe surface and the selenium surface was either 3.0 or 4.0 mm.

Thus, the capacitance C_e between the measuring plate and the selenium surface in air is given by $C_e = \epsilon_0 A/d$, where A is the disc area (1.77 cm^2) and ϵ_0 is the permittivity of a vacuum. The voltage V_m , measured by the electrometer, was only a fraction of the potential V_p on the selenium surface. From Fig 4.4 (a) and (b), it is noted that $Q=(V_p-V_m)C_e=V_mC_m$, where Q is the charge between capacitors C_m and C_e . Hence

$$V_p = V_m \left(\frac{C_m}{C_e} + 1 \right) \quad , \quad (4.1)$$

where C_m is the capacitance of the measuring electrometer with its associated cable. Substitution for C_e and C_m into this relation yields the result $V_p = k_1 V_m$, where $k_1 = C_m/C_e + 1$ is the voltage conversion ratio. This ratio was used to convert the measured potentials to the actual values on the selenium surface with respect to ground. The measured value of k_1 will be treated in section 4.7 of this chapter.

The relationship between the voltage on the charged selenium surface before (V_p) and after positioning under the measuring probe (V_{pf}) is given [2] by:

$$V_p = V_{pf} \frac{C_s C_e + C_s C_m}{C_s C_e + C_s C_m + C_e C_m} \quad , \quad (4.2)$$

where C_s is the capacitance across the selenium sample, given by $C_s = \epsilon_0 \epsilon_r A/L$. Here ϵ_r is the relative dielectric coefficient of selenium and L is the thickness of the selenium film. Substituting the values of $C_m = 78 \text{ pF}$, $C_s = 188 \text{ pF}$ and $C_e = 0.521 \text{ pF}$ into equation

(4.2), yields

$$V_p = 0.9973V_{pf}$$

The result clearly shows that the difference between V_p and V_{pf} can be neglected.

4.4 Xerographic Parameter Determination with Saturated Charging

With the apparatus just described, the procedure (method A) for the measurement of the xerographic parameters of acceptance voltage, dark decay rate and residual voltage was as follows.

1. The sample to be measured was located in the brass sample holder on the turntable, which was first rotated to the position under the corotron wire.

2. With the d.c. power supply switched on and the voltage set to 5,500 to 7,000 volts, the sample was oscillated back and forth (by step-motor control) under the corotron wire to get a uniform charge on the surface of the selenium layer. This process was continued for some 10 seconds, in which time the surface potential essentially reached a saturated value. After this, the sample was moved away from the corotron and its d.c. supply was manually switched off.

3. The sample was rotated to the position under the measurement probe to determine the surface potential in darkness

and maintained in this position for 2 minutes to record the decay of dark voltage.

4. The sample was then rotated to the position under the 8-watt tungsten lamp, which was automatically turned on by a microswitch after the 2 minute dark decay period. The sample was maintained under the lamp for 10 seconds, during which most of the charge was lost.

5. The sample was rotated back to the position under the probe to measure the residual voltage for 30 seconds.

6. The sample was then returned to the position under the 40-watt tungsten lamp, which was also turned on by a microswitch for 30 seconds, to erase the residual voltage.

7. The sample was returned to the position under the probe and the power supplies for the recorder, the electrometer and the high d.c. supply were switched off.

An alternative procedure (method B), which gave the same result, was as follows: the turntable was kept rotating at a speed of about 6.67rpm from the beginning to the end of the measurement. The output signal then consisted of a series of periodic voltage pulses every 9 seconds. Fig 4.5 shows both the voltage plots for the two different methods (A and B) of measurement on the same sample, indicating reasonable agreement between the two.

4.5 Light Fatigue Measurement

Light fatigue measurements were also carried out on the samples. These require many successive charging and illuminating cycles, which are time-consuming and difficult to control uniformly if they are done manually. Thus, in order to do this in an efficient manner, an automatic system was set up for such measurements with repetitive cycles. A cycled-up measurement was hence done as follows:

The sample was placed on the rotating measurement plate and 30 regular charging and discharging cycles were first performed with the sequence described in section 4.4, This was followed by a further program of 300 cycles of fast charging and discharging, where each cycle, lasting only 10 seconds, consisted of dark charging up, 4 seconds of dark delay, followed by illumination. After this, 10 regular cycles were made and finally voltage measurements were taken. The average values of dark decay rate and residual voltage were then taken as the cycled-up values.

4.6 Single Pass Charging for Determination of Dark Decay Voltage Slopes

The charging process described in section 4.4, where the sample was oscillated back and forth under the corotron, lasted about 10 seconds, during which a saturated surface potential V_A was established. However, a shorter single pass charging method was necessary for the measurement of voltage slopes, to study the

mechanism of the dark decay process. This consisted of a single sweep of the sample under the corotron wire, as the sample disc was rotated under it at a constant speed. The sample was then stopped at the measuring probe position to follow the voltage decay with time without the illumination step 4 and residual measurement step 5 of section 4.4. The surface potential on the selenium film just after the charging is defined as the initial voltage V_1 . Voltage slope values of dV/dt were taken from tangents drawn on the plotted variation of dark voltage with time.

4.7 Calibration of Measurement System

As indicated in section 4.3, the plate voltage V_p is proportional to the measured potential V_m with a proportionality constant $k_1 = C_m/C_e + 1$. Since the values of C_m and C_e were known only approximately, it is better to find k_1 by direct calibration, rather than using the formula. The measurement for this cannot be done with the normal selenium sample because direct contact to the top charged selenium surface is necessary. Hence a special metal-insulator test plate was used, consisting of a 2 X 2 inch glass plate with gold sputtered on one surface. This plate was placed in the sample holder with a fine copper wire attached to the edge of the gold film. With the d.c. power supply directly connected to the gold film, the values of potential V_m were taken with the measuring probe using the electrometer. Fig 4.6 shows a plot of the measured probe potential against the actual d.c. supply voltage V_s , which was varied from 0 to 1.5 kV for the two probe-film separations of $d=3$ and 4 mm. From the figure, dV_s/dV_m slopes of 132 and 183 were obtained for $d=3$ and 4 mm respectively. These represent the k_1 -

values in the equation $V_s = V_p = kV_m$.

The electrometer input capacitance C_m (including the capacitance of the leads) was measured using a voltage divider and found to be 78 pF. With C_e values of 0.521 and 0.391 pF, which were obtained with equation $C_e = \epsilon_0 A/d$, for $d=3$ and 4 mm respectively, k_1 -values of 151 and 200 were obtained using $k_1 = C_m/C_e + 1$, representing a 10 to 15% disagreement with the measured k_1 -values. This may be due to inaccuracy in the estimation of C_e .

4.8 Measurements of C_p and R_p of Oxide

To obtain the oxide thickness, capacitance measurements were made on the capacitance samples (Al-oxide-indium) in the following way. The sample was placed in the unit shown in Fig 4.7, which consists of a brass base, a Plexiglass frame and a spring-loaded copper point probe. The sample was placed with its aluminum face on the brass base. In earlier work, a small piece of Wood's metal (50% bismuth, 25% lead, 12.5% cadmium) was placed over one of the deposited indium areas on the sample and the copper point was brought down on it with a sufficient spring pressure to make electrical contact. However, because of possible damage to the oxide with this pressure (especially if the film is very thin or of poor quality), it was found more convenient to eliminate the Wood's metal piece and to have a small drop of mercury between the copper point and the sample indium area, without any spring pressure. While the mercury partially dissolved the indium, the action was slow enough for the measurements to be carried out. Capacitance and conductance (parallel mode) measurements were then made on each indium circle, with areas ranging from 0.049 to 0.255 cm², using a

Hewlett-Packard model HP4192 LF Impedance Analyzer. The frequency employed ranged from 10 Hz to 1 MHz, with an a.c. signal voltage of 0.1 volt. The d.c. bias was varied from -15 to +15 volts to observe the breakdown effect. At zero bias, the capacitance C_p was used to obtain the oxide thickness d_{ox} with

$$C_p = \epsilon_o \epsilon_{ox} A_1 / d_{ox} \quad , \quad (4.2)$$

where ϵ_{ox} is relative dielectric constant of aluminum oxide taken as 9 and A_1 is area of the particular indium contact measured. Thus, if C_p is plotted against A_1 , the result should be a straight line and from the slope, the oxide thickness can be obtained. This was done for Al-oxide-indium samples prepared with oxide films deposited for five different sputtering times, as shown in Fig 4.8. These results and the measurements of C_p and R_p as a function of frequency and bias will be presented in chapter 7.

4.9 Selenium Film Thickness Measurement

For each Al-oxide-Se sample, a small piece of selenium was chipped off from its edge and supported with a little grease on a microscope slide to measure the thickness. The thickness was determined with an optical microscope by comparison with a standard microscope length scale. The results are shown in column 6 of Table 3-1 in chapter 3.

4.10 Control System for Semiautomatic Measurement

In the xerographic measurement apparatus shown in Fig 4.2, a step motor is shown, which was geared to the aluminum turntable. The turntable could thus be rotated to various positions by

controlling the step motor rotation.

Fig 4.9 shows a schematic diagram of the system, where a control program is stored in the computer (IBM-PC 386) and the computer runs the program upon the receiving of the command from the operator. The indexer, SLO-SYN Micro series packaged drive (SE-230), translates the command strings from the computer into the electric pulses, which are sent to the step motor. The motor, which is a 5-lead bifilar-wound SLO-SYN step motor (56VA) and connected to the indexer, controls the turning of the turntable to set positions of the sample for charging, illumination and voltage measurement.

a) Communication between host device and indexer

The communication between the computer and the indexer is done in the following way (Fig 4.10):

1. After receiving the start-command from the operator, the computer sends an attention string "<01" to the indexer, where 01 is the identification number of the indexer.

2. If the indexer is not ready, it gives a response ":" to the computer, and when the computer receives it, the attention string will be sent to the indexer again. These 2 steps are repeated until the indexer is ready.

3. When the indexer is ready, it responds with "=", which means it will do the job that the computer asks it to do.

4. When the computer receives the response "=", it starts to send a set of strings for different actions (positions and speeds) of the turntable. Between every two command strings, there is a CR (Carriage return) or LF (Line feed) command.

b) Command string set to control the rotation of turntable

The command string sets for single and cycled up measurements were as follows:

(I) The command string set for a one-measurement run was set for the steps described in the previous section. All the positions the sample could be rotated to were defined between position 0° to position 360° . For example, the corona wire was located at position 0° , the probe located at position 180° and the exposure lamp at position 270° . Each angular degree contained 15 sub-steps. Thus the stages described in the previous section are now as follows (Fig 4.11):

1. Sample is moved to position 0° ;
2. Sample is oscillated back and forth (charging) within -15° to $+15^\circ$ positions (i.e. ± 225 sub-steps from the starting position);
3. Sample is rotated to 180° position (voltage measurement), and held there for 2 minutes;
4. Sample is rotated to 270° position (illumination) held there for 10 seconds;

5. Sample is rotated counter clockwise to 180° position (voltage measurement) and held there for 1 minute;

6. End.

(II) The command string set for cycling measurements was set for the following steps:

Steps 1 to 5 are same as to those for the one-run measurement but followed by three further steps, which are:

6. Sample is rotated clockwise to 315° position (erase illumination) to erase the residual charge;

7. Sample is rotated to 0° for step 1;

8. Repeat steps 1 to 8.

c) Test of control system

A xerographic measurement run was made on sample X1 first manually and second semiautomatically with the motor-control system described in this section. In the second run, the switching on of the d.c. power supply, the chart recorder and the electrometer was done manually. Fig 4.12 shows a comparison of the two voltage-time characteristics, where it is clear that they are essentially the same; the difference in the acceptance voltages is of the same magnitude as that found with successive manual measurement runs.

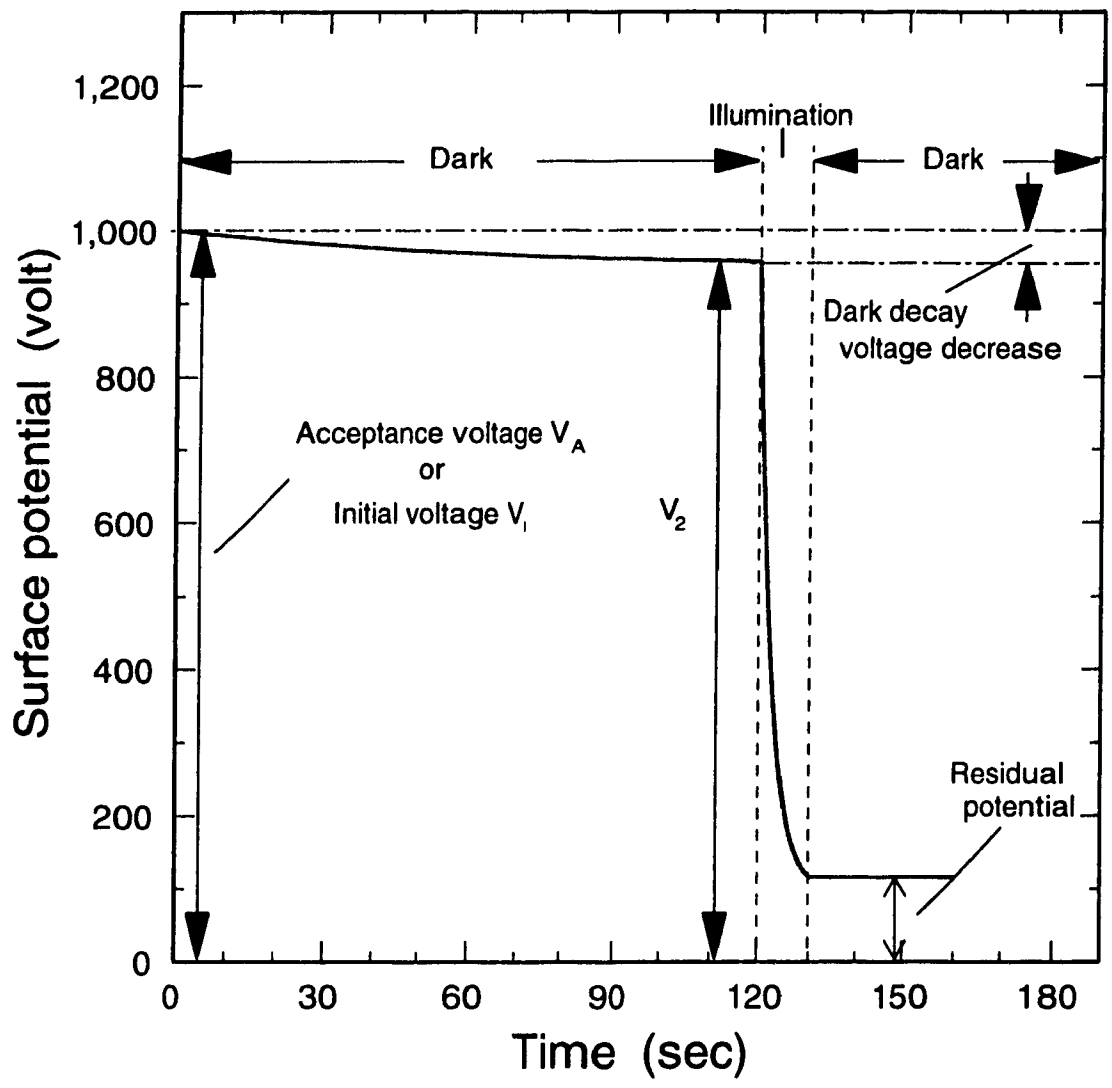


Fig 4.1 Typical variation of voltage with time for a precharged photoreceptor, showing the parameters of acceptance voltage, dark decay voltage and residual voltage.

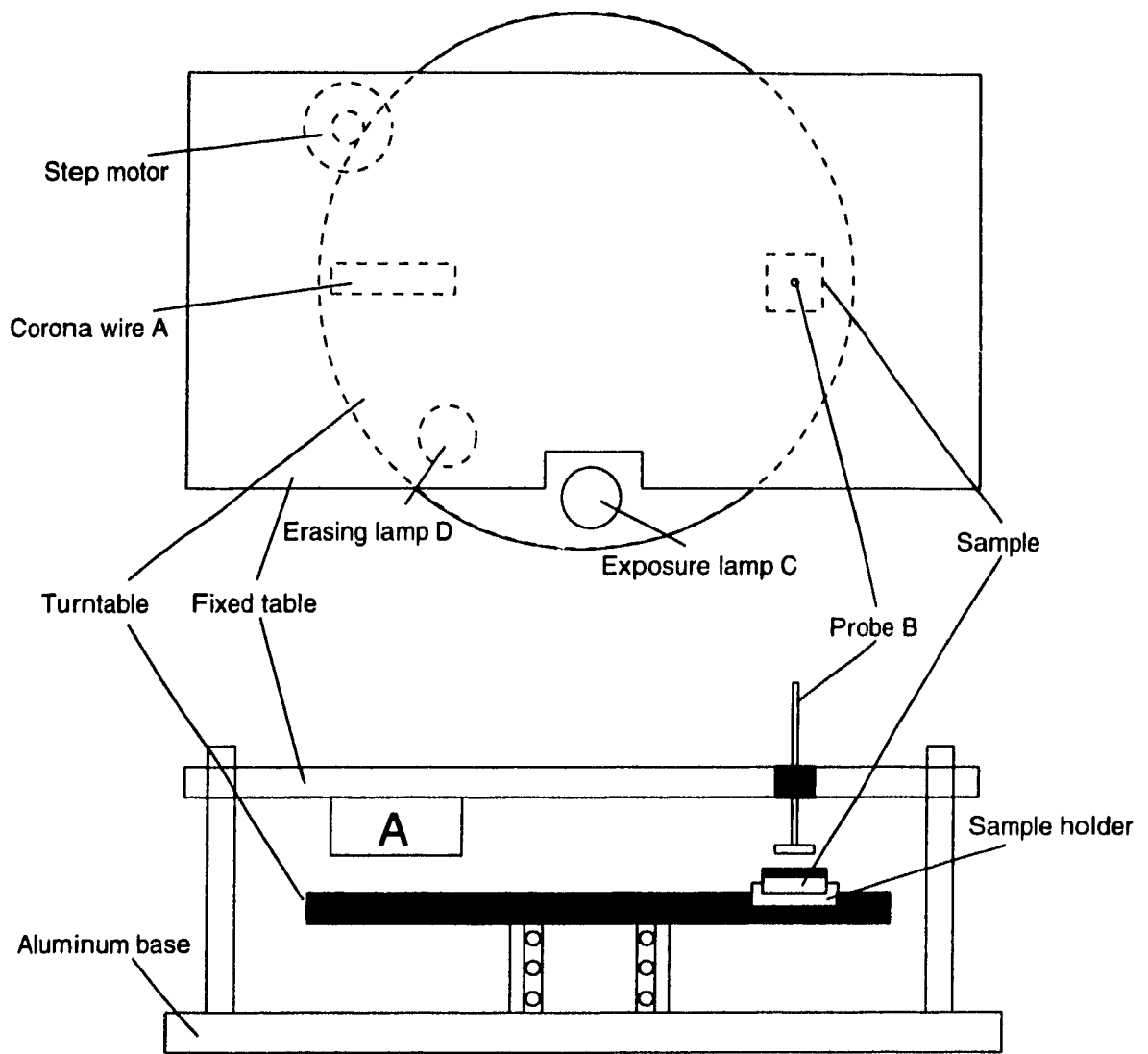


Fig 4.2 Schematic diagram of apparatus used for measurement of xerographic characteristics.

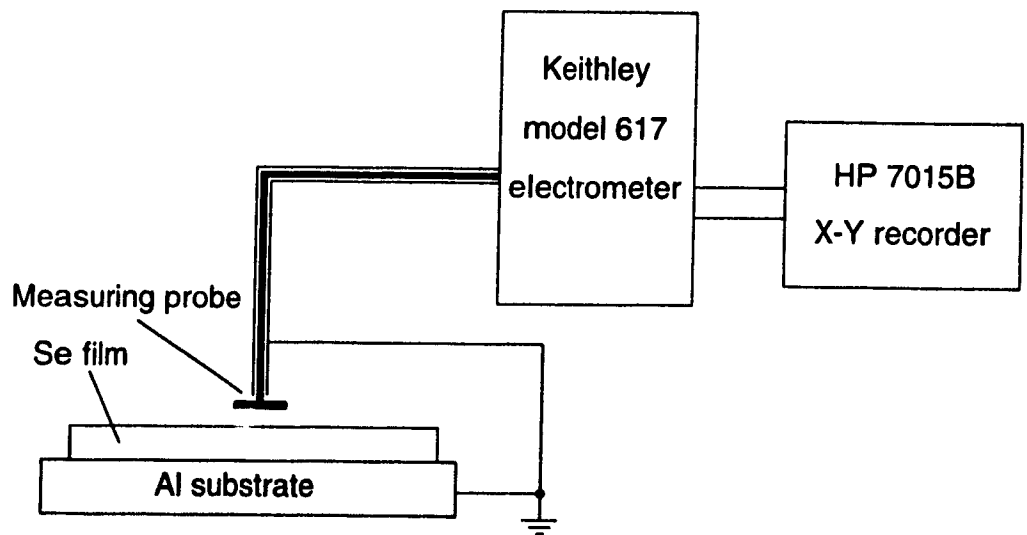


Fig 4.3 Complete system for potential measurement on Se surface.

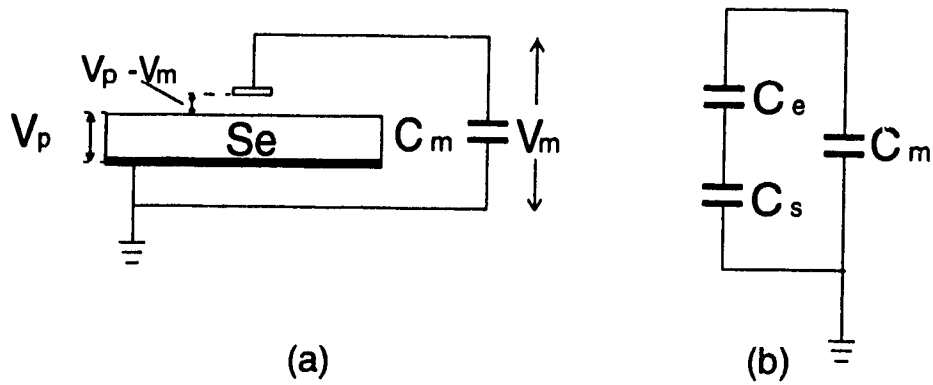


Fig 4.4 Measurement circuit: (a) simplified diagram of measurement system, (b) equivalent capacitor circuit.

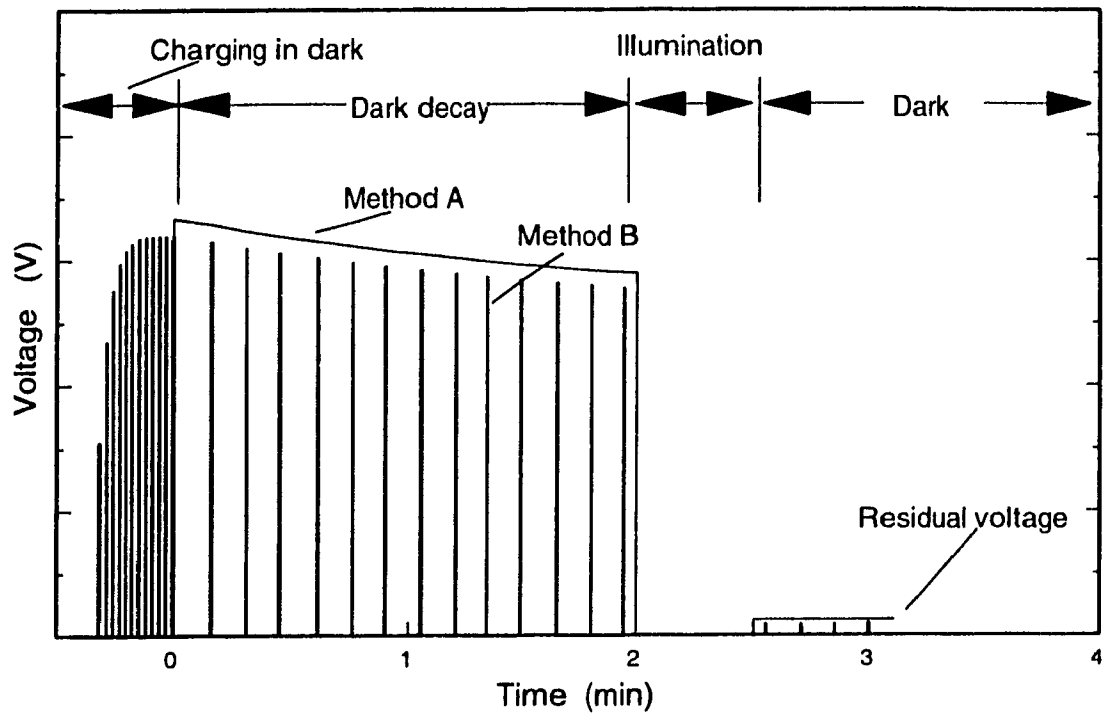


Fig 4.5 Xerographic measurements on a selenium sample with two different methods

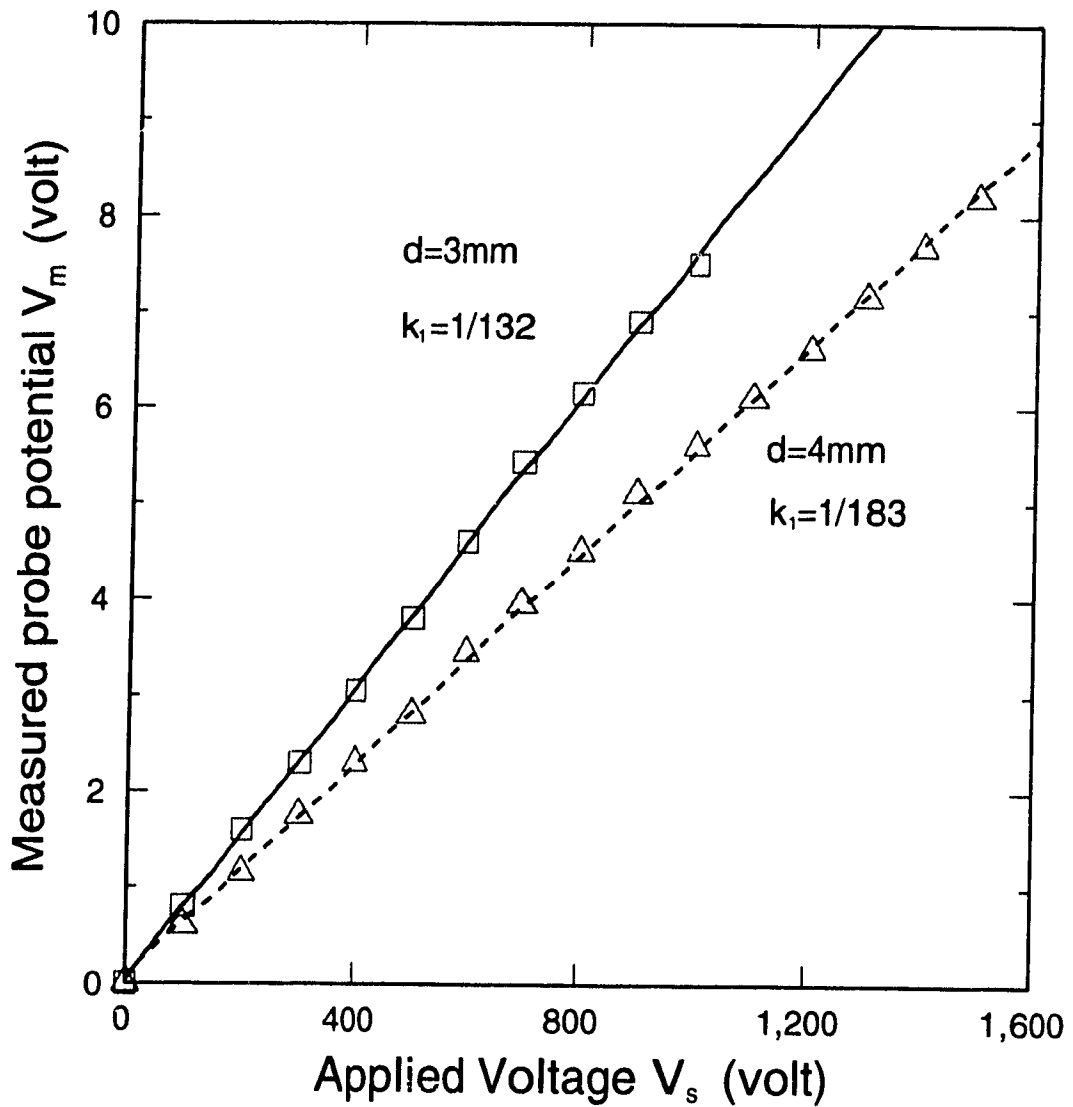


Fig 4.6 Plot of measured probe potential against applied surface voltage for two different probe-surface separations (d), where $k_1 = V_s/V_m$

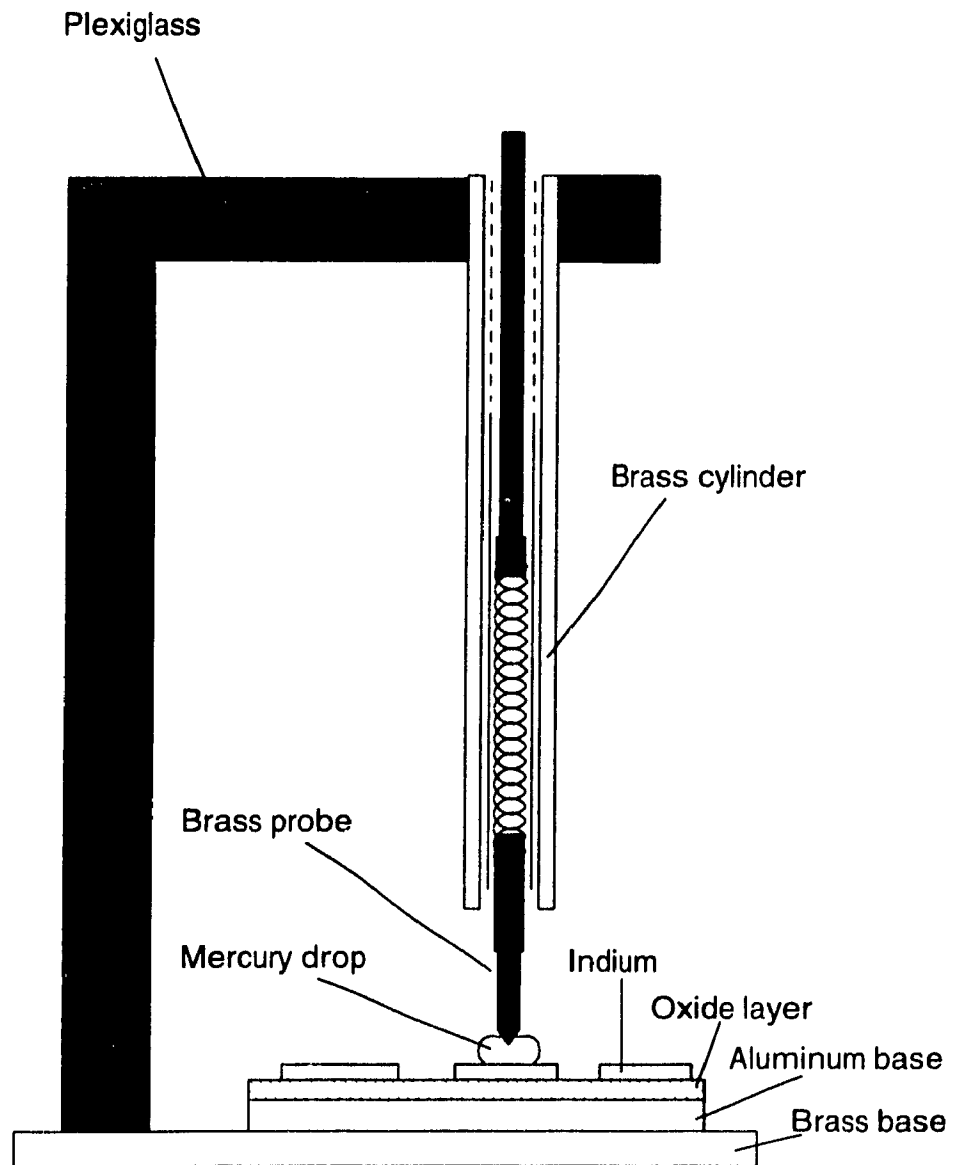


Fig 4.7 Unit used for making contact to samples for capacitance measurements.

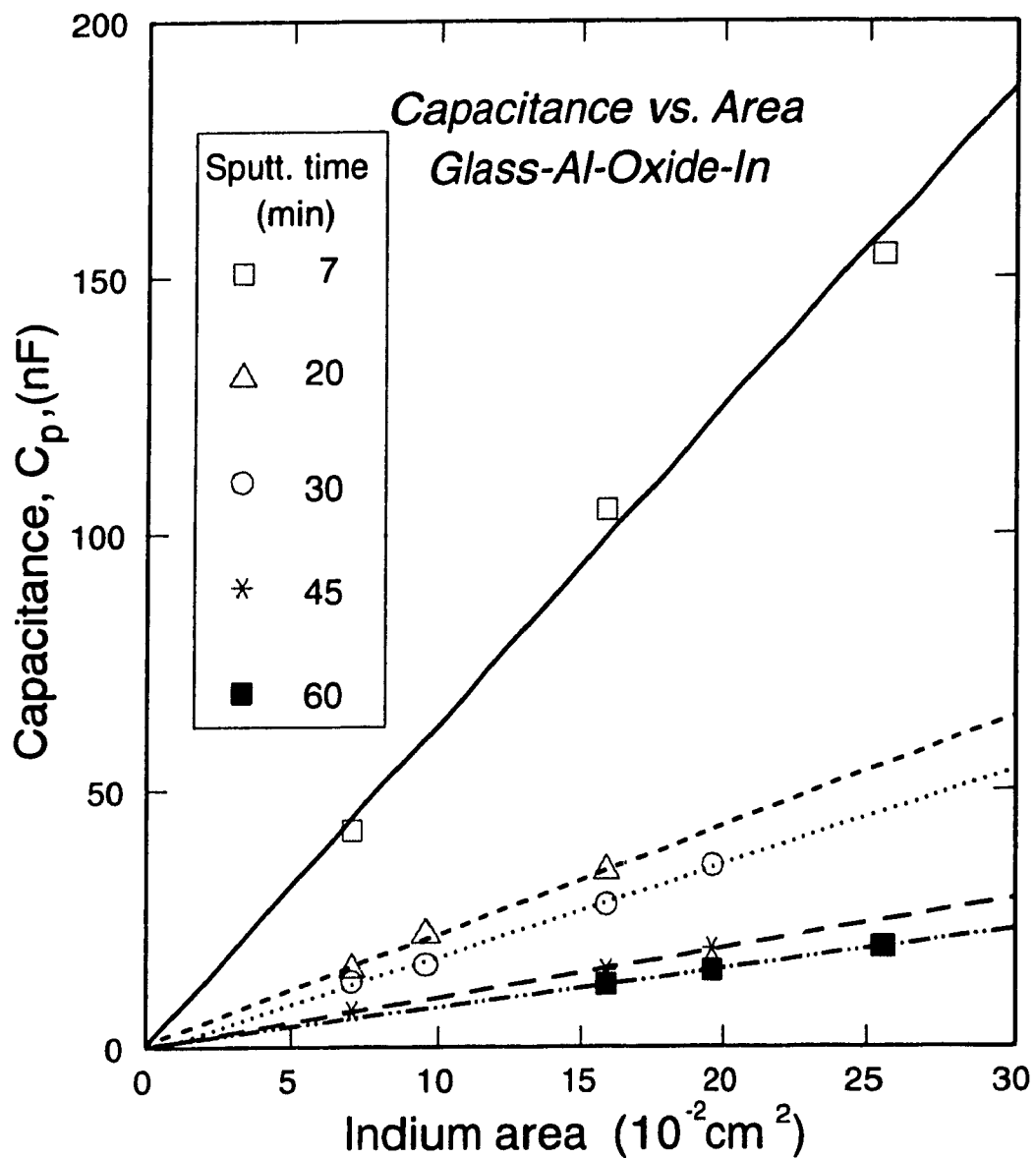


Fig 4.8 Plot of measured parallel capacitance against indium contact area for 5 samples, where r.f. sputtering was used to form the oxide layers.

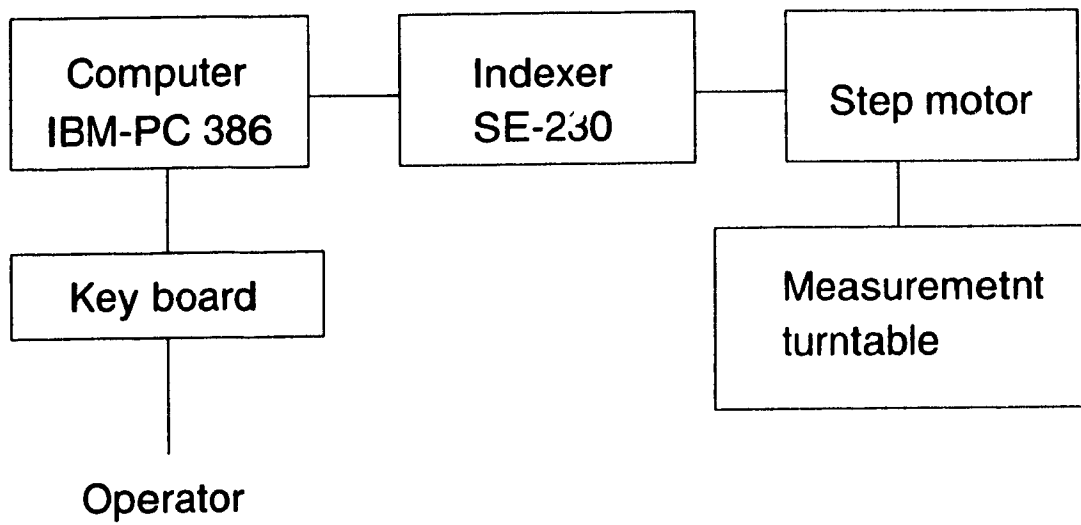


Fig 4.9 Block diagram of the step motor control system.

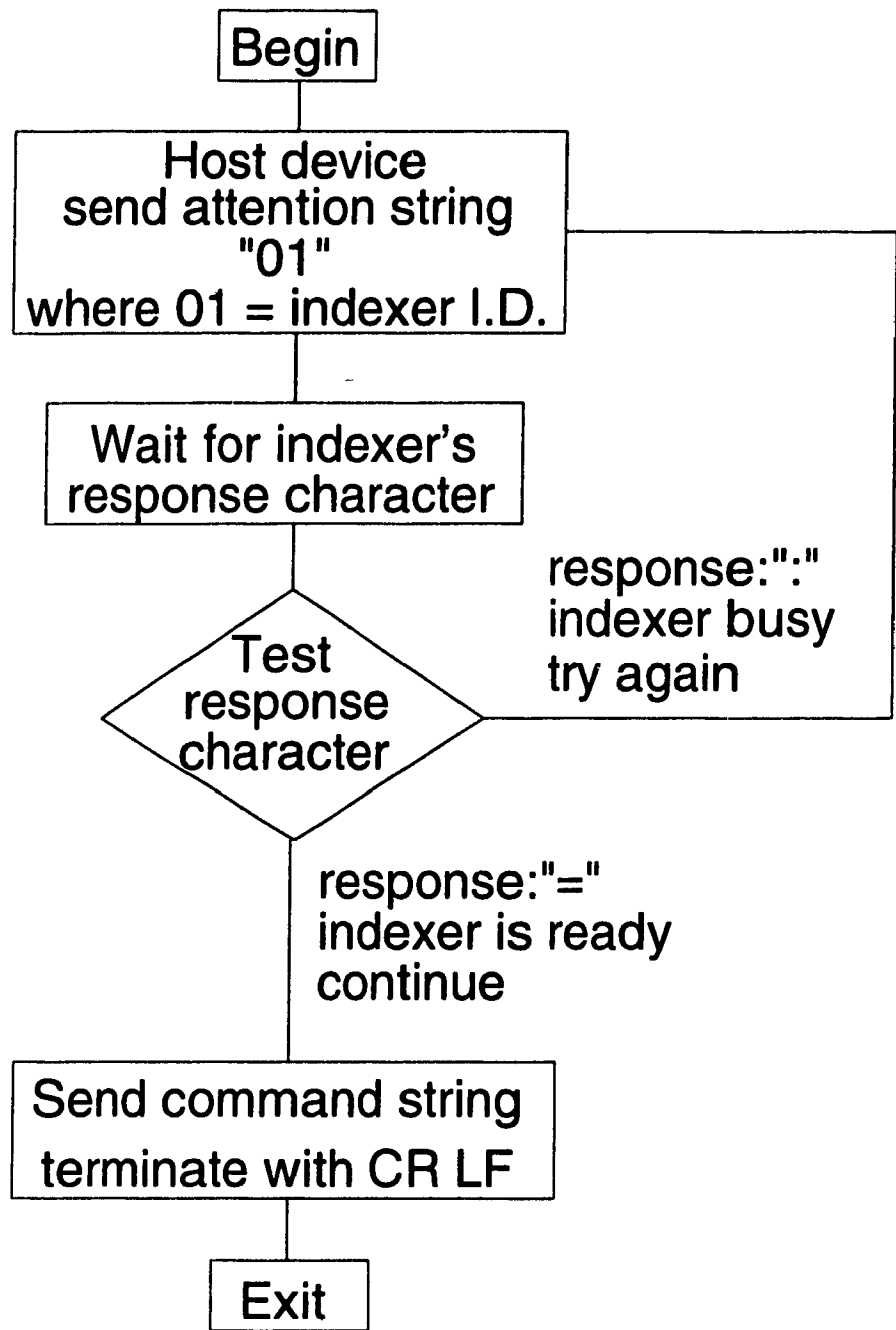


Fig 4.10 Measurement control sequence

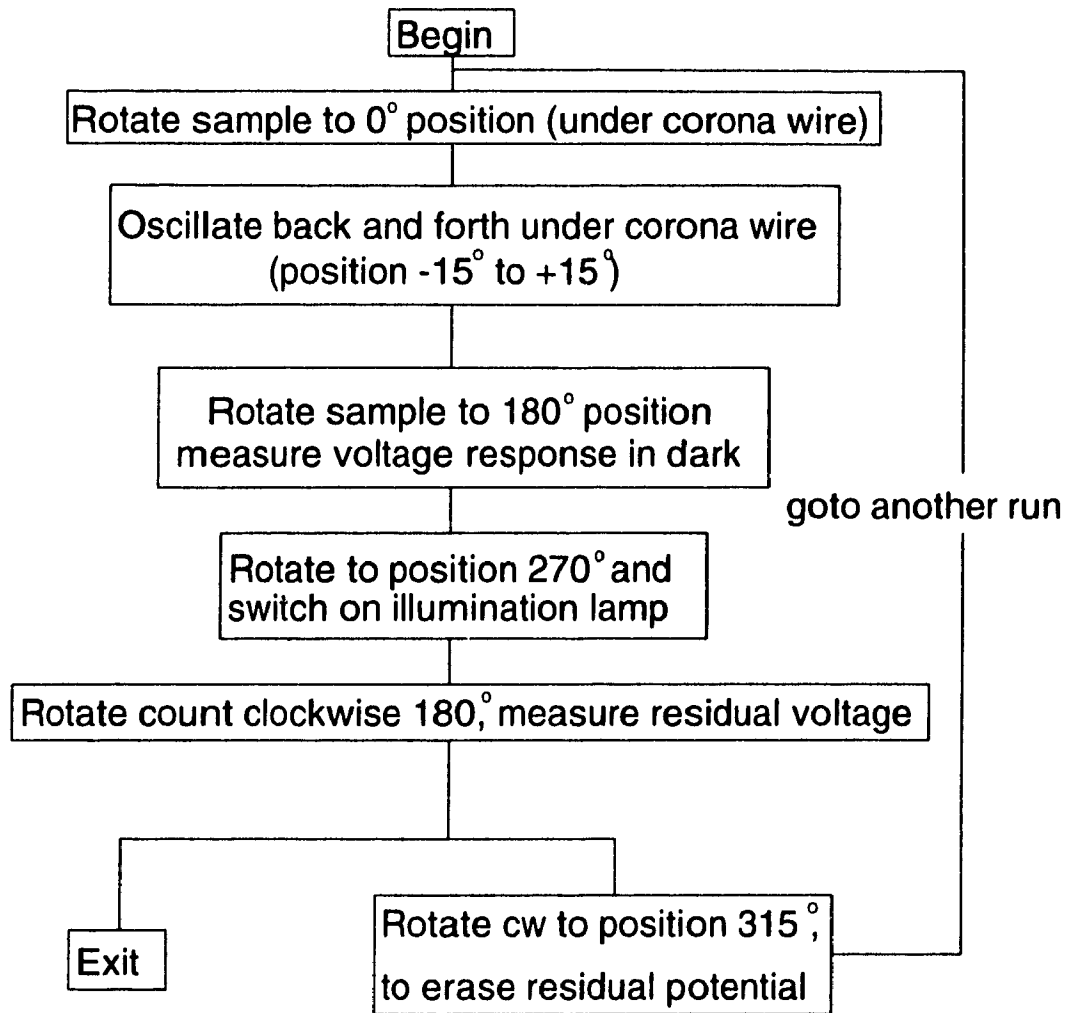


Fig 4.11 Procedure of automatic measurements.

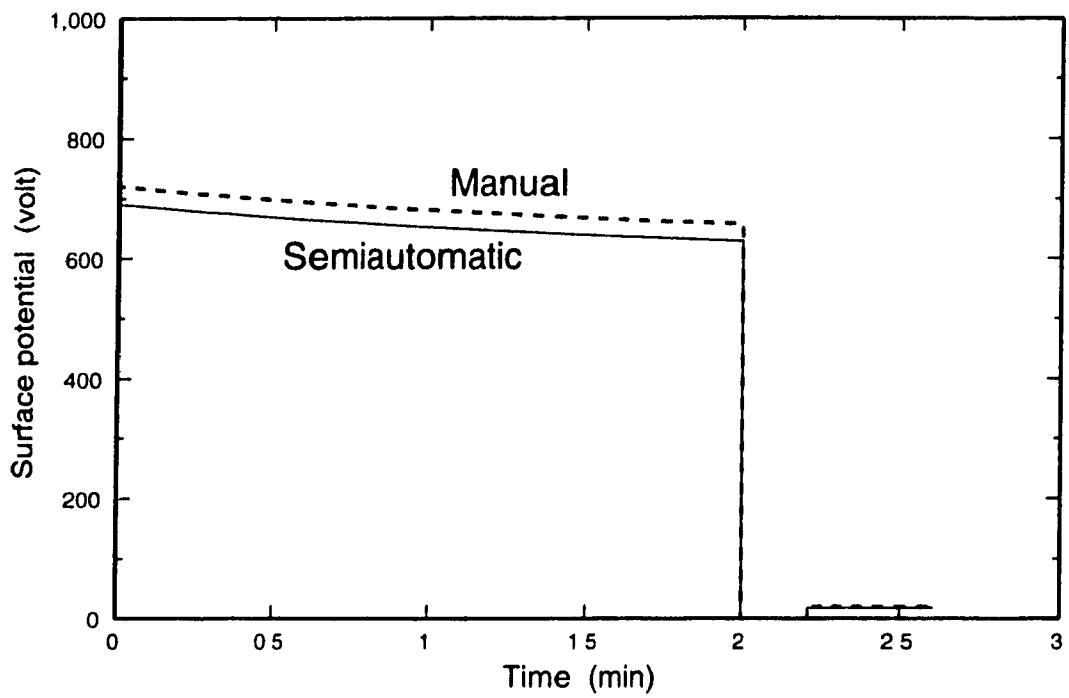


Fig 4.12 Plot of decay of surface potential with time in darkness using manual and semiautomatic measurements

Chapter 5

XEROGRAPHIC RESULTS OF CHLORINE-DOPED SELENIUM

5.1 Introduction

As described in chapter 3, samples were prepared with selenium doped with five different concentrations of chlorine up to about 100ppm. On these samples plus a nominally undoped sample (see Table 5-1), the xerographic measurements described in chapter 4 were carried out and the results are presented in detail in this chapter. In all the plots, the chlorine concentrations reported are those determined by chemical analysis (and not the nominal values from the initial preparations).

The measurements were carried out in 3 sections, the first as single cycles of charge, dark-decay, light-exposure, and the second as measurements after many repeated cycles and the third as single cycle readings after exposure of a sample to strong illumination.

5.2 Results of Single Cycle Xerographic Measurements

(a) Acceptance voltage

A plot of acceptance voltage V_A (saturated value as described in section 4.4) against chlorine concentration is shown in Fig 5.1

for three values of voltage V_{PS} of the d.c. power supply creating the charging corona. It is seen that for constant V_{PS} , V_A decreased with increase of chlorine content, with a rapid fall near 100 ppm. For a fixed chlorine concentration, V_A increased with V_{PS} but it was found that below a V_{PS} value of about 5kV, no charging took place.

(b) Dark decay rate

Fig 5.2 shows plots of dark decay rate (as defined in chapter 4) against chlorine concentration for 6 different values of acceptance voltage. It is noted that the dark decay rate increased with chlorine concentration, and at higher concentration (65ppm), increased also with acceptance voltage.

The same data were replotted in Fig 5.3 to show the dark decay rate against the acceptance voltage for 5 samples with different chlorine concentrations. It may be noted that for all the samples, except that doped with 65 ppm, the dark decay rate was almost unchanged with increasing acceptance voltage up to about 1.3 kV. However, above this value, the dark decay rate increased rapidly like a breakdown effect. For the sample doped with 65 ppm Cl, the dark decay rate increased with the acceptance voltage in the range 400 to 950 volts.

(c) Residual voltage

A plot of residual voltage V_r (defined in chapter 4) against chlorine concentration is shown in Fig 5.4 for different V_A values. It is clearly shown that the residual voltage decreased strongly

with increase of the chlorine, especially up to about 1.5 ppm. With lower V_A , this tendency was even stronger. For example, V_r at 6 ppm was 0.2 volt for 400 volts of V_A but 2 volt for 1400 volts of V_A ; that is an order of magnitude increase in V_r for a 3.5-fold increase in V_A .

In Fig 5.5, a plot of residual voltage against acceptance voltage V_A is shown, where the five sets of data correspond to the 5 samples with different chlorine concentrations. It is noted that the residual voltage increased with the increase of the acceptance voltage, particularly at the higher chlorine levels. Thus, for the 0.7 ppm chlorine sample, V_r increased only slightly.

5.3 Results of Cycled Xerographic Measurements

The procedure for taking cycled measurements was described in detail in chapter 4, but is briefly described again here for convenience. Essentially, the sample was placed on the rotating measurement plate with the high d.c. power supply kept at a charging voltage of 6 kV to charge up the selenium layer. When the acceptance voltage V_A reached its saturated value, the surface potential was measured in darkness for 2 minutes during the decay process. After this, an 8-watt tungsten lamp was turned on for 30 seconds (corresponding to 2 seconds of direct illumination on the sample during the rotation), following which, measurements of residual voltage were made for a period of 1 minute. After taking the residual voltage measurements, the sample was illuminated from a stronger tungsten lamp (40 watt) for 20 seconds (corresponding to 1.3 seconds of direct illumination during the rotation) to erase

the residual charge. This cycle of measurement was then repeated for a total of 30 times. After this, a series of more rapid cycles was made without taking surface potential measurements. Each cycle, lasting only 10 seconds, consisted of dark charging up and illumination with only 4 seconds for the dark decay period. This was done for 300 of these rapid cycles, after which, another 10 regular cycles were made with voltage measurements.

(a) Residual voltage

Fig 5.6 shows residual voltage against number of cycles for four different samples with 0.7, 1.4, 6.0 and 65 ppm chlorine. For the first two samples with low chlorine content, it is seen that the residual voltage only slightly increased with the number of cycles. For the 6ppm sample, V_r increased significantly in the first 10 cycles and reached a saturated value after this. For the last sample, 65ppm, V_r was almost constant, with only a slight decrease. For all the samples, the cycled-up residual voltage after the 300 rapid cycles was not significantly different from the value immediately prior to this fatigue treatment.

Some of the data from Fig 5.6 are also shown in Fig 5.7 to indicate the relation between the residual voltage and chlorine concentration for the initial (V_r) and the cycled-up ($V_{r\infty}$) values. It is clear that both V_r and $V_{r\infty}$ decreased with increase of chlorine content in the selenium. At low chlorine content, $V_{r\infty}$ was greater than V_r , but at higher concentration, $V_{r\infty}$ was the smaller.

(b) Dark decay rate

Dark decay rate against number of cycles is also plotted in Fig 5.8 for these same four samples. It is noted that the dark decay rate for the 6 ppm sample was essentially unchanged with increase in the number of cycles, while the 65 ppm sample showed a slight decrease. The dark decay rate for the 1.4 ppm sample dropped rapidly during the first three cycles and then became essentially constant, while the dark decay for the 0.7 ppm sample showed a slight overall increase. In the case of 300 rapid cycle treatment, the dark decay rate, like the residual voltage, showed no significant change.

Fig 5.9 shows the initial and saturated (cycled-up) dark decay rates versus chlorine concentration. Apart from a small initial decrease in the cycled-up value, both quantities increased with added chlorine in the selenium.

5.4 Results of Strong Initial Illumination

A study of the effect of strong illumination on xerographic properties was carried out in the laboratory. Xerographic measurements were made on a pure selenium sample (with a chemically determined chlorine concentration of 0.7 ppm), by first subjecting it to strong illumination from a 40-watt tungsten lamp for 24 hours. After this, xerographic measurements were repeated at different intervals in darkness.

Plots of dark decay rate and residual voltage against time

after strong illumination are shown in Fig 5.10, where it is first noted that both quantities were increased initially by factor of about 3 over the values measured prior to the strong illumination. Thereafter, they decreased monotonically, eventually approaching nearly constant values with the dark decay rate reaching 13% after about 300 minutes (5 hours). The residual voltage decreased at a lower rate, starting at about 30 volts and decreasing to half this value after 3,000 minutes (2.1 days), which was still higher than the value (20V) before the strong illumination.

5.5 Discussion

For a fixed concentration of chlorine in the selenium, Fig 5.1 shows that the acceptance voltage V_A increases with V_{PS} , the corotron power supply voltage. This is because the value of V_A results from an equilibrium in the process of charging and discharging, so that if the latter is fixed, then increasing the charging rate by increasing the corona voltage V_{PS} results in an increase of V_A . The decrease of V_A with increasing chlorine content is consistent with the results in Fig 5.2 showing an increase of dark decay with increase in chlorine level in the selenium. This is due to an increase in the "discharging" rate with increased chlorine in the equilibrium process to establish V_A . For the depletion discharge model, "discharge" means charge redistribution rather than actual charge loss.

It might be thought that the higher V_A , the higher the dark decay rate should be, (in an analogy with Newton's law of cooling). However, Fig 5.3 shows this not to be the case, since, for the most

part, the dark decay rate was independent of acceptance voltage, although the 65 ppm sample was an exception. The rapid rise of the dark decay rate at a V_A value of about 1.3 kV must represent breakdown, since with a selenium thickness of 50 μm , the electric field across the selenium at this voltage amounts to about 2.6×10^5 volt/cm, a very high field.

Fig 5.4 shows that chlorine is very effective in reducing residual voltage. For example, the presence of only about 1.4 ppm of chlorine brings V_r down by about an order of magnitude. At the same time, Fig 5.2 indicates that this amount only caused the dark decay rate to double.

Using the Warter relation $V_r = L^2 / (2\mu\tau_c)$ (equation 2.27), $\mu\tau_c$ products were calculated from the V_r values and these are given in Table 5-1. It is noted that $\mu\tau_c$ values increased by about an order of magnitude in increasing the chlorine content from 0.7 to 65 ppm. Fig 5.5 showing that V_r increases with V_A , is replotted in Fig 5.11 on double logarithmic scales. For low chlorine content the dependence is sublinear and for high content superlinear, approaching a V_A^2 dependence. Such an increase of V_r with V_A implies, from the Warter relation, a strong reduction in the values of $\mu\tau_c$ with increasing V_A .

The cycled up values of residual voltage $V_{r\infty}$ from Fig 5.6 would be expected to be independent of V_A , but this has not been checked experimentally. Using equation (2.28) $N_t = 2\epsilon_0\epsilon V_{r\infty} / (eL^4)$, values were found for N_t , the concentration of charged traps, which

are listed also in Table 5-1. As seen, N_t decreased by more than an order of magnitude as the chlorine content was increased. Thus the chlorine acts to reduce the concentration of trapping centres in the selenium, leading to an increase in the free time τ_c of the holes before capture.

Table 5-1

Sample Number	Meas. Cl conc. in Se Source (ppm)	N_t from $V_{r\infty}$ (at $V_A=1000$ V) (10^{12}cm^{-3})	$\mu\tau_c$ from V_r (at $V_A=1000$ V) (cm^2/volt)
X25	0.7	6.2	7.8×10^{-7}
X36	1.2	--	--
X28	1.4	4.5	1.6×10^{-6}
X32	6	0.86	8.3×10^{-6}
X31	65	0.23	8.9×10^{-6}
X34	95	Not measurable at $V_A=1000$ V	

The reduction of V_r with increased chlorine and decreased V_A means that the contrast ratio, if defined as V_A/V_r , is improved using a high chlorine content with a low acceptance voltage. For example, the ratio for the 65 ppm sample at a V_A of 400V is 2000, but for the 0.7ppm sample at a V_A of 1400, it is only 70.

Fig 5.8 shows that charge-discharge cycling leads to a slightly higher cycled-up dark decay rate for low Cl-doped selenium but a slightly lower value for high Cl-doped material. Thus, practically speaking, the addition of chlorine has no detrimental effect on the cycling-up dark decay rate.

The results in Fig 5.10 confirm that strong illumination is detrimental xerographically in temporarily increasing both dark decay rate and residual voltage. It is seen that it would take almost a week of subsequent storage in darkness for the residual voltage to recover to its pre-illumination value.

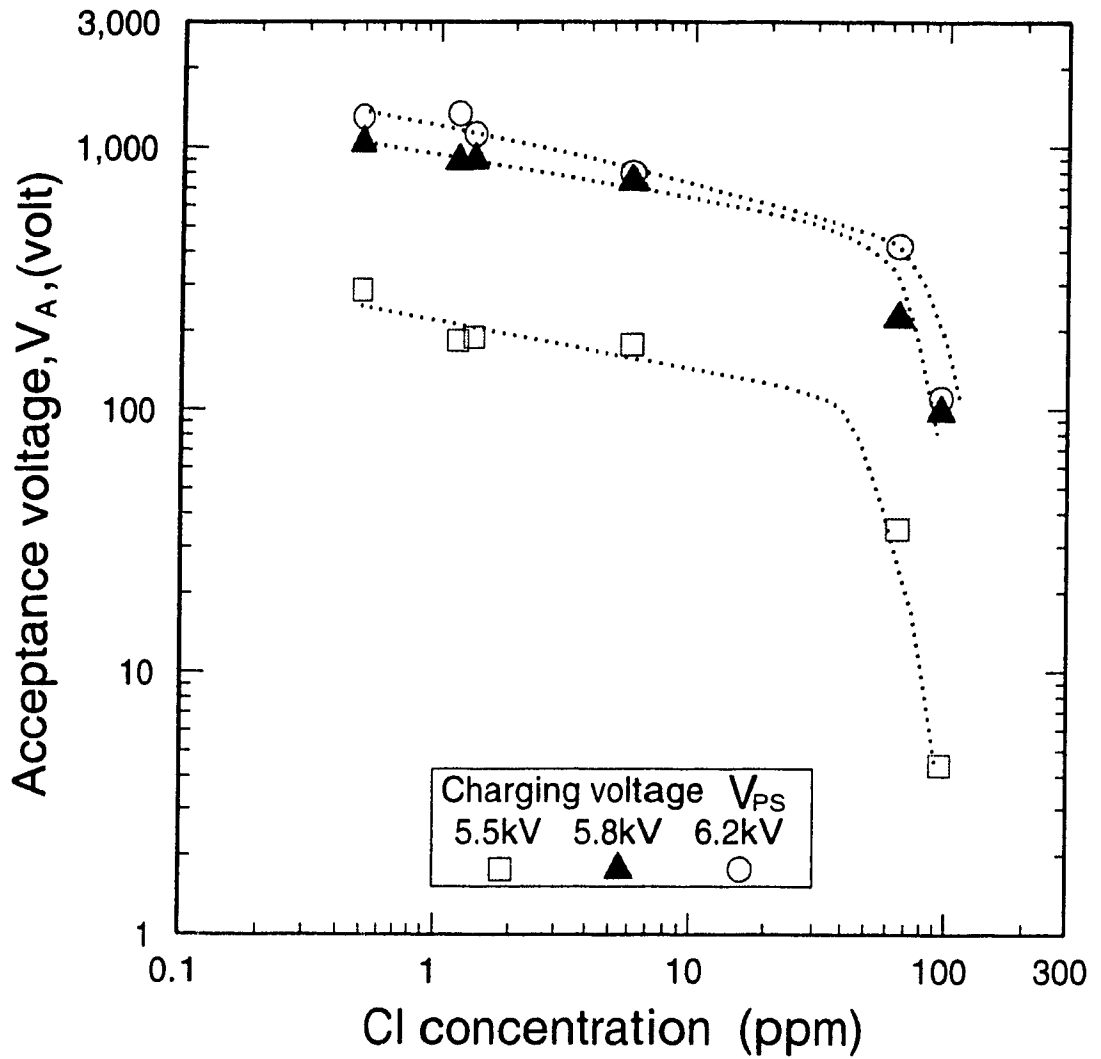


Fig 5.1 Plot of acceptance voltage against chlorine concentration in the selenium for 3 different charging voltages of the corotron power supply.

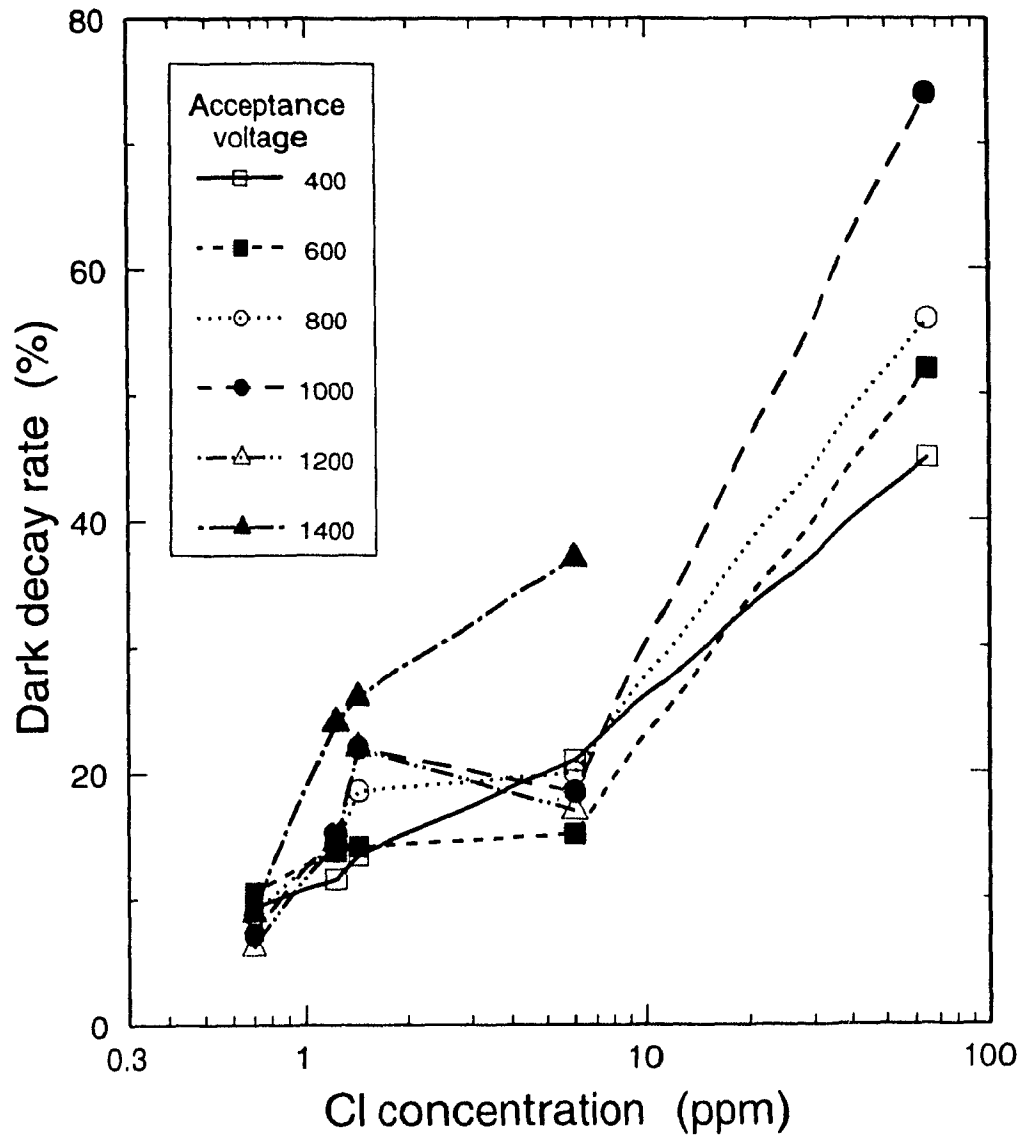


Fig 5.2 Plot of dark decay rate against chlorine concentration in the selenium for 6 different acceptance voltages.

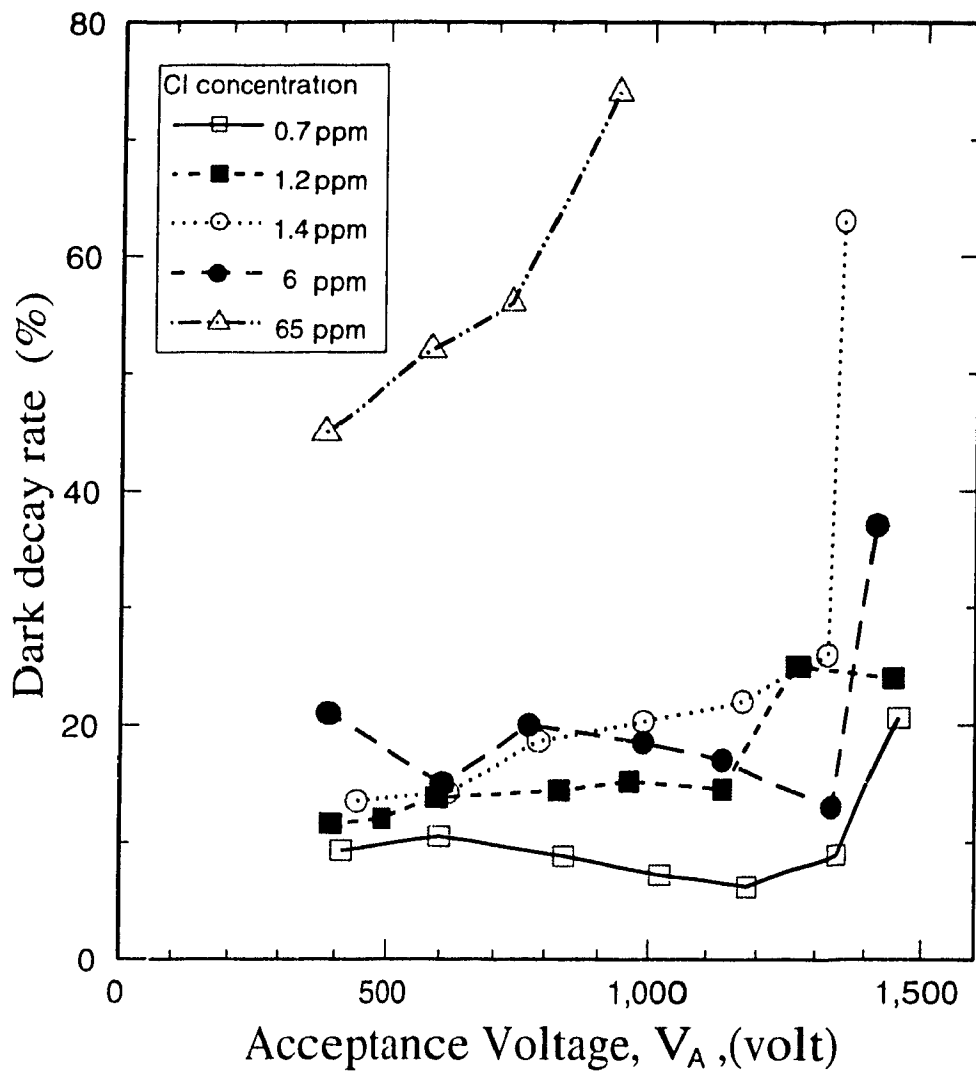


Fig 5.3 Plot of dark decay rate against acceptance voltage for samples with different chlorine concentrations in the selenium.

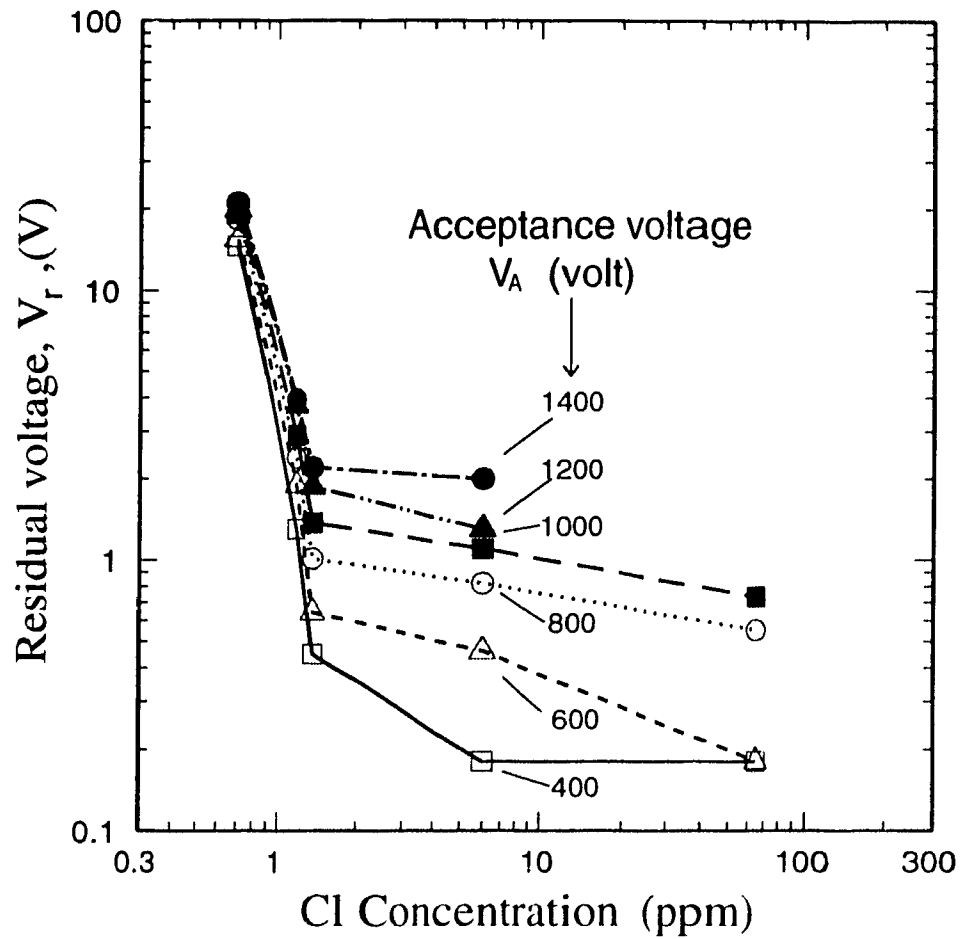


Fig 5.4 Plot of residual voltage against chlorine concentration in the seleniun for 6 different acceptance voltages.

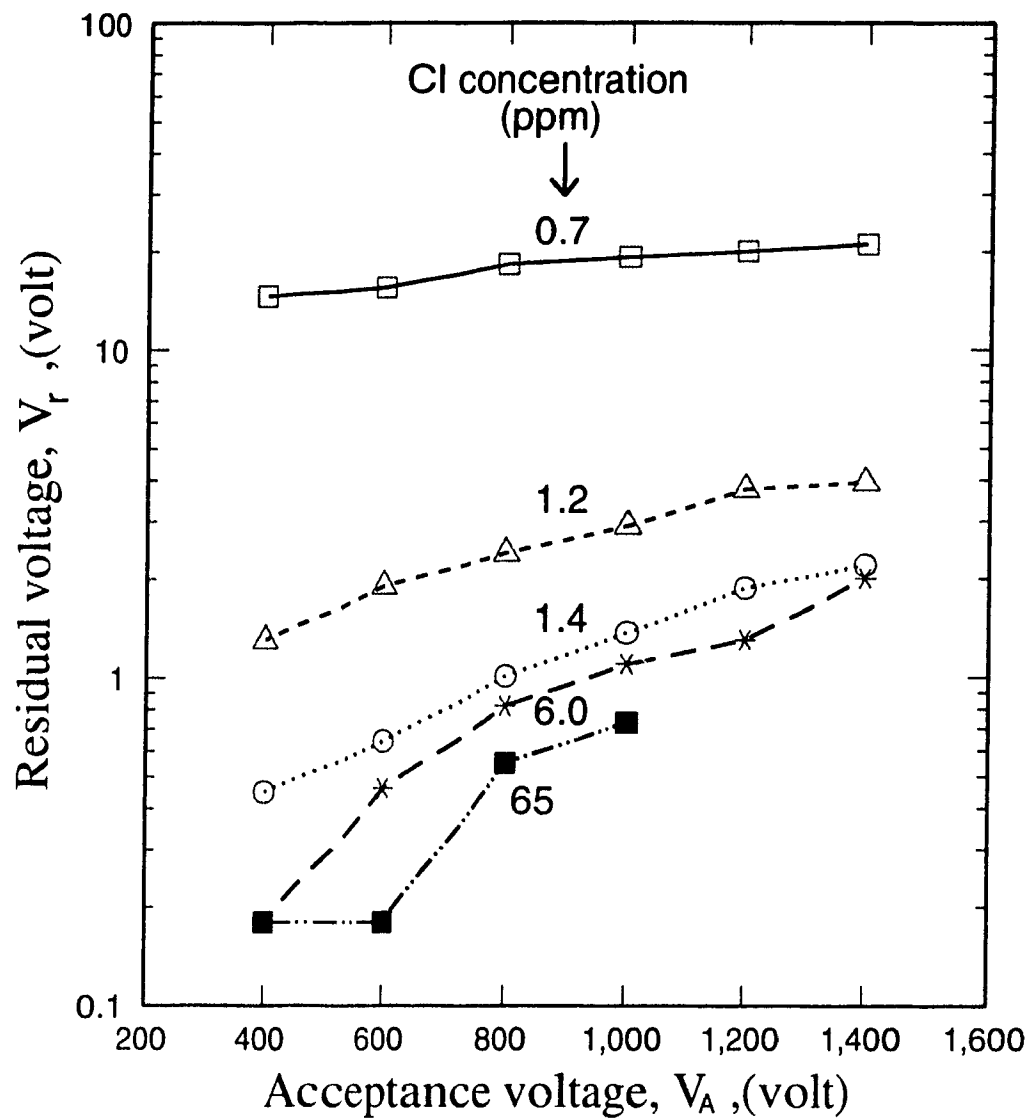


Fig 5.5 Plot of residual voltage against acceptance voltage for 6 different chlorine concentrations in the selenium.

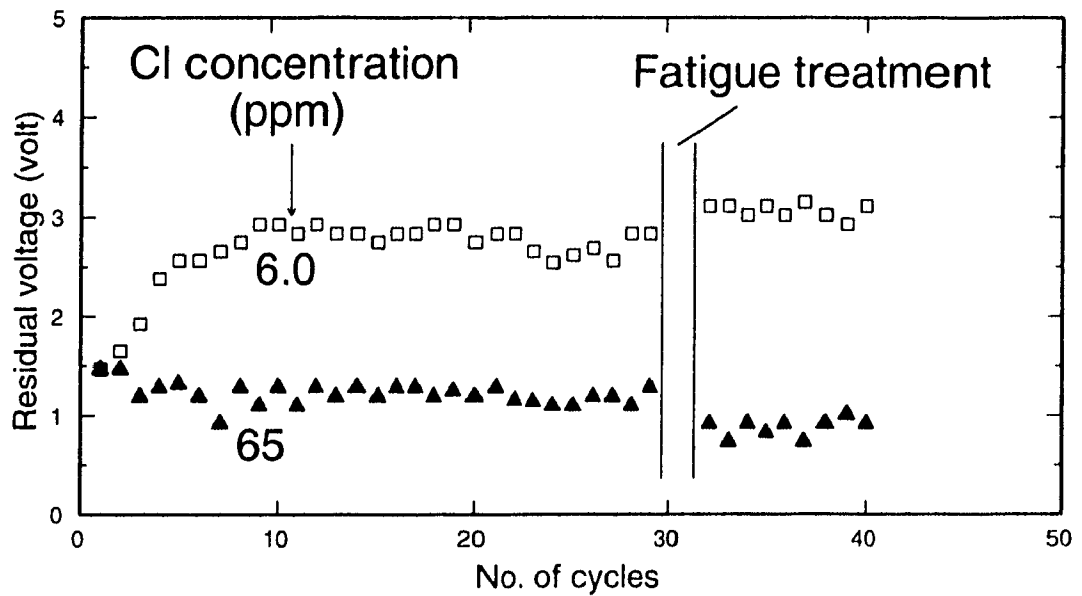
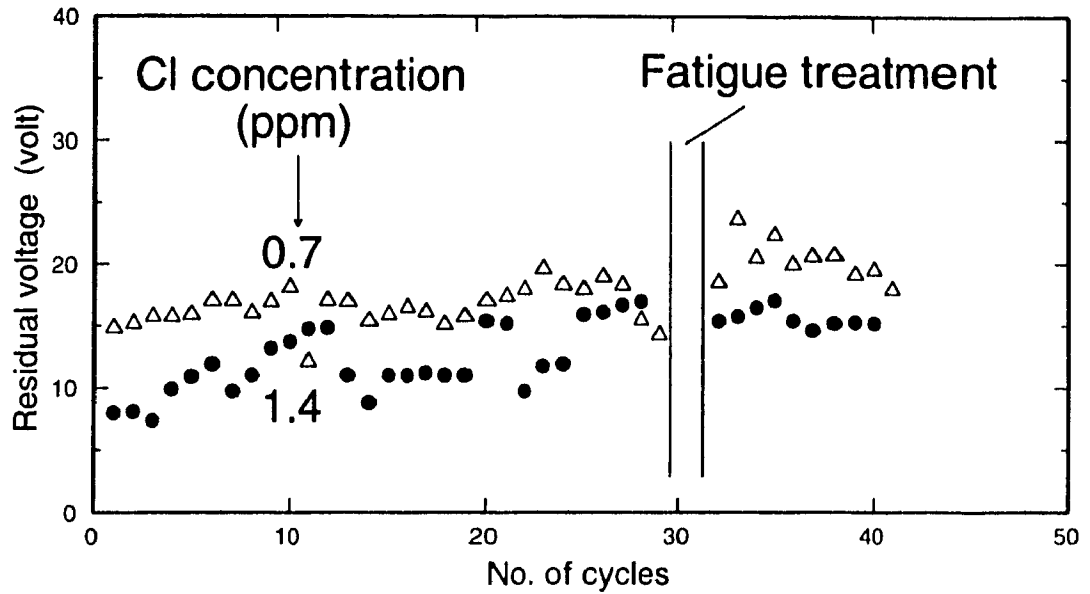


Fig 5.6 Plots of residual voltage against number of charging-decay-measurement cycles for samples with different chlorine concentrations in the selenium.

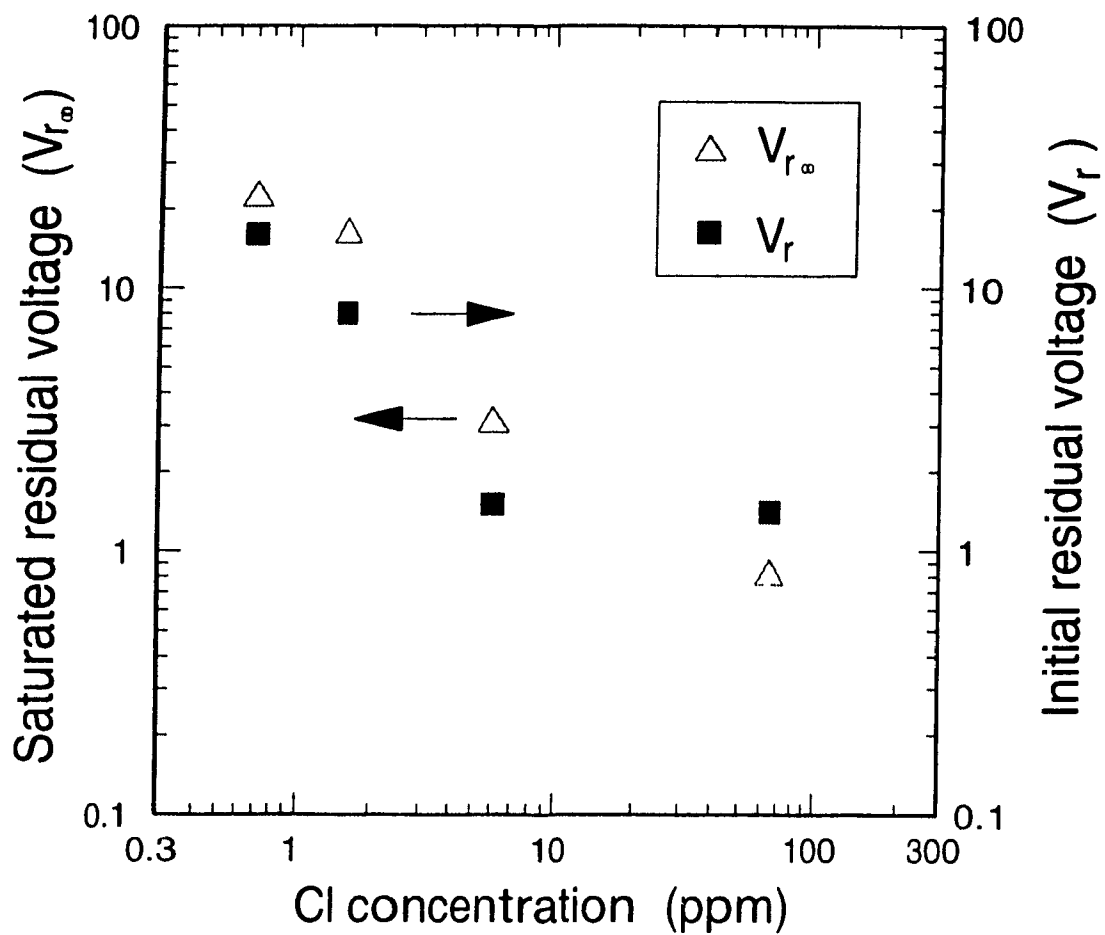


Fig 5.7 Plot of initial residual voltage V_r and saturated (i.e. cycled up) residual voltage V_{r_∞} against chlorine concentration in the selenium.

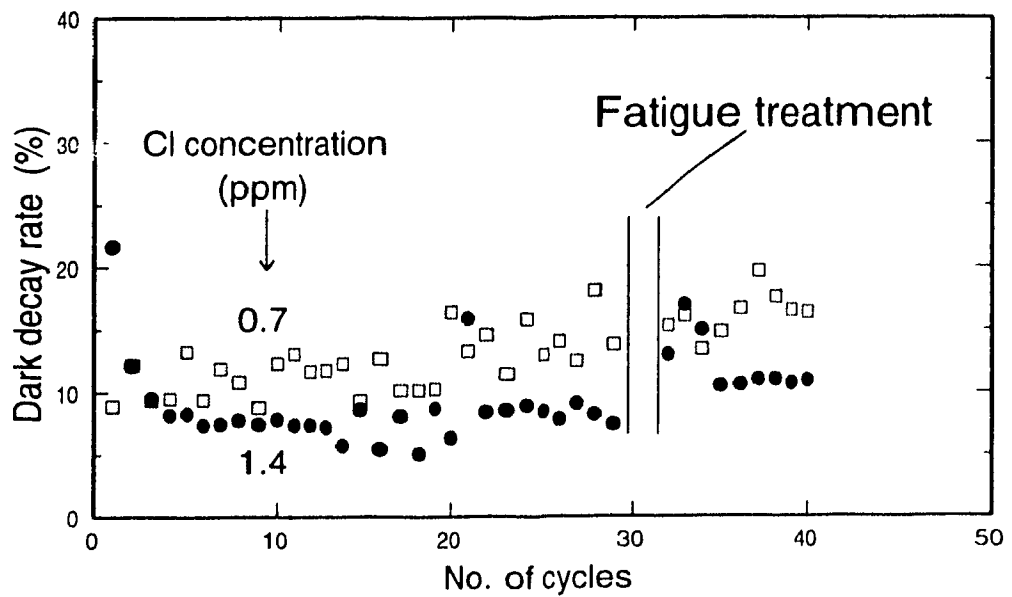
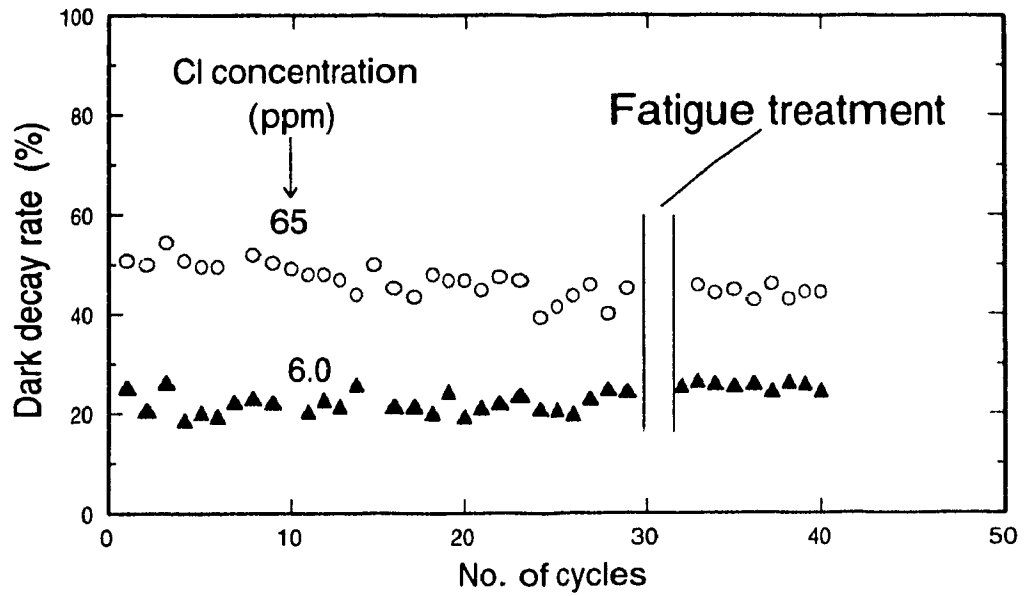


Fig 5.8 Plots of dark decay rate against number of charging-decay-measurement cycles for samples with different chlorine concentrations in the selenium.

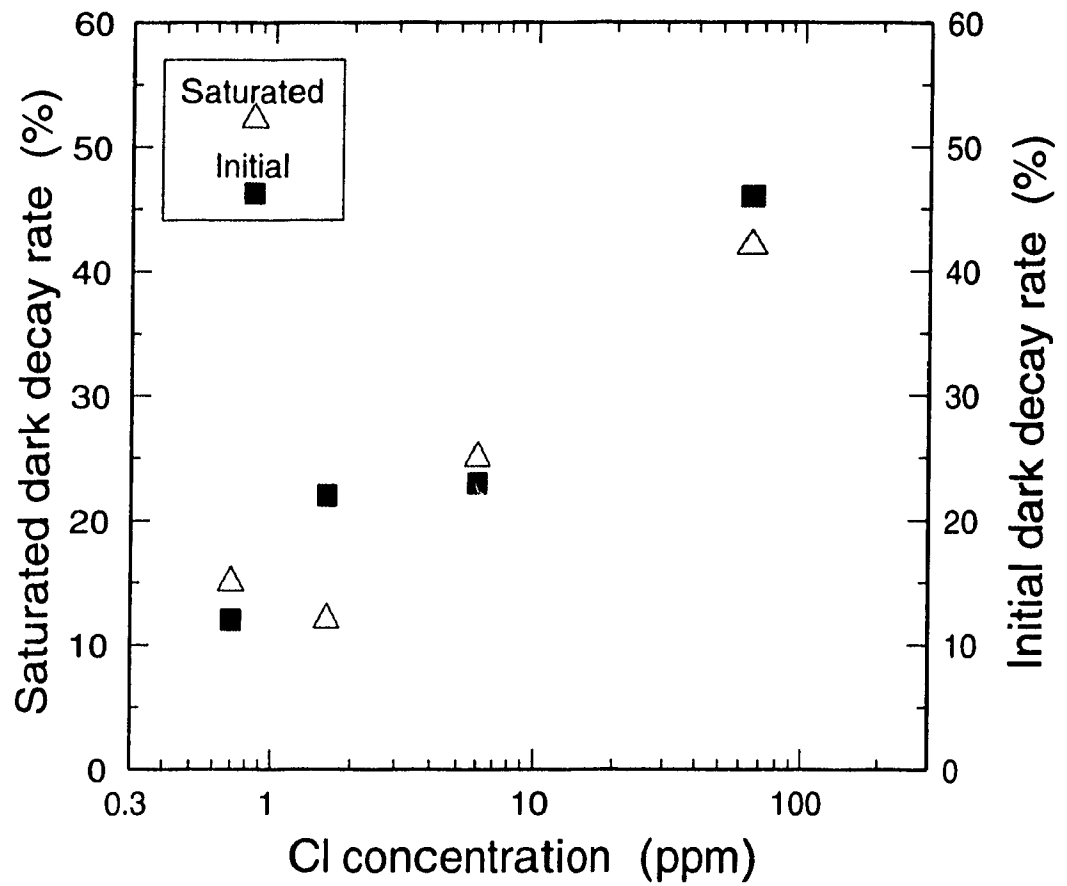


Fig 5.9 Plot of saturated dark decay rate and initial dark decay rate against chlorine concentration in the selenium.

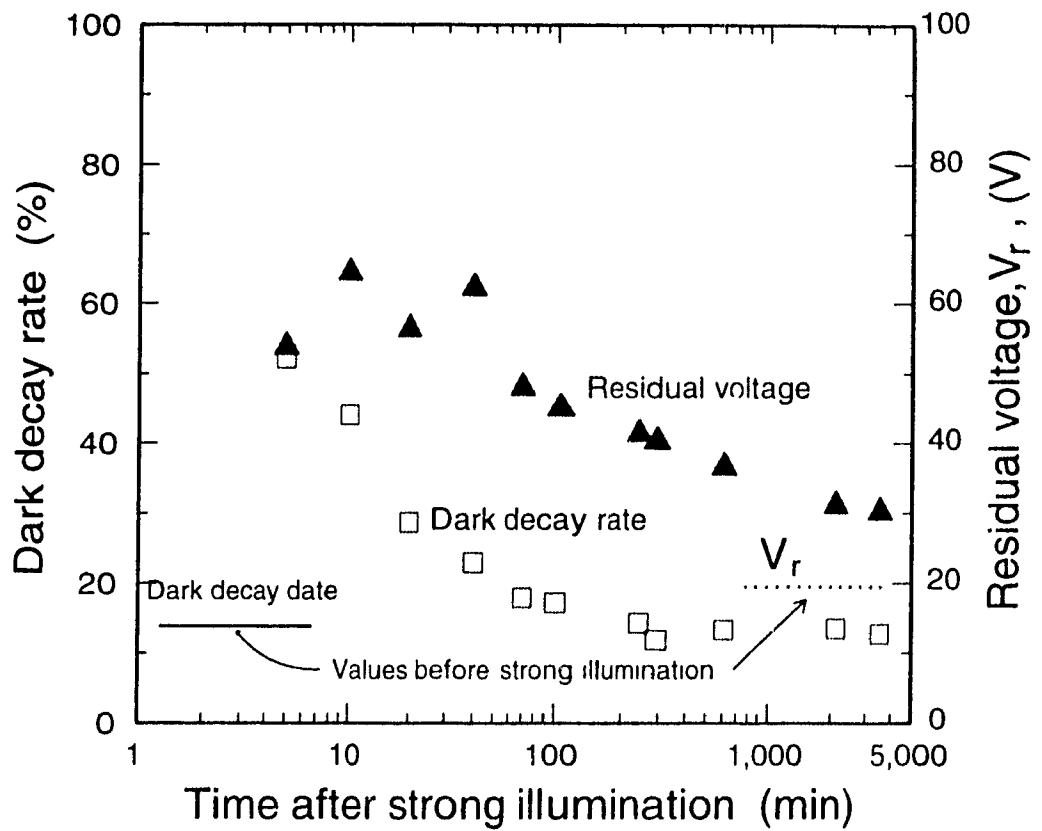


Fig 5.10 Plot of dark decay rate and first residual voltage against time after strong illumination for an undoped selenium sample (0.7 ppm chlorine).

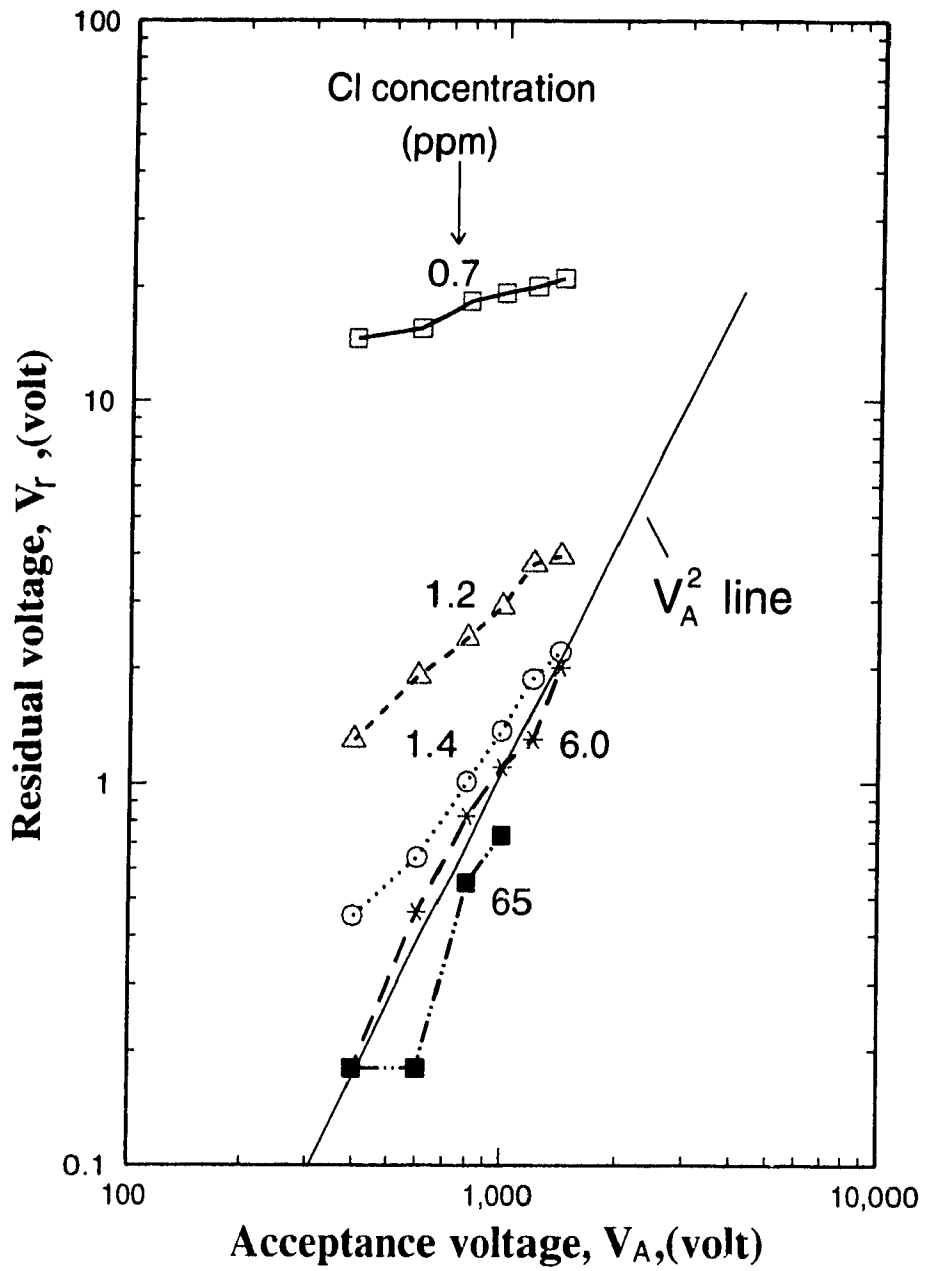


Fig 5.11 Replot of Fig 5.5 using double logarithmic scales, with a comparison to a V_A^2 dependence.

Chapter 6

DARK DECAY TIME GRADIENT MEASUREMENT

6.1 Introduction

As mentioned earlier in chapter 2, various workers have found that in chlorine-doped chalcogenide photoreceptors, the dark decay is determined predominantly by the depletion discharge of deep-lying centres in the material. This is readily shown up in plot of dV/dt versus dark decay time t , as described in chapter 2. Accordingly, the present chapter is devoted to such plots from the experimental results on amorphous selenium. The effect of chlorine content and charging voltage is specifically studied on the six xerographic samples listed in Table 5.1.

6.2 Effect of Chlorine Content

Double logarithmic plots of dV/dt against time are shown in Figs 6.1 and 6.2 for the six samples with average initial voltages of $V_1=123\pm 30$ volts and 281 ± 35 volts respectively. Except for the 95 ppm sample in Fig 6.1 and the 0.7 ppm (nominally undoped) sample in both figures, there is a clear slope change as the dark decay time increases for all the samples. There is also a clear general increase in the initial magnitude of dV/dt with increasing chlorine

content, which is consistent with the previously reported increase in the differently-defined dark decay rate in Fig 5.2. By drawing tangents to the curves, the time to the break-point or kink can be found to represent the depletion time t_d (section 2.2). Comparison of Figs 6.1 and 6.2 shows that such t_d values, at each chlorine level, are larger in Fig 6.2 than those in Fig 6.1, arising from the higher V_1 value.

Fig 6.3 shows a plot of depletion time t_d versus the chlorine content of the selenium samples, for the two V_1 values of 281 and 123 volts, corresponding to electric fields of 5.6 and 2.5 V/ μm respectively. It is seen that the depletion time decreased essentially linearly, on the double logarithmic scales, with increase of chlorine content. Extrapolated results from Abkowitz, Jansen and Melnyk [3], also shown in Fig 6.3, with an electric field of 5 V/ μm , are generally consistent with the present results.

6.3 Effect of Initial Voltage

Plots of dV/dt against time were measured with variation of the initial voltage for samples with fixed chlorine levels of 0.7 ppm (nominally undoped), 6 ppm and 65 ppm. These are shown in Figs 6.4, 6.5 and 6.6. For the 0.7 ppm sample, with initial voltages ranging from 99 to 1280 volts in Fig 6.4, it may be noted that larger voltage slope values were found with increasing V_1 . However, in the variation of dV/dt with time, no "kink point" could be clearly observed. The dV/dt versus time plots in Figs 6.5 and 6.6 for the 6 and 65 ppm samples respectively are similar to each

other, except that the voltage range was smaller for the higher doped sample. Separation into two time regions, with different slopes, is clearly apparent here. In the first time zone, the curves are nearly coincident with almost a small common slope. The depletion time t_d , representing the starting time of the second slope, clearly increased with increase of V_1 .

6.4 Effect of Absence of Oxide Blocking Layer

The two time zone behaviour of the chlorine-doped samples, such as that for the 65 ppm sample in Fig 6.6, is taken to be due to depletion discharge, with injection of electrons from the substrate either absent or playing a minor role. To check this, a sample was prepared with the selenium doped with 65 ppm of chlorine but deposited on the aluminum substrate without the usual sputtered aluminum oxide layer. Measurements of dV/dt against t for this sample were carried out and the result is shown in Fig 6.7. The curves for this sample show no discernible kink points and the character of the variation is seen to be quite different from that of Fig 6.6. This is brought out more clearly in Fig 6.8, where curves from the two samples are compared at similar values of V_1 . For example, at the approximate 300 volts level of V_1 , the value of dV/dt for the no-oxide sample starts at a higher value than that of the sample with an oxide layer, soon crosses below it and finally has a lower slope. The same trend is apparent for the curve of the no oxide sample at the lower V_1 value of about 120 V.

6.5 Analysis of Results

(a) Plots of dV/dt versus t

(i) Effect of chlorine

Fig 6.9 shows a dV/dt versus t plot for the 65 ppm chlorine doped sample, representing measurements over a longer dark decay time than in Fig 6.6 to more than 200 seconds with an initial voltage of 308 volt. The broken line shows the dependence expected from equations (2.13) and (2.15) of chapter 2 with the parameters $a=6.9 \times 10^{-7} \text{ C cm}^{-3}\text{sec}^{-p}$ and $p=0.95$. However, it is clearly seen that this line does not fit the trend of the experimental points. Accordingly, equations (2.20a) and (2.21a) were invoked, involving the modified charge density time dependence of equation (2.18). The solid line, so obtained in Fig 6.9, corresponding to the parameters $p=0.95$, $V_x=950$ volts and $\tau=25$ sec, appears to fit the experimental points well in both time zones. From the relation $V_x = \rho_o L^2 / (\epsilon_o \epsilon_r)$, the ultimate charge density ρ_o was calculated with $L=50 \mu\text{m}$ and $\epsilon_r=6.5$ to yield $2.2 \times 10^{-5} \text{ coulomb/cm}^3$. This corresponds to an ultimate surface voltage of $V_{oo} = V_1^2 / (2V_x) = 49.9 \text{ V}$ and a space charge thickness of $z_{oo} = \sigma / \rho_o = \epsilon_o \epsilon_r V_1 / (L \rho_o) = L(V_1 / V_x) = 16.2 \mu\text{m}$.

Fig 6.10 shows a similar fit, with equations (2.20a) and (2.21a), to results on the 6 ppm chlorine doped sample with an initial voltage of $V_1=158$ volt. The fit for the dV/dt versus t plot, corresponding to the parameters $p=0.98$, $V_x=980$ volt and $\tau=51$ sec, is reasonable. The corresponding values of ρ_o , V_{oo} and z_{oo} are

2.3×10^{-5} coulomb/cm³, 12.7 V and 8.06 μm respectively. Shown also in Fig 6.10 are experimental points of dV/dt versus dark voltage V and an attempted curve calculated with equations (2.25a) and (2.26a) using the same parameters as those employed for the dV/dt versus t plot. It is seen that the calculated line lies slightly under the experimental points but shows the shape satisfactorily.

(ii) Effect of V_1

The dispersion of the dV/dt versus t curves with different V_1 values after the kink is quite evident in Figs 6.5 and 6.6. For the most part, this arises from the V_1^2 term in equation (2.21a). However, this alone does not quite explain the shape of the post-kink curves, particularly for the 6 ppm sample in Fig 6.5. Therefore, consideration is given to the possibility of a slight loss of surface charge σ with time. For simplicity, it is supposed that this loss can be taken into account using a linear relation of the form

$$\sigma = \sigma_0(1-Kt) \quad , \quad (2.22)$$

where K is a constant with dimensions of (time)⁻¹. Fig 6.11 shows again the experimental points of Fig 6.5 with curves calculated for four V_1 values, using equations (2.20b) and (2.21b), which include a term arising from equation (2.22) and $K=5 \times 10^{-4}$ sec⁻¹. It is seen that the curves follow the trend of the experimental points well. Fig 6.12 shows a repeat of the experimental points of Fig 6.6 with 6 curves calculated in a similar way but with $K=0$ (ie no loss of surface charge). Again the curves follow satisfactorily the trend of the experimental points.

(b) Plots of t_d versus $2V_d$

Figs 6.13 and 6.14 show double logarithmic plots of depletion time t_d against $2V_d$ for the 6 and 65 ppm samples respectively. According to equation (2.16), a line drawn through the experimental points on this plot should be a straight line of slope $1/p$ but, in fact, the trend of the $2V_d$ experimental points is a curve, rather than a straight line. If equation (2.23) is invoked with the parameters from the corresponding fits of Figs 6.9 and 6.10 applied respectively to Figs 6.13 and 6.14, the resulting calculated lines are those shown as the broken lines. These have a similar shape but differ in position from the experimental points. However, if new parameters are chosen, it is possible to fit the observed results, as shown by the solid lines in Figs 6.13 and 6.14. The parameters needed were $p=0.98$, $V_x=820$ volts and $\tau=69$ seconds for the 6 ppm sample and $p=0.75$, $V_x=670$ volts and $\tau=20$ seconds for the 65 ppm sample. These values thus differ from those obtained from the corresponding dV/dt versus t plots.

In both Figs 6.13 and 6.14, experimental points for t_d versus V_1 are also included. The fact that these points lie the right of the $2V_d$ points (that is $V_1 > 2V_d$) suggests a slight loss of surface charge with time, i.e. $d\sigma/dt < 0$, since for $d\sigma/dt = 0$, V_1 would be identical to $2V_d$.

6.6 Discussion

The observed two time-zone behaviour of the dV/dt versus t

plots clearly shows that the depletion discharge model is the dominant process of dark voltage decay in amorphous selenium, even with chlorine concentrations below 100 ppm in the source material. However, when the aluminum oxide blocking layer is absent, the present results show that this may no longer be true.

The shape of the variation of dV/dt with time is better explained using the modified space charge density increase function of equation (2.18) than the simpler power law function of Abkowitz et al [3] (equation 2.11). For longer dark decay times, such as those found in the measurements on the 6 ppm sample, it was necessary to assume some surface charge loss via equation (2.22) with $K=5 \times 10^{-4} \text{ sec}^{-1}$. However, it should be noted that, even with this value, the surface charge loss would amount to only 10% after 200 seconds.

The parameters of p , V_x and τ , obtained for the 6 and 65 ppm samples, differed between the dV/dt versus t plots on the one hand and the t_d versus $2V_d$ plots on the other. The discrepancy may be due again to a slight loss of surface charge. Never-the-less, the results of both sets of data show an unequivocal decrease of τ with chlorine content, indicating that the hole release time τ_r changes in a similar way.

The influence of the Poole Frenkel effect has been considered by Kasap, Baxendale and Juhasz [12]. However, application of this treatment to the present results does not seem to be helpful because the Poole Frenkel effect seems to cause the t_d versus $2V_d$ curve to bend downwards, away from a straight line, instead of

bending upwards, as indicated by the experimental results.

The dV/dt versus t results also yield ρ_0 , the ultimate bulk charge density in the selenium and hence $N_0 = \rho_0/e$, the density of the ionized deep centres. For both the 6 and 65 ppm samples, ρ_0 was found to be about 2.2×10^{-5} coulomb/cm³, corresponding to a value for N_0 of about 1.4×10^{14} cm⁻³. This suggests that the chlorine does not affect the concentration of deep centres but never-the-less speeds up the release process.

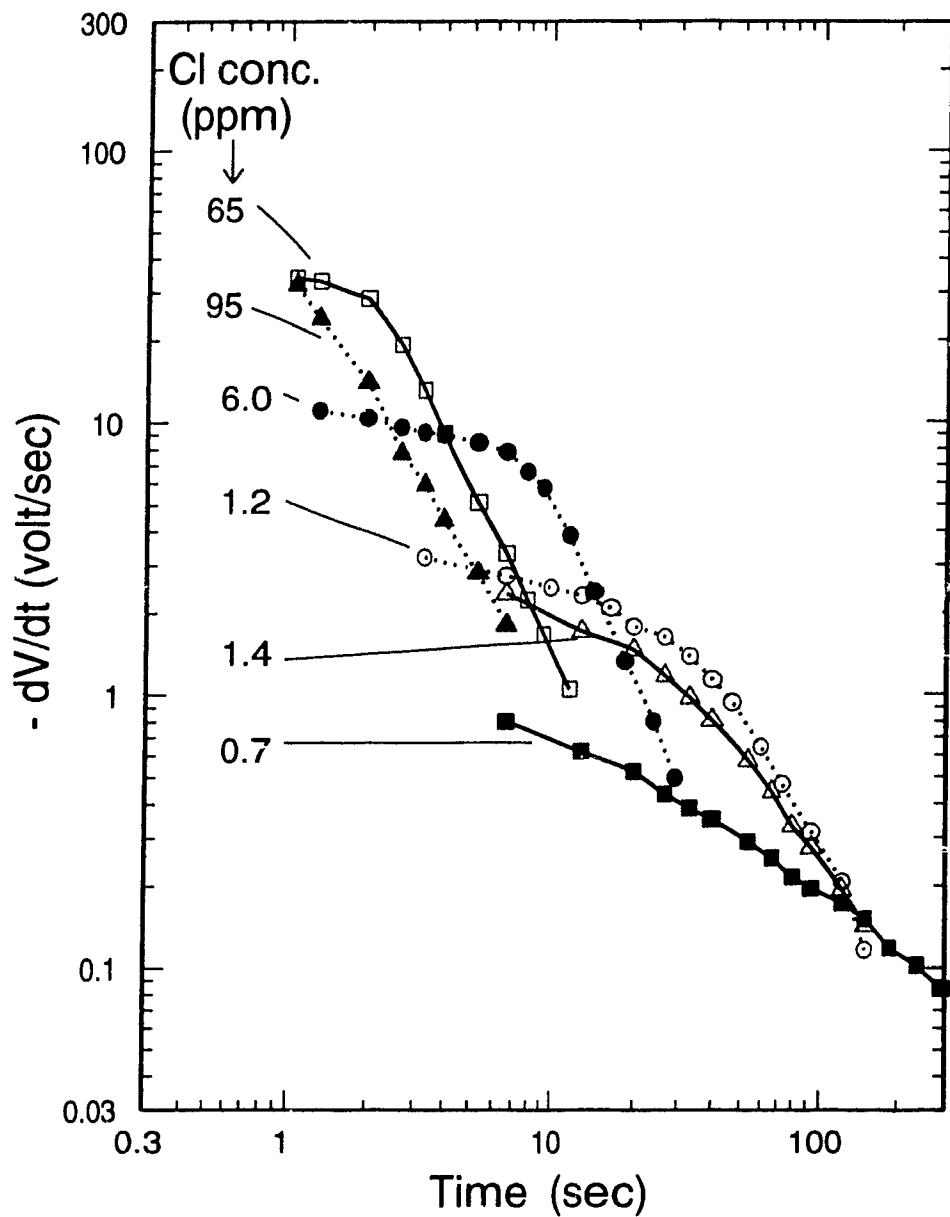


Fig 6.1. Plots of voltage slope $-dV/dt$ against time t for 6 samples with different Cl concentrations in the selenium charged to an initial voltage of 123 ± 30 volts.

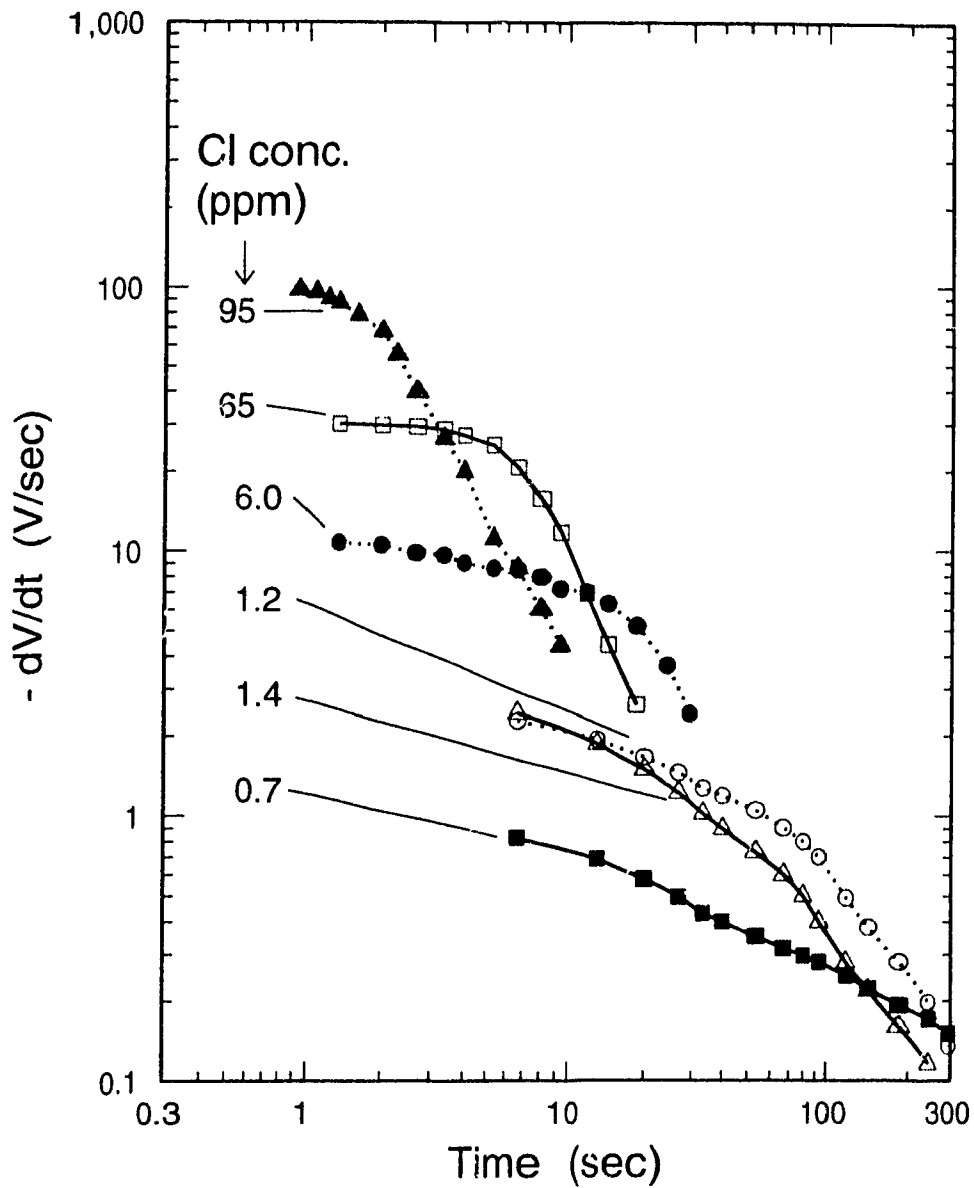


Fig 6.2. Plots of voltage slope $-dV/dt$ against time t for 6 samples with different Cl concentrations in the selenium charged to an initial voltage of 281 ± 35 volts.

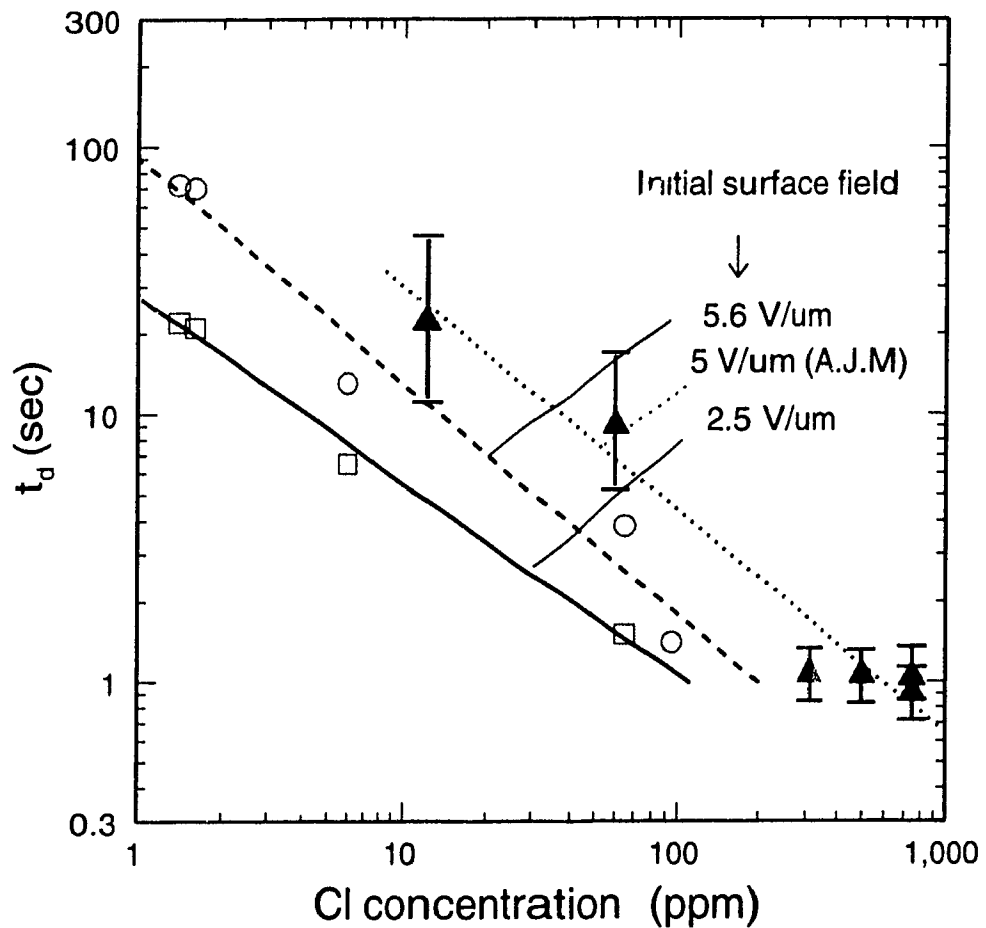


Fig 6.3 Plot of measured depletion time against chlorine concentration in the selenium for samples charged initially to 123 and 281 volts, corresponding to electric fields of 2.5 and 5.6 volt/micrometer respectively. Plotted also are values from AJM, reference [3], corresponding to a field of 5 V/micrometer

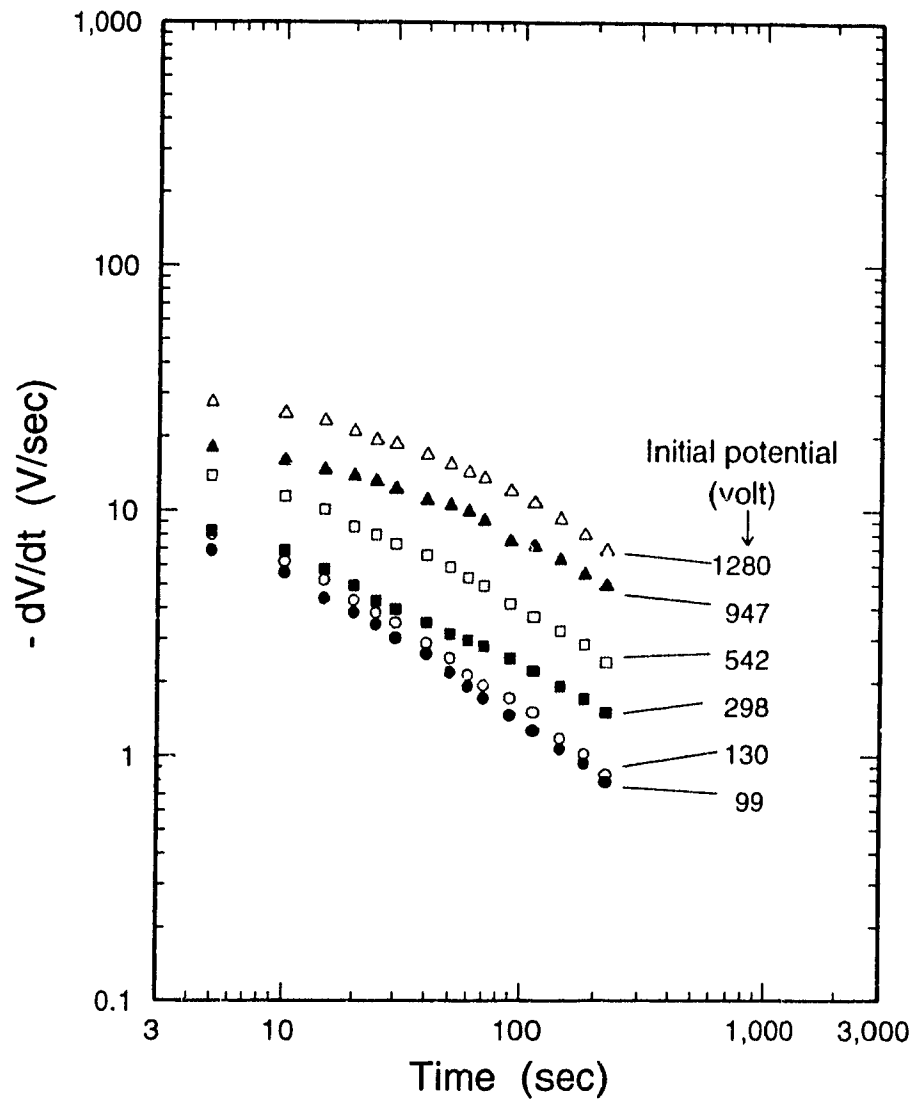


Fig 6.4 Plot of voltage slope $-dV/dt$ against t for a nominally undoped sample with 6 different initial charging voltages.

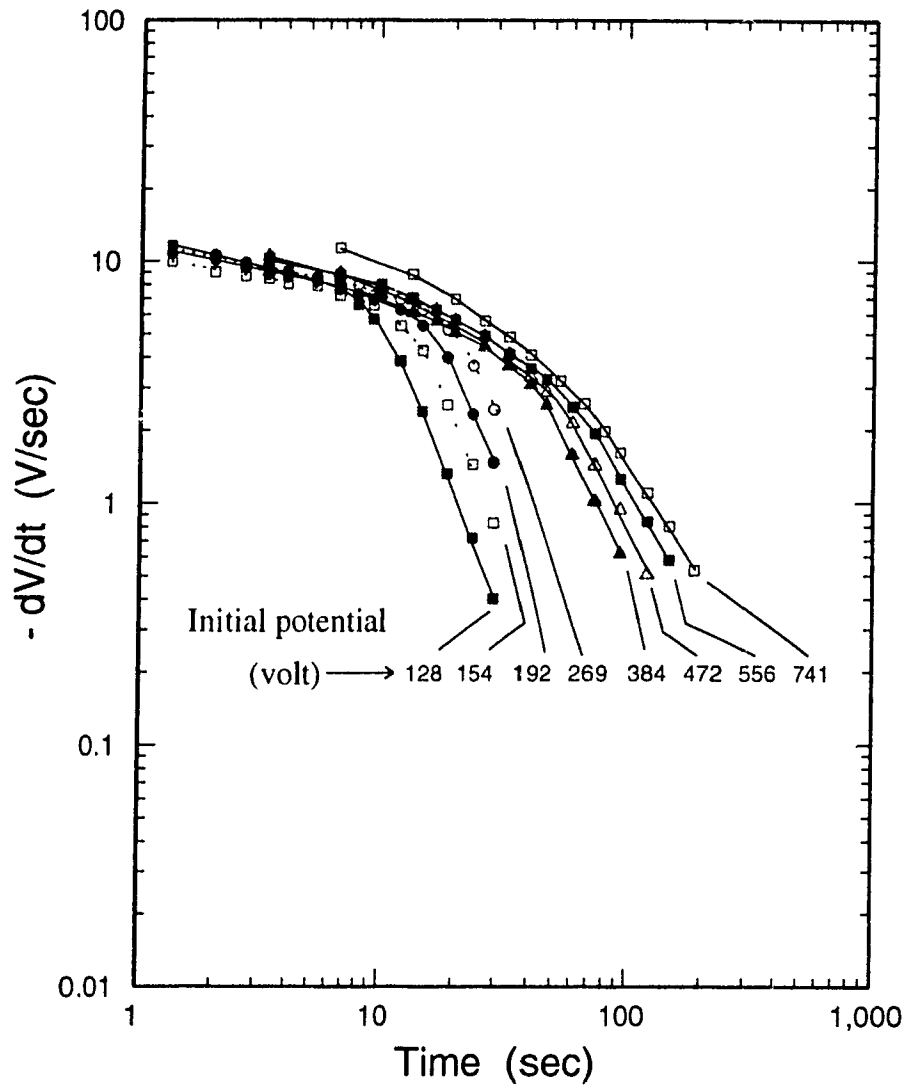


Fig 6.5 Plot of voltage slope $-dV/dt$ against t for a sample with doped with 6.0 ppm chlorine in the selenium with eight different initial charging voltages.

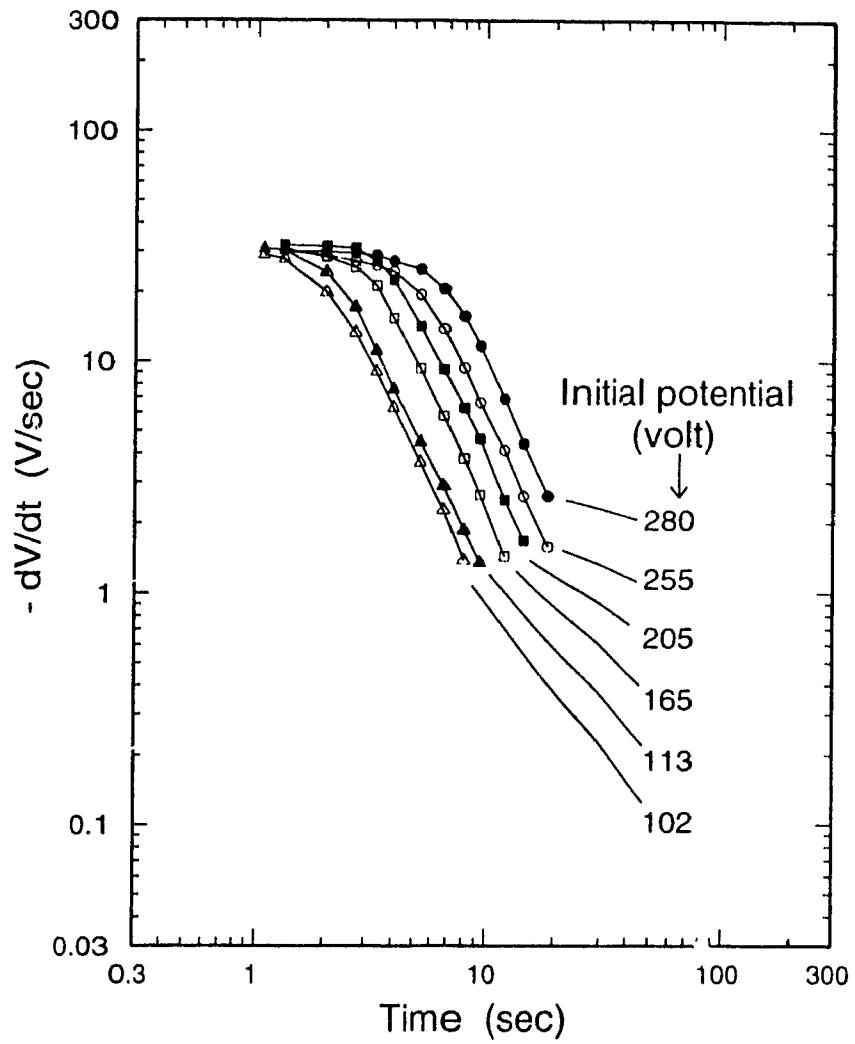


Fig 6.6 Plot of voltage slope $-dV/dt$ against t for a sample with doped with 65 ppm chlorine in the selenium with six different initial charging voltages.

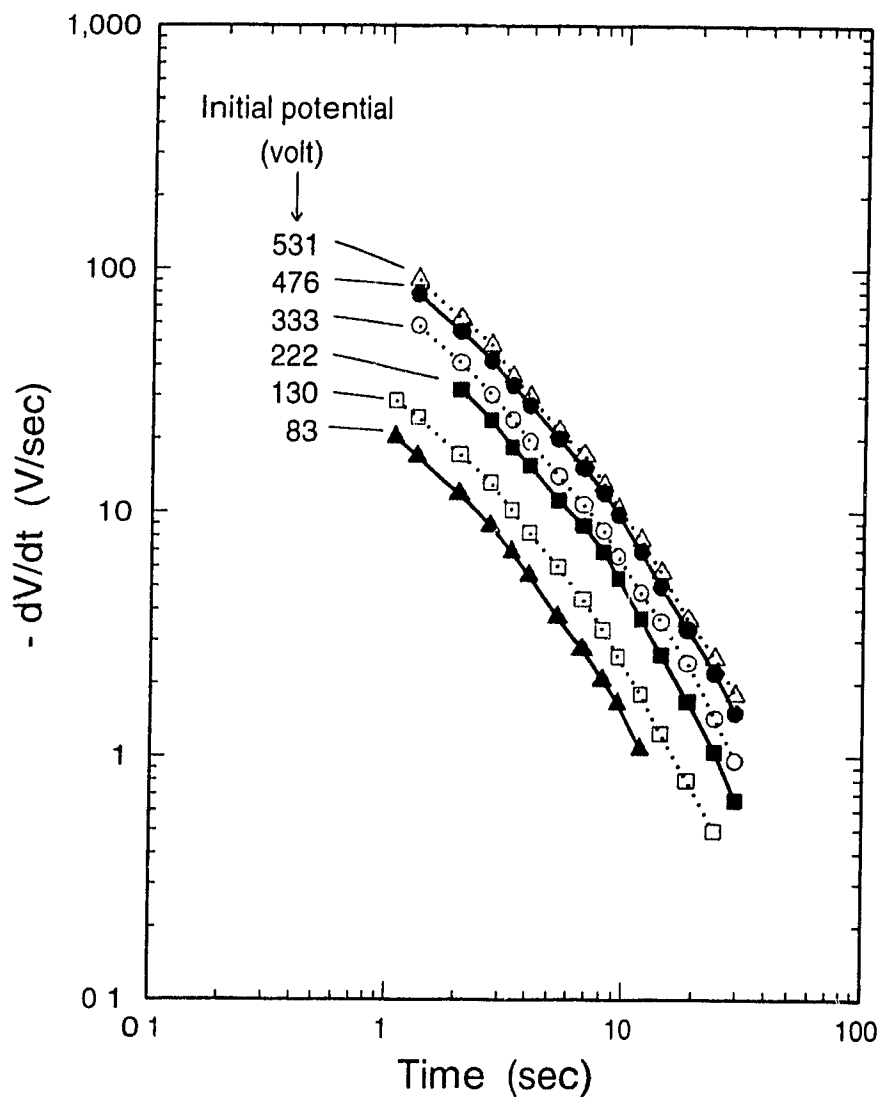


Fig 6.7 Plot of voltage slope $-dV/dt$ against t for a sample doped with 65 ppm chlorine in the selenium but with no oxide layer between Se and substrate for 6 different initial charging voltages.

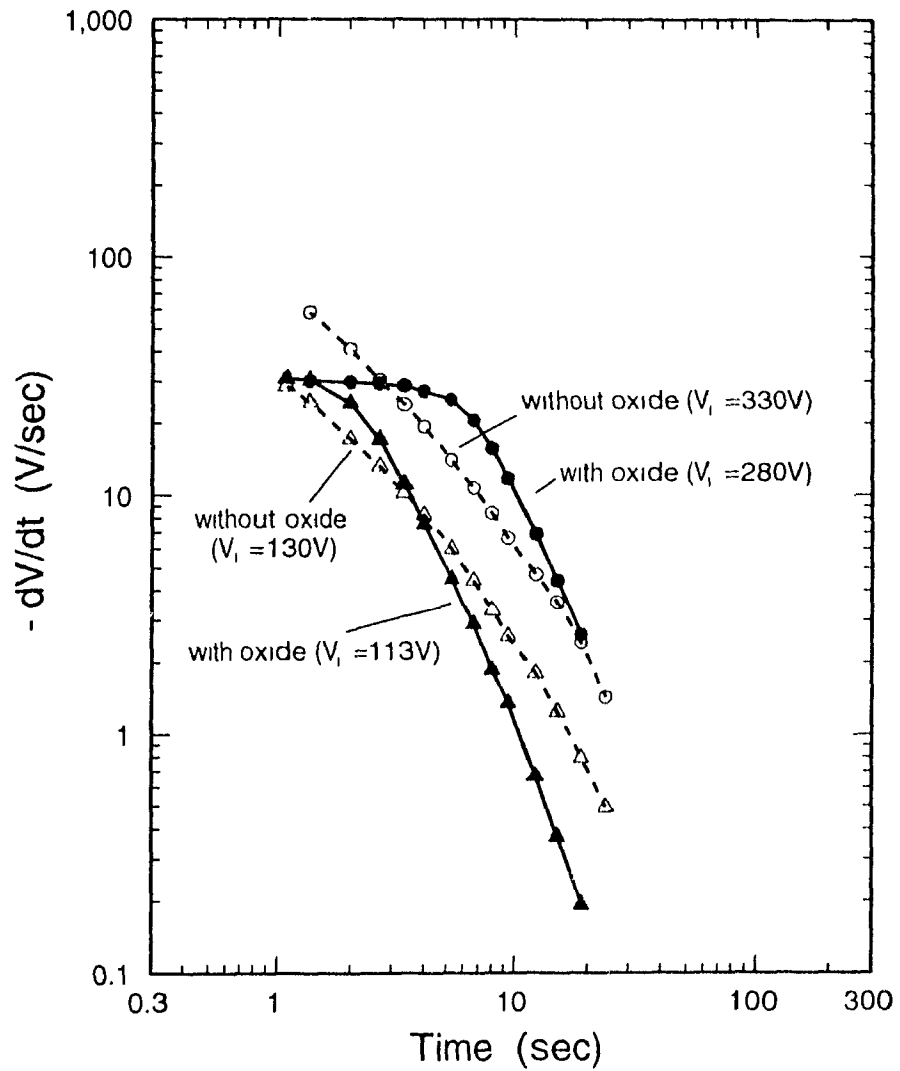


Fig 6.8 Comparison of $-dV/dt$ against t plots for the 65 ppm Cl doped samples with and without the interfacial oxide layer for two average levels of the initial charging voltages.

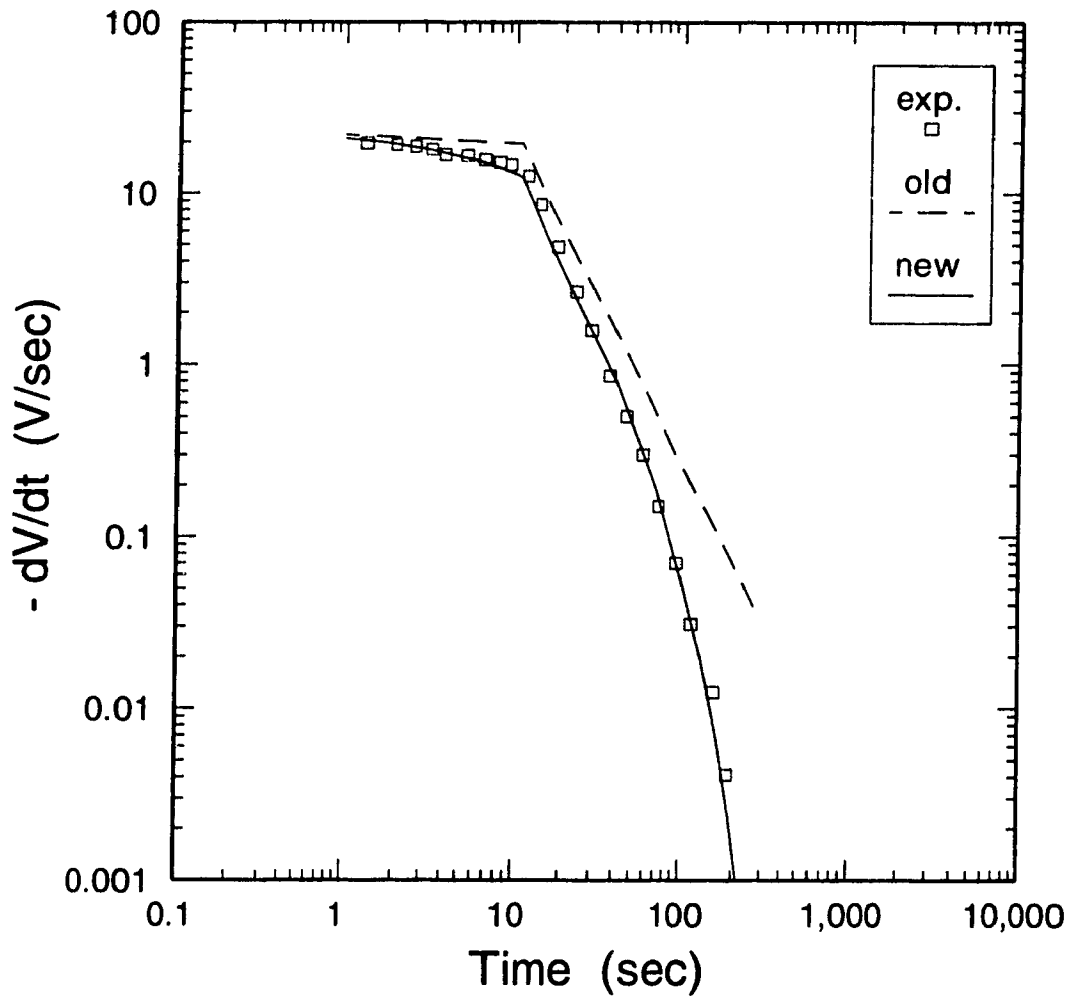


Fig 6.9 Plot of voltage slope $-dV/dt$ against time for a sample doped with 65 ppm chlorine with an initial charging voltage of 308 V. The broken line was calculated with equations (2.13) (2.15), and the solid line with equations (2.20a) and (2.21a) using the parameters $t_{orr}=25$ sec, $p=0.95$ and $V_x =950$ volts.

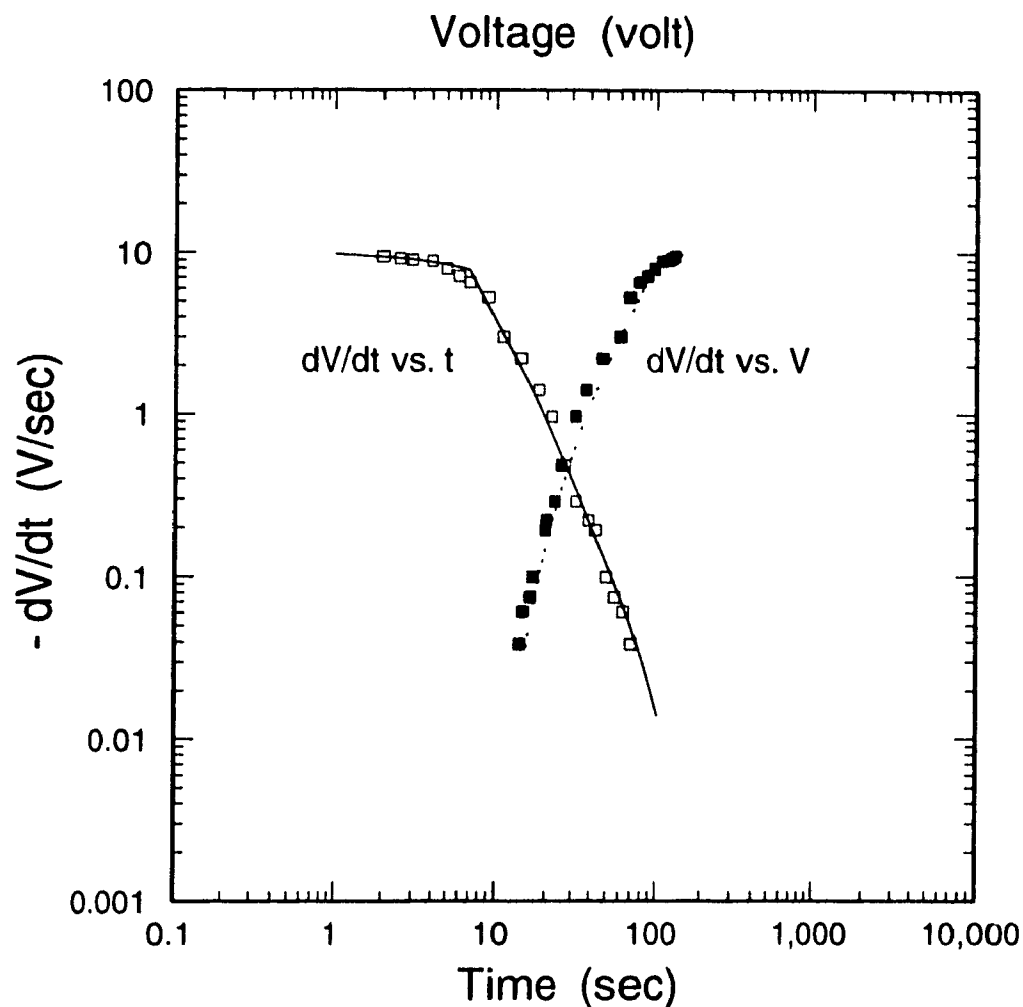


Fig 6.10 Plot of voltage slope $-dV/dt$ against time and against voltage for a sample doped with 6 ppm chlorine with an initial charging voltage of 158 V. The solid line was calculated with equations (2.20a) and (2.21a), and the dotted line using equations (2.18), (2.5) and (2.20) for zone 1, (2.18), (2.6) and (2.21) for zone 2, where the parameters used were: $\text{torr}=25$ sec, $p=0.95$ and $V_x=950$ volts.

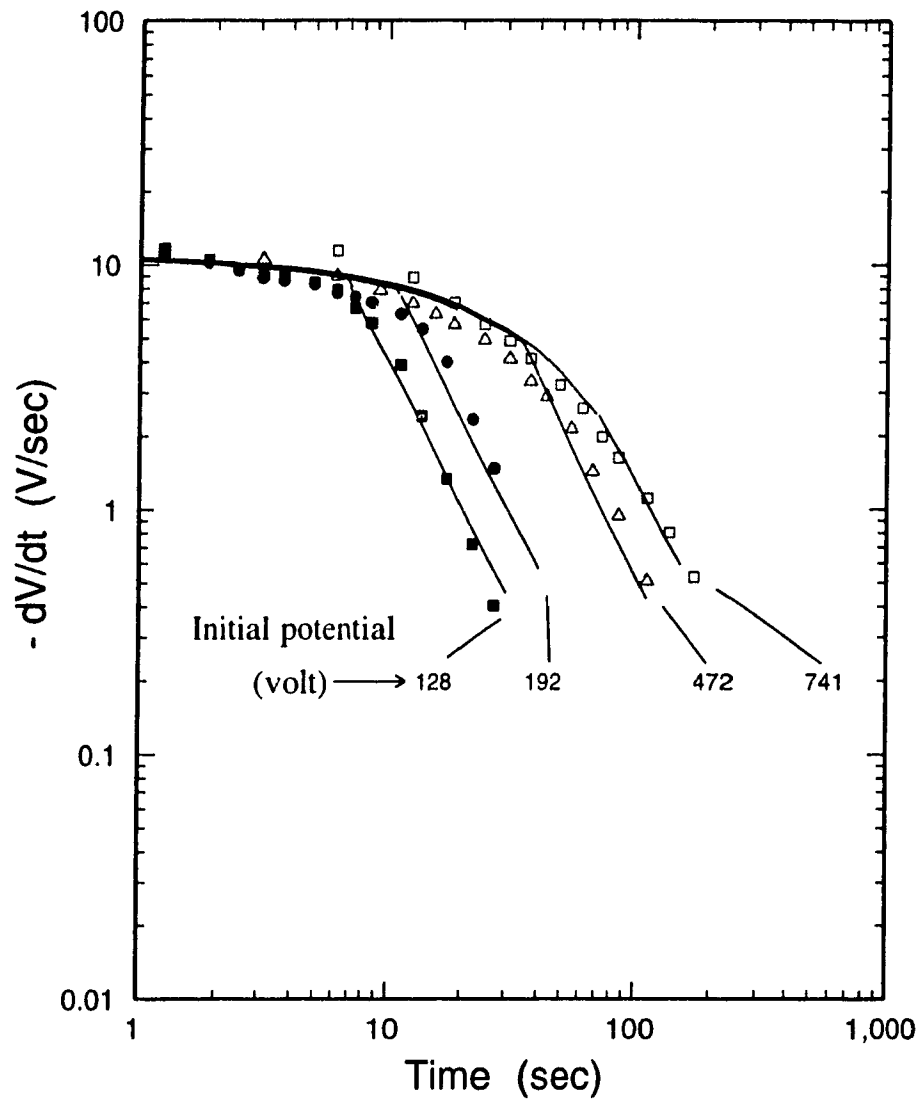


Fig 6.11 Plots of voltage slope $-dV/dt$ against time t for a sample doped with 6.0 ppm chlorine with four different initial charging voltages, together with four theoretical curves calculated using equations (2.20b) and (2.21b), with the parameters $t_{orr}=51$ sec, $p=0.98$, $V_x=980$ volts and $K=5 \times 10^{-4} \text{ sec}^{-1}$.

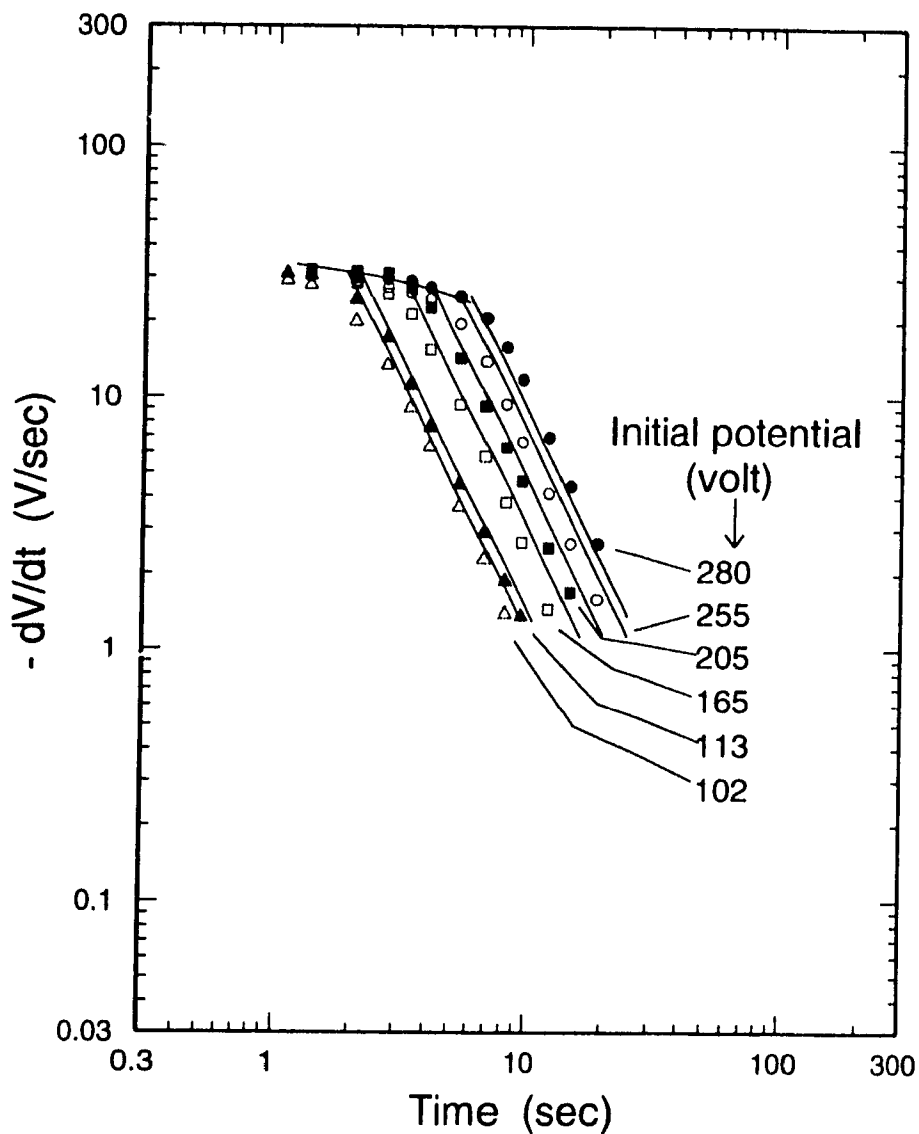


Fig 6.12 Plots of voltage slope $-dV/dt$ against time t for a sample doped with 65 ppm chlorine with six different initial charging voltages, together with six theoretical curves calculated using equations (2.20b) and (2.21b), with the parameters $t_{orr}=25$ sec, $p=0.95$, $V_x=950$ volts and $K=0$.

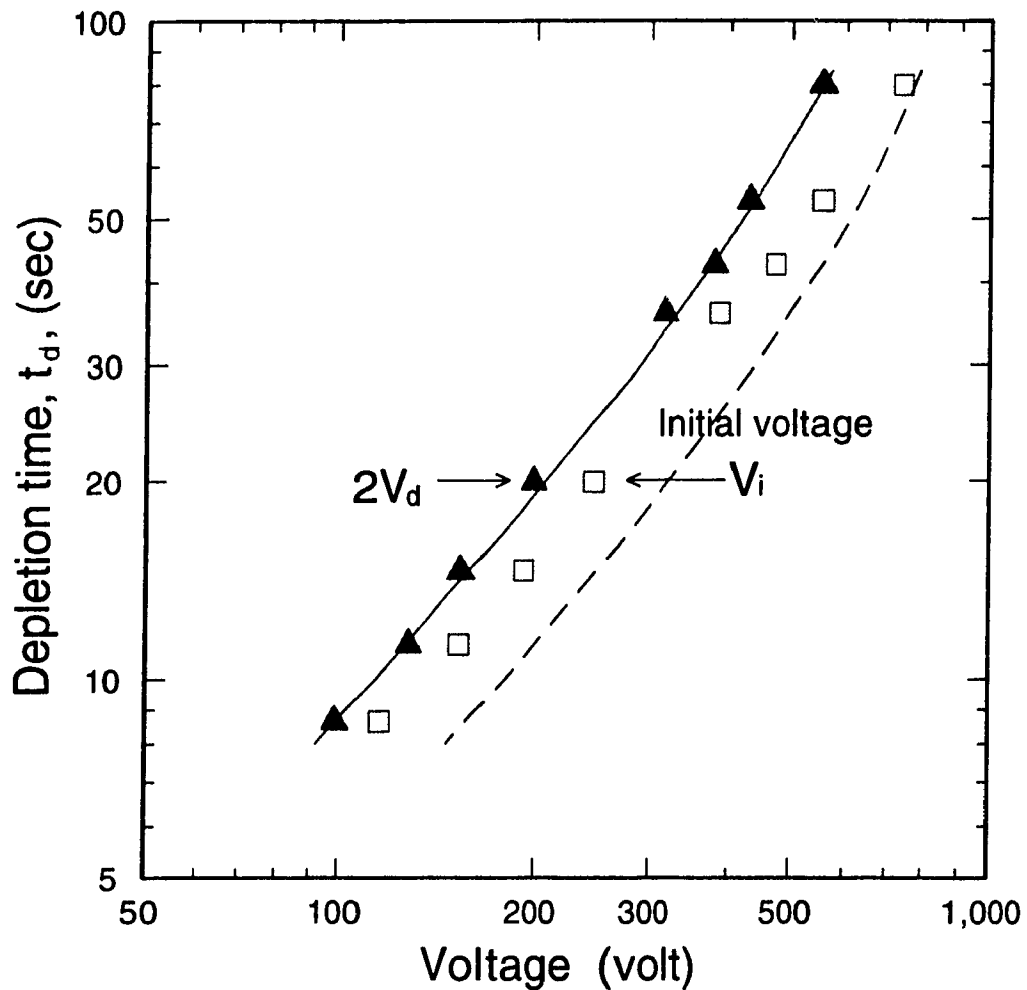


Fig 6.13. Log-Log plot of depletion time against initial charging voltage (V_i) and twice the depletion voltage ($2V_d$) for a 6 ppm chlorine doped sample. The broken line was calculated using equation (2.23) with the parameters obtained from Fig 6.10. The solid line was computed with the parameters $t_{orr}=69$ sec, $p=0.98$ and $V_x=820$ volts, obtained by fitting to the $2V_d$ experimental points.

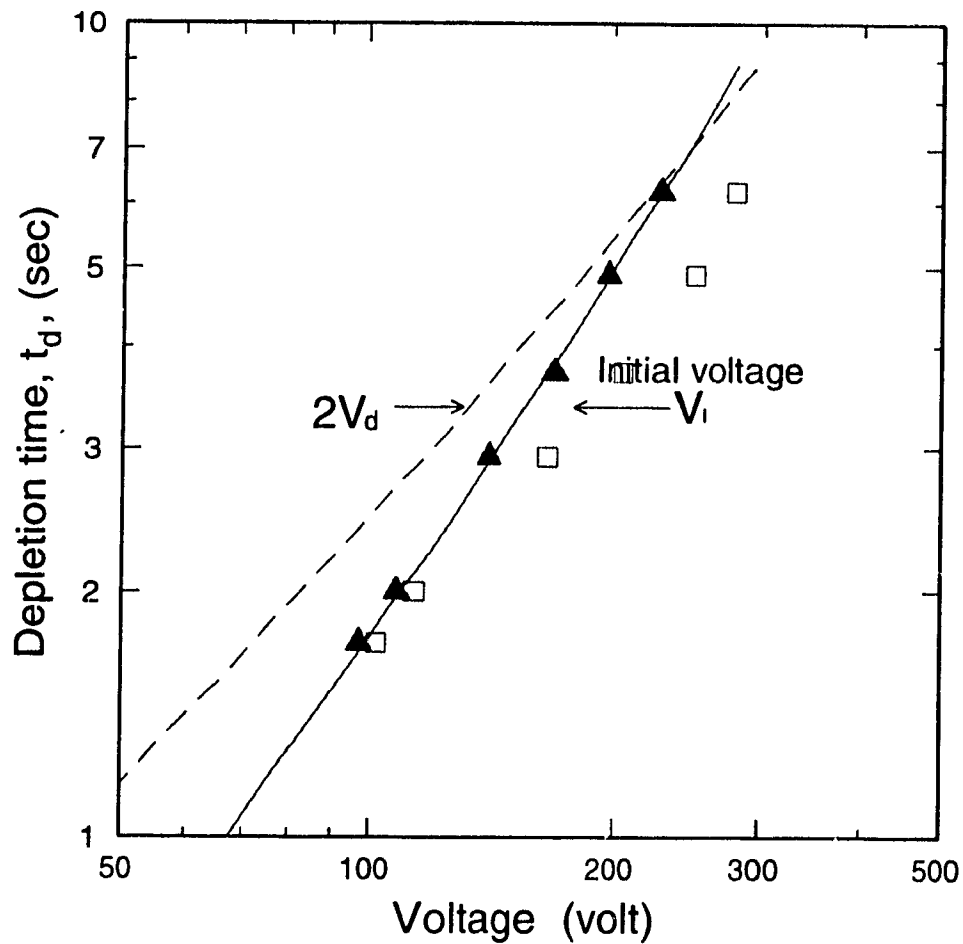


Fig 6.14. Log-Log plot of depletion time against initial charging voltage (V_i) and twice the depletion voltage ($2V_d$) for a 65 ppm chlorine doped sample. The broken line was calculated using equation (2.23) with the parameters obtained from Fig 6.9. The solid line was computed with the parameters $\tau=20$ sec, $p=0.75$ and $V_x =670$ volts, obtained by fitting to the $2V_d$ experimental points.

Chapter 7

RESULTS OF MEASUREMENTS ON OXIDE LAYER

7.1 Introduction

As described in chapter 4, the blocking layer employed in the xerographic samples in the present work was a thin film of aluminum oxide between the substrate and the selenium, deposited usually by r.f. sputtering from an Al_2O_3 target. The present chapter reports some thickness, capacitance and conduction measurements performed on the so-called capacitance samples of the form Al-oxide-In or glass-metal-oxide-In, where the metal was either aluminum, nickel or gold. The methods used for these measurements are described in chapter 4.

7.2 Oxide Deposition Rate

A set of glass-Al-oxide-In capacitance samples (C7 to C15, Table 3-1) was prepared and capacitance measurements were made on the indium areas (A) on each sample. The oxide thickness, d_{ox} , was then determined for each sample from a plot of capacitance against indium area, as indicated in Fig 4.8.

The results are shown in Fig 7.1 as a plot of oxide thickness against sputtering time from 100 to 1100 Å. Within this range, the

dependence appears to be linear with a slope of about 17.7 Å/min. These results may be compared with data obtained earlier using d.c. sputtering, shown in the same figure, where the dependence is seen to be generally nonlinear. Using a larger target-sample distance s of 8 cm compared with 4 cm [2], reduced the initial d.c. sputtering deposition rate by a factor of almost 6.

Fig 7.2 shows a few measurements on samples with nickel or gold substrates (ie glass-Ni-oxide-In and glass-Au-oxide-In structures) compared with the experimental broken line for aluminum-base samples from Fig 7.1. Here only r.f. sputtering of the oxide was used. While the scatter in the points is larger than for aluminum, the dependence of r.f. sputtered oxide thickness on deposition time is seen to be about the same as that for the aluminum substrate.

7.3 Xerographic Comparison of d.c and r.f. Sputtered Oxides

While a detailed comparison of xerographic performance between samples, prepared with d.c. reactively sputtered oxides and r.f. sputtered ones, has not been carried out, a preliminary test was made on 6 samples with an oxide thickness of 300 Å. Three of these were fabricated using d.c. reactive sputtering with air and three using r.f. sputtering from an Al_2O_3 target. Fig 7.3 compares the voltage-time characteristics for 4 undoped samples from the set of 6, two prepared with d.c. sputtering and two with r.f. sputtering. It is seen that the dark decay rates, for all the 4 samples over

the 4-minute dark period, were about 5 to 8 percent, with similar acceptance and residual voltages of about 1500 and 20 volts respectively. Thus, there was no significant xerographic difference between the two types of sputtering. The same can be said of Fig 7.4, showing results for the remaining two samples, where the selenium was doped with 65 ppm of chlorine. The dark decay rates, acceptance voltages and residual voltages of about 70%, 650 volts and less than 5 volts respectively were almost the same.

7.4 Capacitance and Resistance Results with r.f. Sputtered Oxide

Plots of parallel capacitance per unit area, C_p/A , and product of resistance and area, R_pA , respectively against frequency are shown in Fig 7.5, for 3 areas of indium ($A=7.1, 9.6$ and 15.9 mm^2) on the same glass-Al-oxide-In sample. As indicated, the capacitance showed only a small decrease with the increase of frequency but the resistance decreased rapidly over about six decades of frequency. The near coincidence of the experimental C_p/A and R_pA points, for the three areas, indicates that C_p and $1/R_p$ were both approximately proportional to the indium contact area. Fig 7.6 is a similar plot to Fig 7.5, but for three samples with different oxide thicknesses (d_{ox}) on the same nickel substrate. Here the products $C_p d_{ox}$ and R_p/d_{ox} were plotted against frequency for the same indium contact area. It is noted that the capacitance varied little in the frequency range from 100 Hz to 100 kHz, with a sharp decrease near 1 MHz. The resistance, however, decreased rapidly with frequency over about five decades. The lack of good coincidence of the R_p/d_{ox}

experimental points for the three thicknesses indicates that R_p was not simply proportional to oxide thickness. The coincidence of the C_p points, however, arises from the fact that d_{ox} was actually determined from C_p . Fig 7.7 shows a plot of C_p and R_p against frequency for two samples on a gold substrate with different oxide thicknesses. The capacitance and resistance showed little change for frequencies lower than about 1 MHz for both oxide thicknesses, resulting from the different sputtering times of 20 and 60 minutes.

The dependence of $R_p A$ on oxide thickness at low frequency where possible, is examined specifically in Fig 7.8. The points plotted for the aluminum substrates at 10 and 100 Hz (which correspond to the conductance through the film better than at higher frequency) suggest that R_p was approximately proportional to $(d_{ox})^{3/2}$, rather than d_{ox} , which would be expected from simple considerations. For nickel, a steeper dependence is apparent but there are only three points plotted. For gold, the number of points is insufficient to obtain a specific dependence.

7.5 Voltage Breakdown of Oxide Layers

The C_p and R_p measurements, reported in section 7.4 were all carried out at zero voltage bias on the samples. To observe the bias dependence, C_p and $G_p=1/R_p$ were measured as a function of voltage applied to each glass-Al-oxide-In sample for both voltage polarities at a fixed frequency of 100 Hz. Figs 7.9 and 7.10 show plots of C_p and G_p against applied bias for two typical samples with oxide thicknesses of 800 and 1000 Å. It is clearly seen that, with either voltage polarity an abrupt increase in G_p occurred at about

7 volts for the 800 Å sample and 9 volts for the 1000 Å sample. These changes were accompanied by abrupt decreases of C_p at the same voltages. The results were repeatable, indicating that no irreversible change had taken place in the samples. Breakdown fields were then obtained by dividing the critical or breakdown voltages by the oxide thicknesses d_{ox} and these values are plotted against thickness in Fig 7.11. It is seen that, while the breakdown voltage increased apparently linearly with d_{ox} , extrapolation of the straight line did not go through the origin, so that the breakdown field decreased initially with thickness, approaching a value of the order of 10^6 volt/cm for larger thicknesses.

7.6 Discussion

For deposition of the oxide blocking layer, a "glow discharge" method is often used, which, while similar to the physical arrangement for d.c. reactive sputtering, involves a relatively large anode-cathode distance, so that the oxidation is largely the result of a reaction between the aluminum substrate and atomic oxygen from the electrical discharge. In d.c. reactive sputtering, however, the oxide is formed from the oxygen reacting with the aluminum of the target and not the substrate. In d.c. sputtering, the target can have a much higher purity than the substrate and additionally, Zhang [2] showed that oxide thicknesses up to 3000 Å at least, can be reached, if needed, by continuous sputtering, whereas this was not normally possible with the glow discharge method. In the present work, it was found that, even with d.c. reactive sputtering, it was difficult to form the aluminum oxide on metals, such as gold, platinum and nickel, so that r.f. sputtering

from a sintered Al_2O_3 target was investigated. As reported in this chapter, this method worked well. At least up to about 1000 Å, the oxide thickness increased linearly with deposition time using an aluminum substrate. Deposition on nickel and gold followed approximately the same dependence. The deposition rate of about 18 Å/min was obtained with a sample-target distance s of 8 cm, an r.f. power of 60 watts and an argon pressure of 2 millitorr. Slower or faster rates can be obtained by suitable adjustment of these parameters.

While the xerographic performance of the r.f. sputtered oxide films on nickel and gold has not so far been evaluated experimentally in this laboratory, measurements of capacitance and resistance, as reported in this chapter, do give some interesting characteristics of these films.

A circuit model to explain exactly the observed variation of C_p and R_p with frequency is likely to be rather complicated. However, a simple model, consisting of a capacitor C_1 shunted by a resistor R_1 as a parallel pair in series with a small resistor R_2 (Fig 7.12), can qualitatively explain the main variation. Equivalent values of parallel capacitance C_p and parallel resistance R_p for this circuit for $R_1 \gg R_2$ are given by:

$$C_p = C_1 / (1 + \omega^2 R_2^2 C_1^2) \quad (7.1)$$

$$R_p = R_1 (1 + \omega^2 R_2^2 C_1^2) / (1 + \omega^2 R_1 R_2 C_1^2) \quad (7.2)$$

The dashed lines in Fig 7.5 were calculated using these equations to fit approximately the experimental points with the

R_1A , R_2A and C_1/A values of $3 \times 10^5 \Omega\text{cm}^2$, $0.35 \Omega\text{cm}^2$ and 220 nF/cm^2 respectively. From Fig 7.6, the C_p and R_p values for the nickel substrate sample C16 have been replotted in Fig 7.13 and a fit made with equations (7.1) and (7.2). Here the calculated lines, shown dotted and dashed, fit the experimental points better than in Fig 7.5 and correspond to the parameters R_1 , R_2 and C_1 with values of $3 \text{ M}\Omega$, 37Ω and 7.8 nF respectively. From these results, it is clear that the measured R_p value represents R_1 below a frequency of about 100 Hz and R_2 above about a megahertz. For determining thickness, it appears also that measurement of C_p at 1 to 10 kHz is appropriate.

Fig 7.14 is a plot of resistance x area, measured at a frequency of 10 Hz, against thickness for the Al substrate samples, where the aluminum oxide was deposited by d.c. reactive sputtering and also r.f. sputtering. The comparison shows that the resistance of the latter samples was about an order of magnitude larger than that of the d.c. sputtered samples. This may be due to obtaining a more compact oxide with r.f. sputtering. Thus, r.f. sputtering would appear to be superior to d.c. reactive sputtering in obtaining higher film resistance but in the preliminary tests carried out in this laboratory, no significant difference in xerographic performance was obtained between samples with the oxide deposited by the two methods. The fact that the low frequency resistance (i.e. R_1) through the oxide films on an aluminum substrate was found to be roughly proportional to $d_{\text{ox}}^{3/2}$, rather than d_{ox} , suggests that possibly injection of carriers into the oxide layer may take place.

Regarding the observed electrical breakdown of the oxide film at only a few volts, the breakdown field of the order of 10^6 volt/cm is about an order of magnitude larger than the breakdown strength reported [19] for dense alumina (85% Al_2O_3).

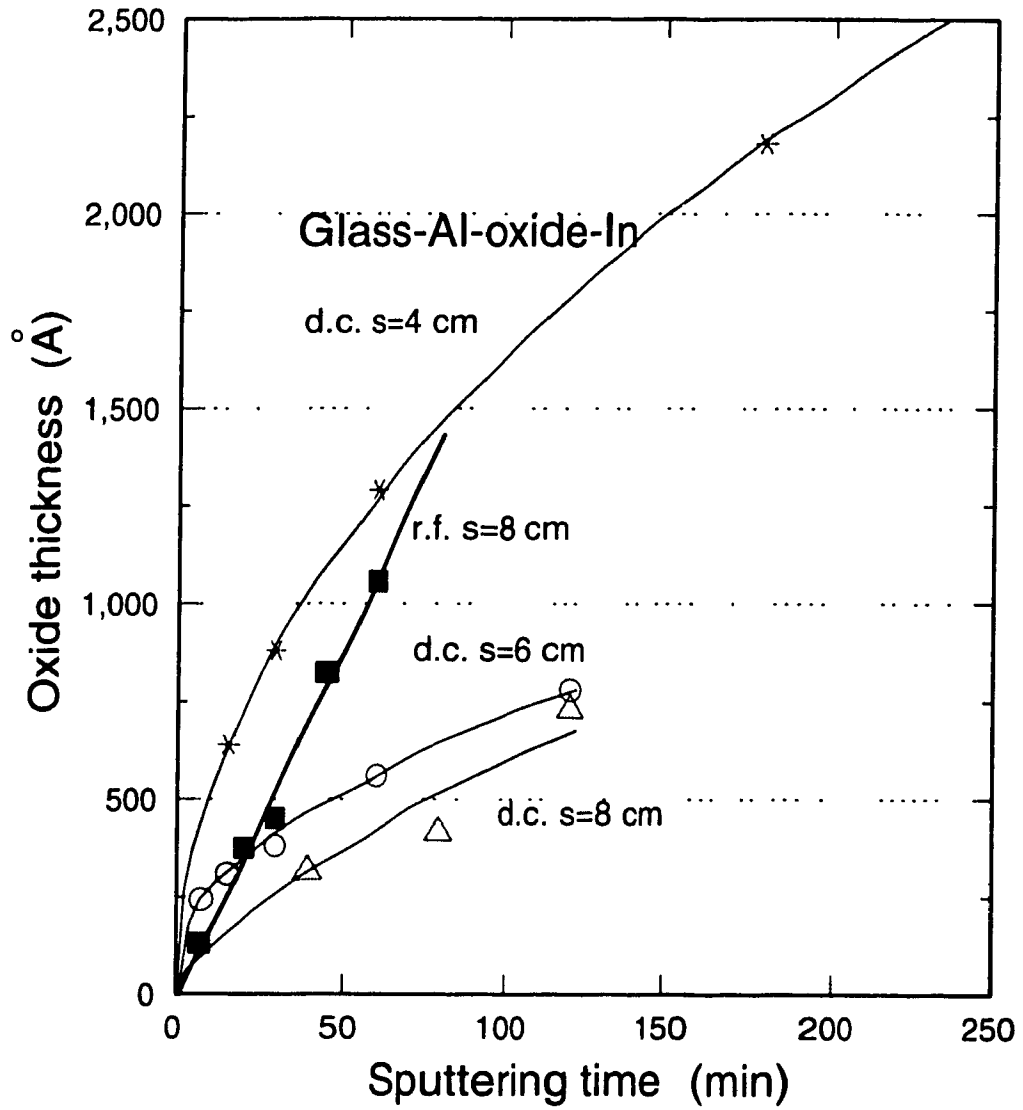


Fig 7.1 Plot of oxide thickness against sputtering time for r.f. sputtering and d.c. reactive sputtering of aluminum oxide on an aluminum film on glass. The quantity s is the target-substrate separation.

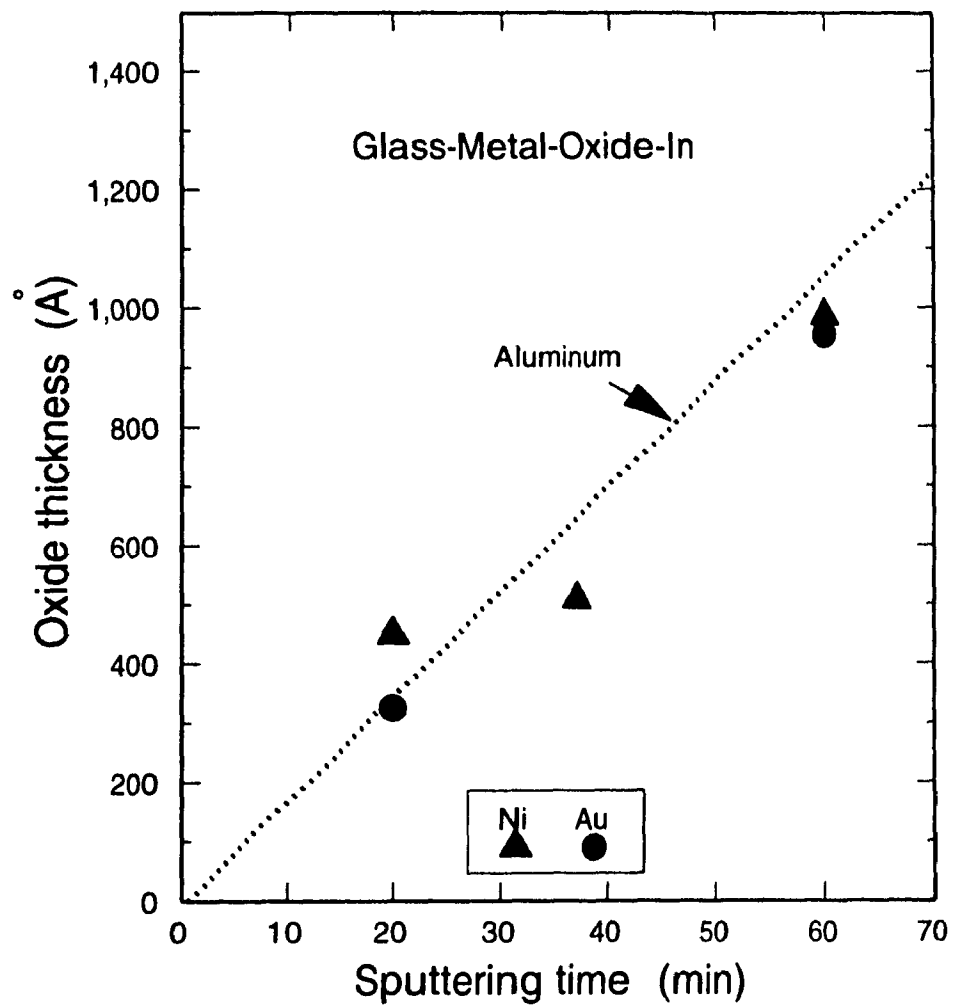


Fig 7.2 Plot of oxide thickness against r.f. sputtering time for aluminum oxide deposited on gold and nickel. The dotted line shows the dependence for oxide on an aluminum base, taken from Fig 7.1.

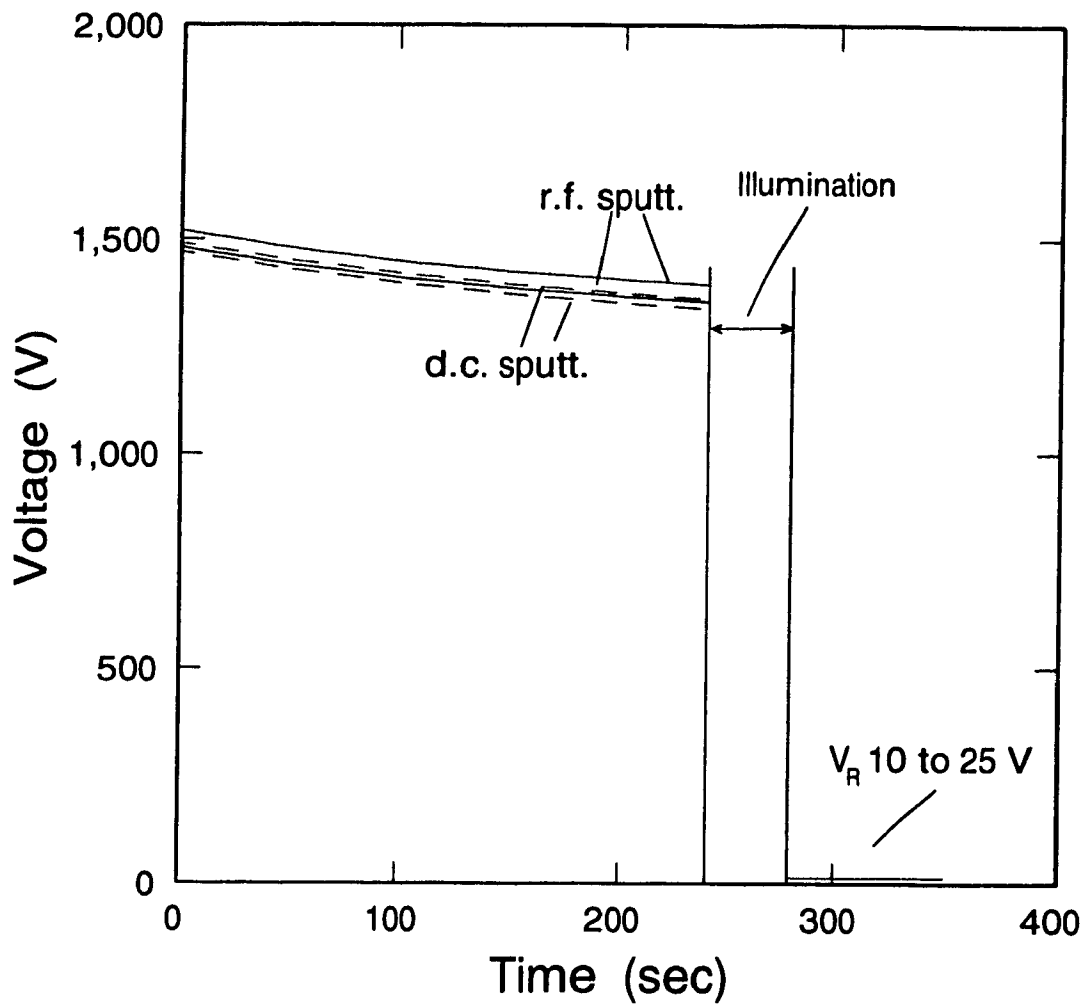


Fig 7.3 Comparison of dark voltage decay curves of undoped selenium samples made with r.f and d.c. sputtered oxide barrier layers of equal thickness (300 \AA).

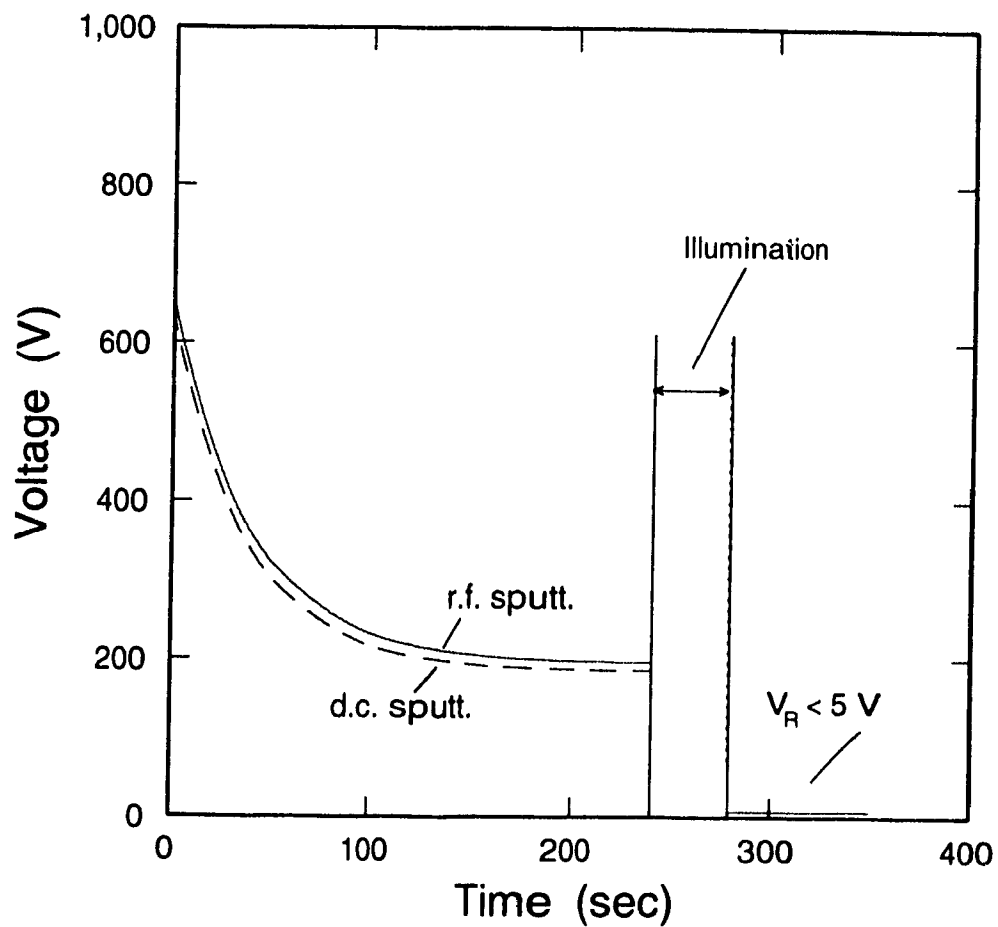


Fig 7.4 Comparison of dark voltage decay curves of selenium doped equally with 65 ppm of chlorine for r.f and d.c. sputtered oxide layers of equal thickness (300 \AA).

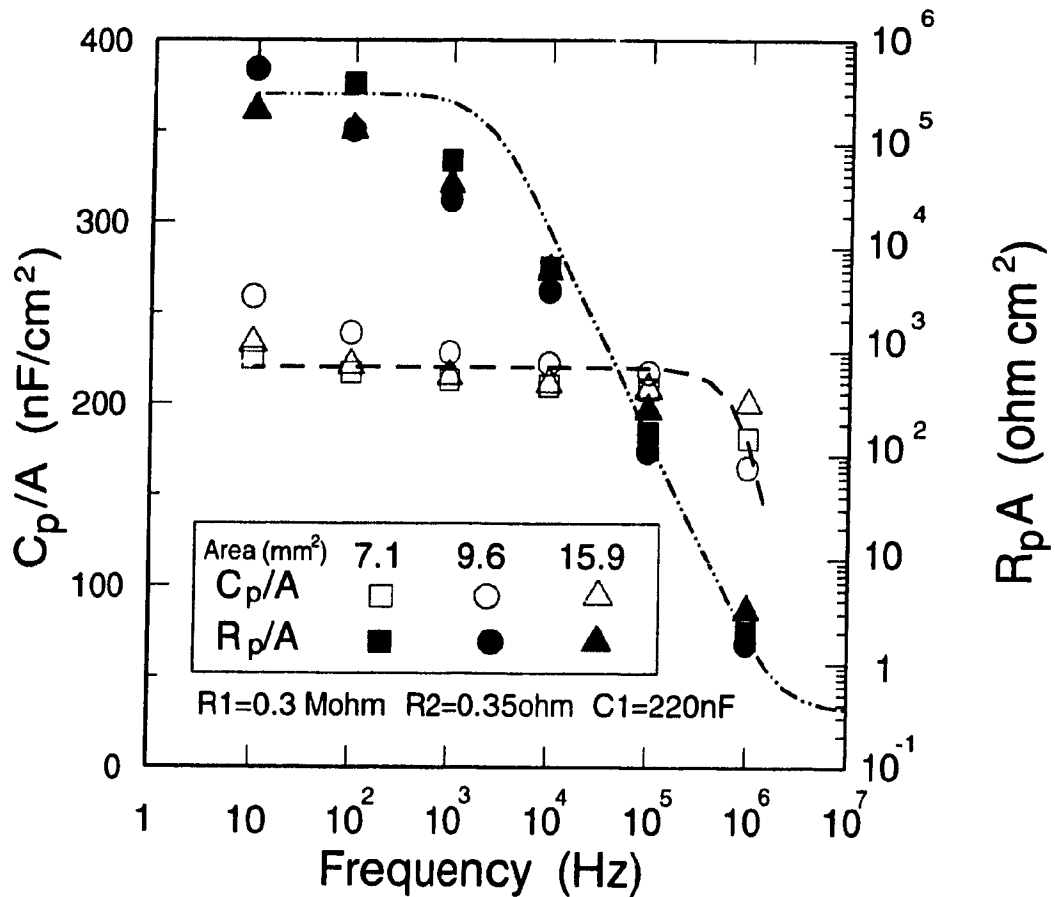


Fig 7.5 Plot of capacitance per unit area and resistance x area against frequency for a glass-Al-oxide-indium structure with 3 different indium contact areas. The r.f. sputtering time was 20 min, yielding an oxide thickness of 360 Å. The drawn lines were calculated from equations (7.1) and (7.2).

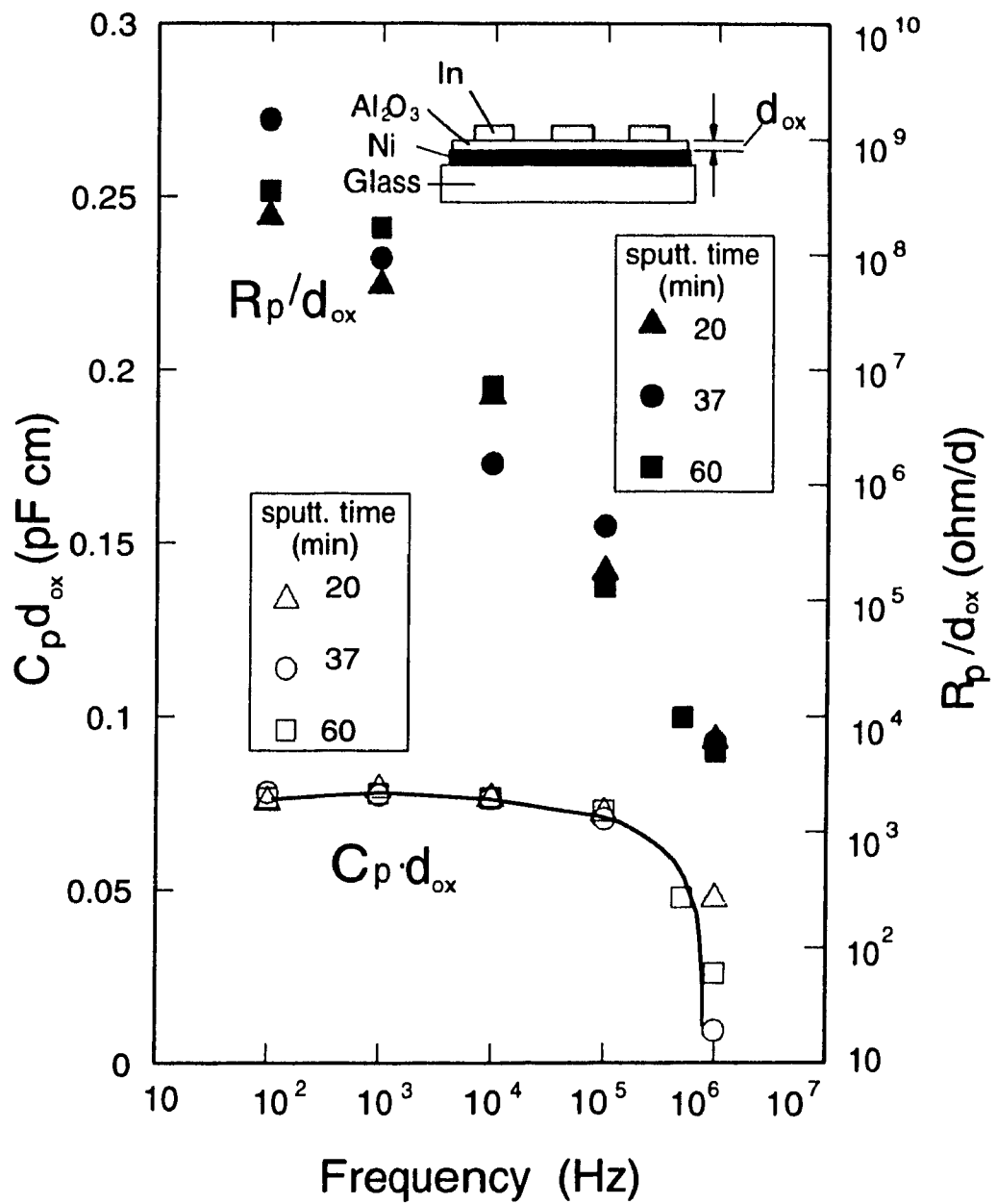


Fig 7.6 Plot of capacitance x thickness and resistance/thickness against frequency for 3 thicknesses of aluminum oxide r.f. sputtered on nickel for different times.

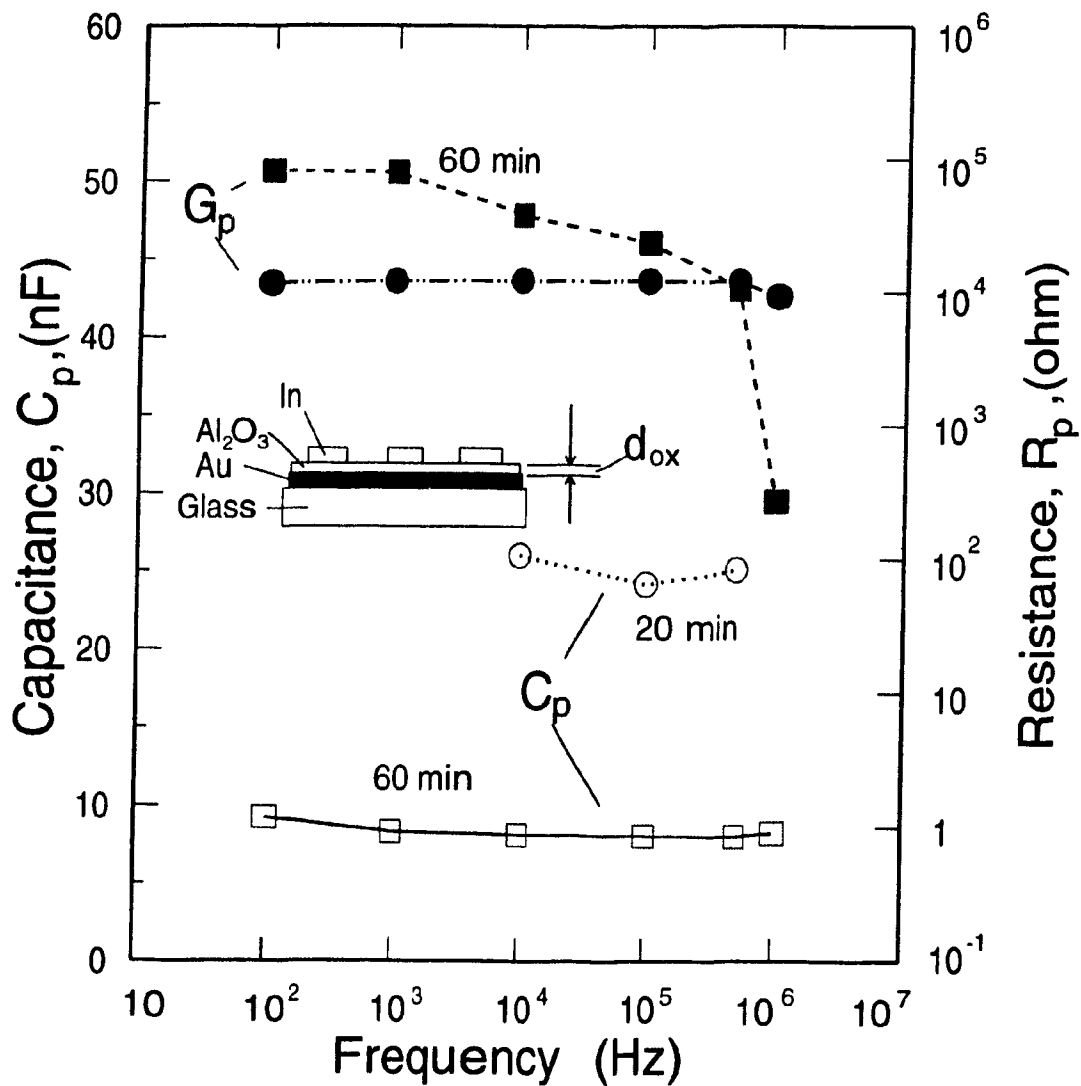


Fig 7.7 Plot of capacitance and resistance of Al₂O₃ on gold against frequency for two oxide thicknesses, deposited by r.f. sputtering for 20 and 60 minutes.

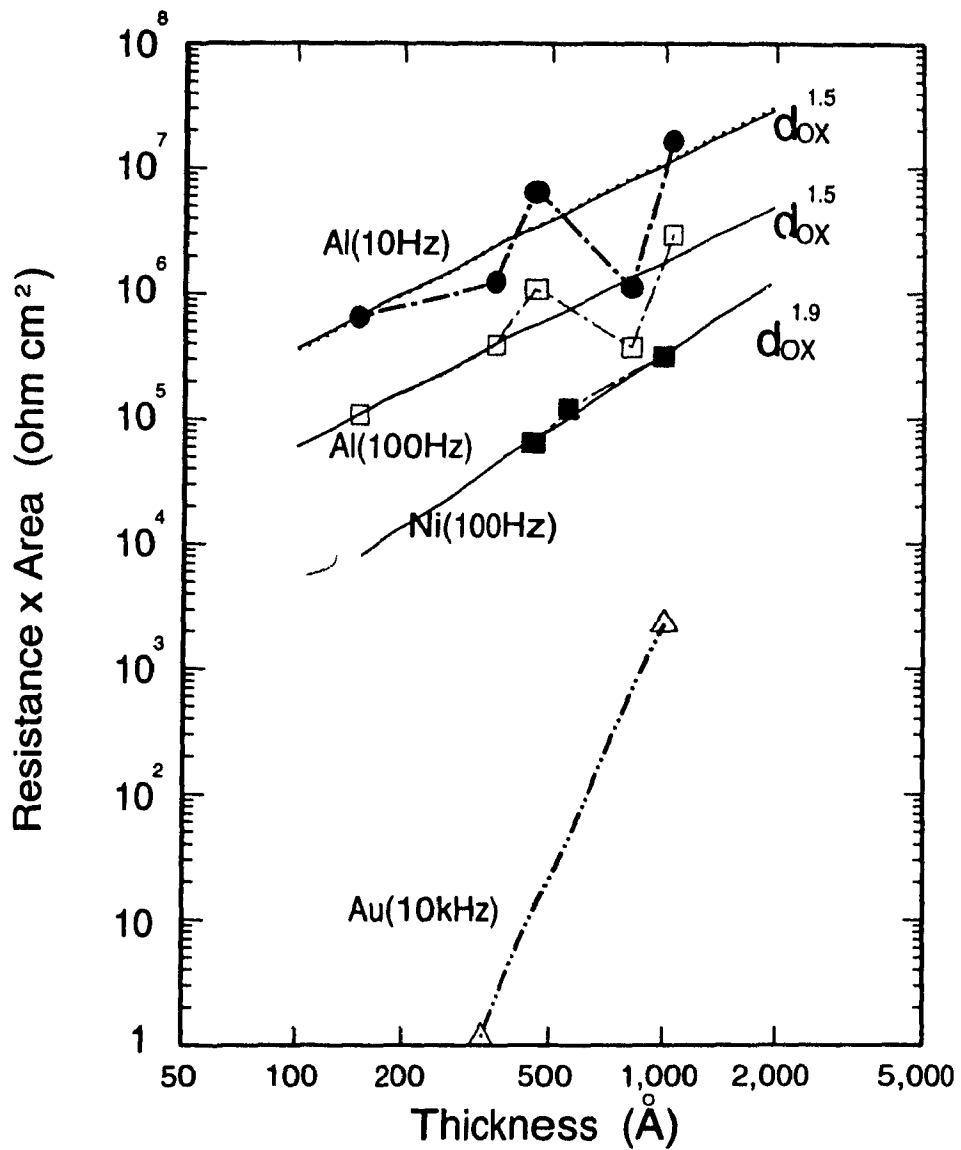


Fig 7.8 Plot of resistance x area of oxide against oxide thickness for different metal substrates, with the indicated frequencies of resistance measurement.

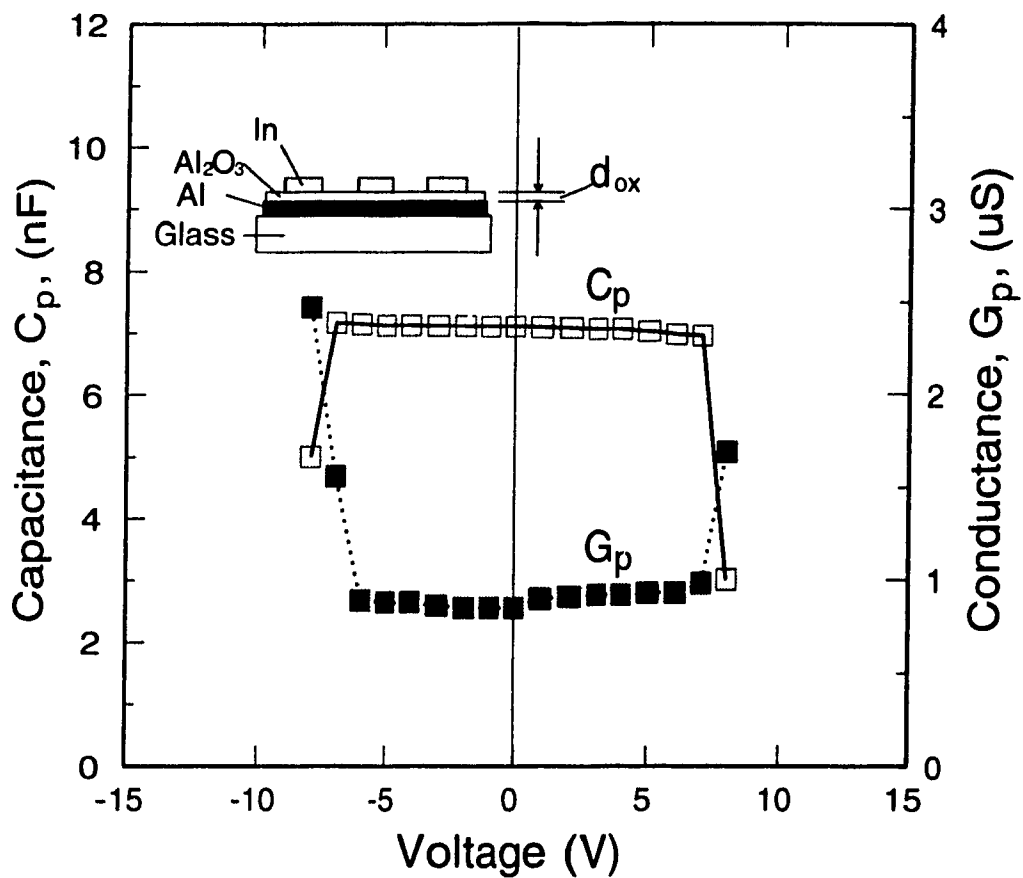


Fig 7.9 Plot of parallel capacitance and conductance against bias voltage for a capacitance sample with an r.f. sputtered oxide thickness of 800 Å. The measurement frequency was 100 Hz.

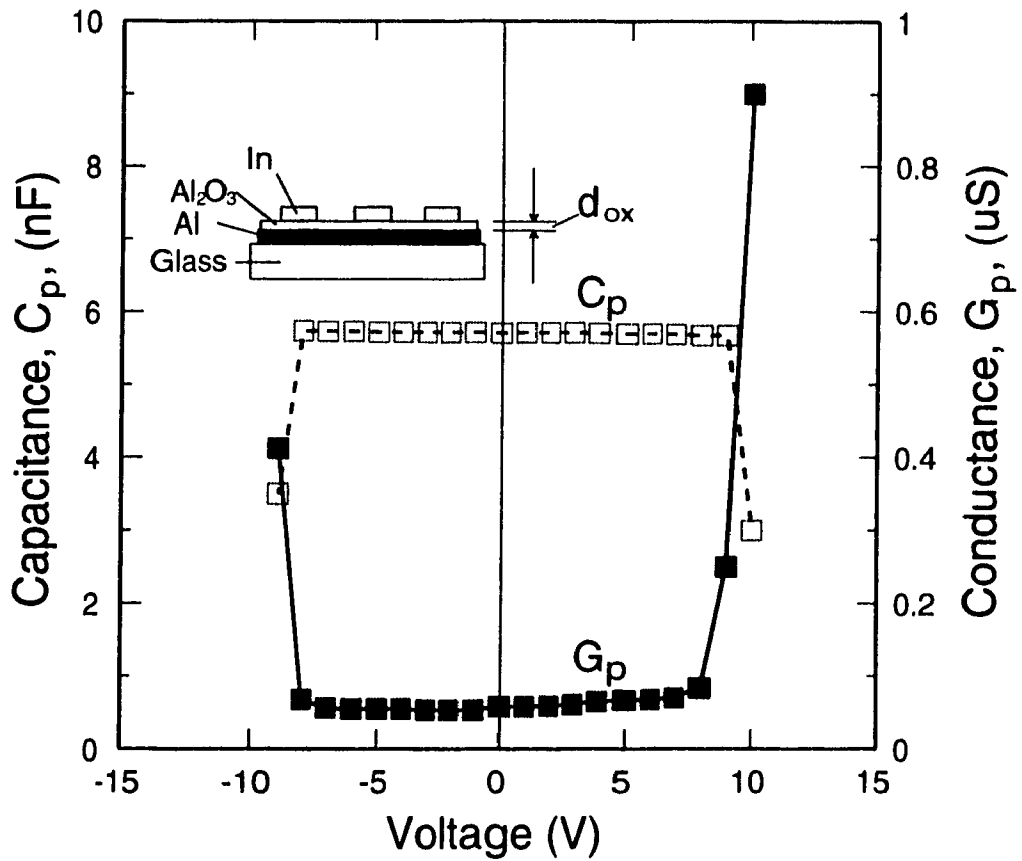


Fig 7.10 Plot of parallel capacitance and conductance against bias voltage for a capacitance sample with an r.f. sputtered oxide thickness of 1000 Å. The measurement frequency was 100 Hz.

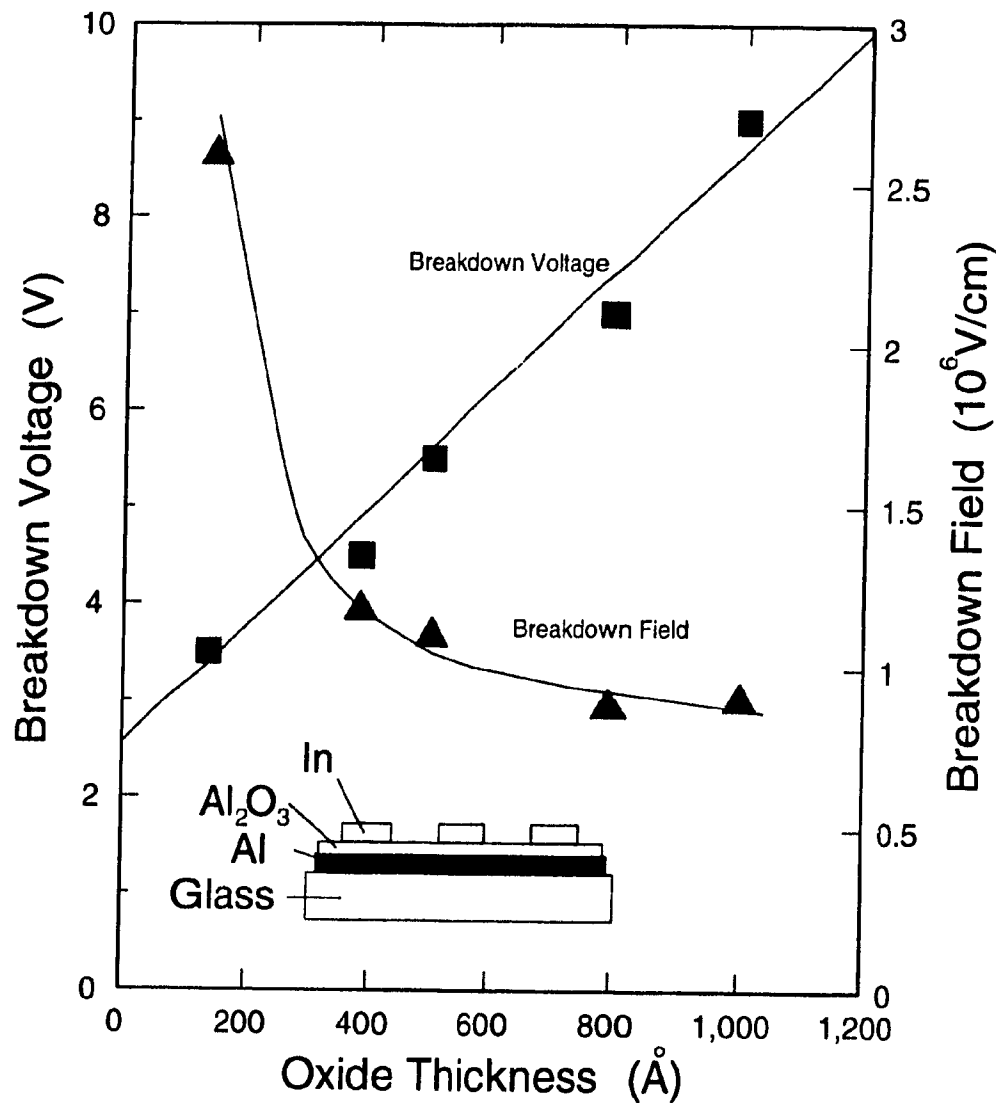


Fig 7.11 Plot of breakdown voltage and breakdown field against thickness for capacitance samples, with oxide deposition by r.f. sputtering on aluminum substrates.

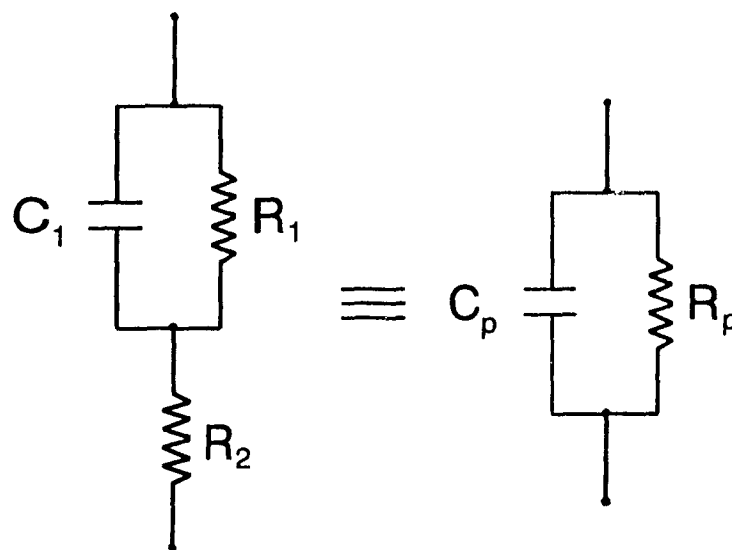


Fig 7.12 Postulated 3-element equivalent circuit of a metal-oxide-In capacitance structure and its 2-element parallel equivalent circuit.

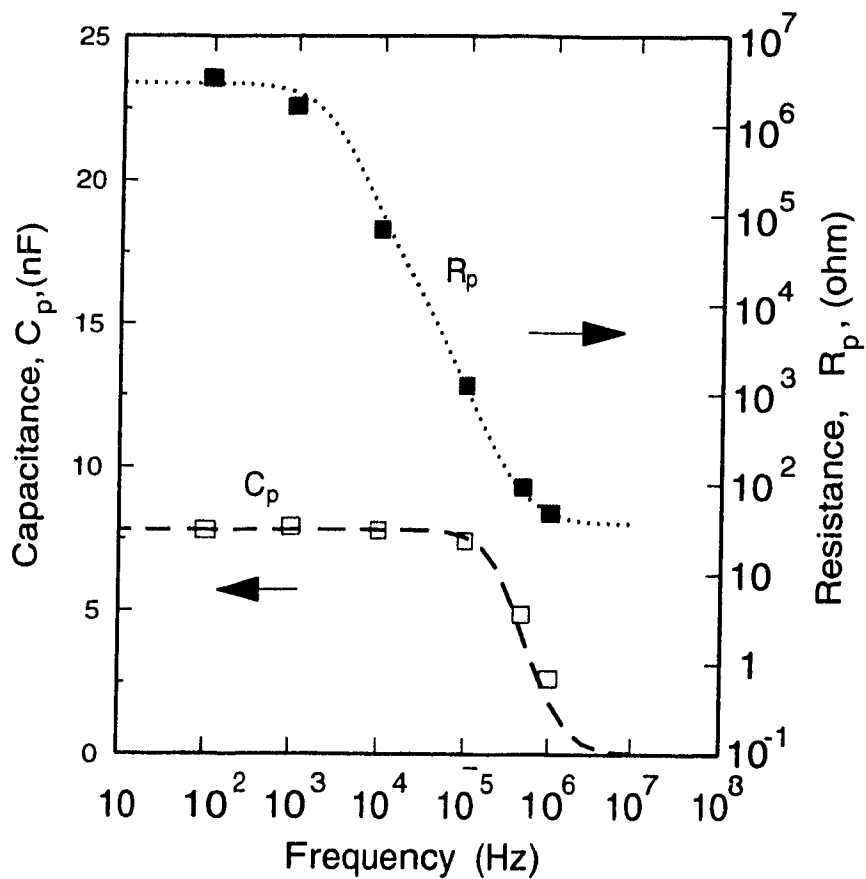


Fig 7.13 Plot of C_p and R_p against frequency for glass-Ni-oxide-In structure sample number C16 from Fig 7.6 with an r.f. sputtering time of 60 min. The dotted and broken lines were calculated from equations (7.1) and (7.2) with the fitted parameters $R_1 = 3$ megohm $R_2 = 37$ ohm and $C_1 = 7.8$ nF.

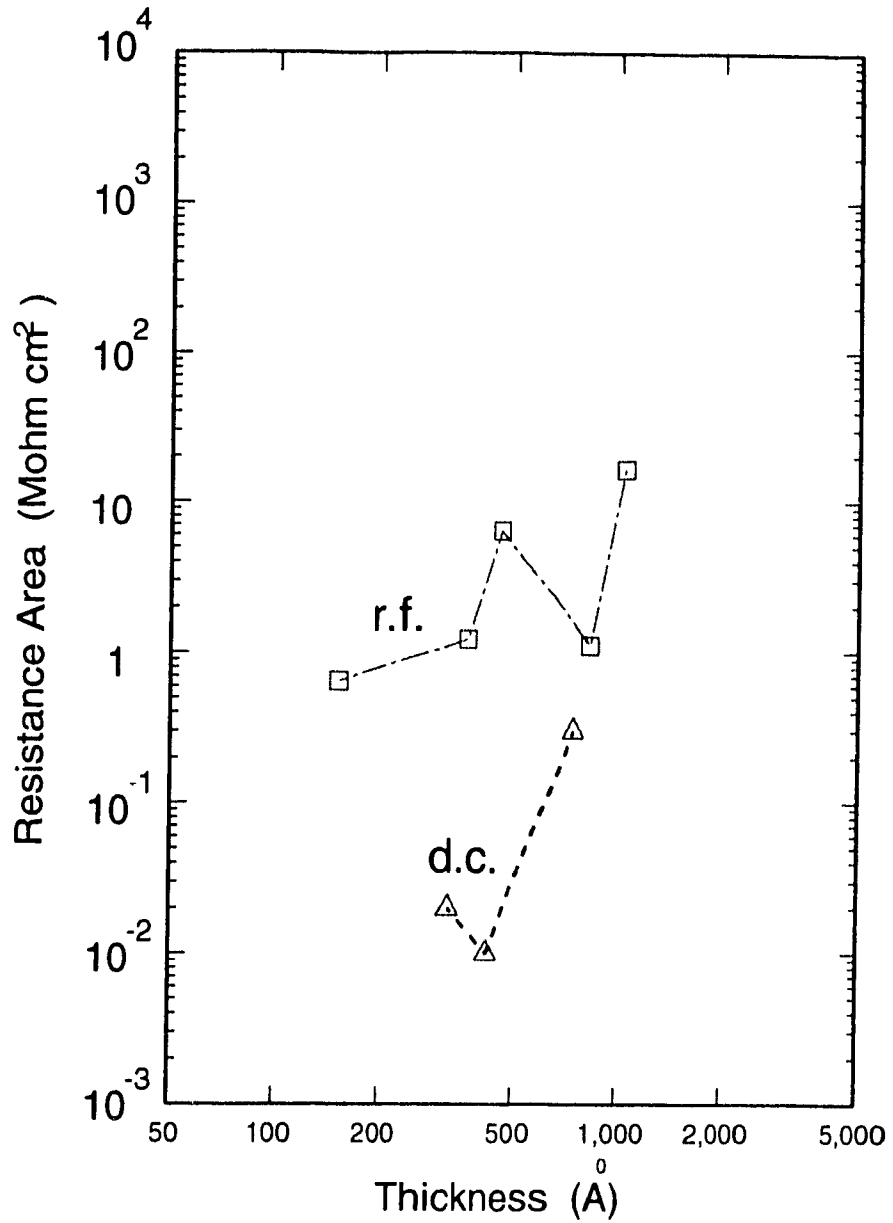


Fig 7.14 Comparison of resistance x area measured at 10 Hz of aluminum oxide layers on aluminum obtained with d.c. and r.f. sputtering.

Chapter 8

GENERAL CONCLUSIONS AND FURTHER DISCUSSION

In this chapter, the general conclusions of the work carried out will be stated, with further discussion of the results. Some suggestions for future work will also be given.

8.1 Conclusions and Discussion

In respect of the measurements, the techniques employed to obtain the xerographic data have been greatly improved and refined over those used previously in this laboratory in two respects. Firstly, the relation between measured probe potential and sample surface potential has been made more exact by actual calibration, rather than simply relying on calculation. Secondly, the introduction of semiautomatic computer control of the turn-table apparatus, described in chapter 4, has enabled the measuring procedure of sample charging, dark delay, exposure and potential measurement to be carried out in a more uniform and exact manner. This is particularly important in the cycled-up measurements.

While previous xerographic work has been done on chlorine-doped selenium elsewhere, measurements, such as those of Abkowitz et al [3], have only been reported in detail on a level of 750 wt ppm or more of chlorine. However, the present work shows that the

major xerographic effects take place at a lower concentration of chlorine, and in fact at the level of a few ppm, at least in selenium without arsenic or tellurium. The addition of a very small amount of chlorine brings the first residual voltage down by an order of magnitude for a low charging voltage. While the dark decay rate is increased somewhat, the increase is modest in comparison with the reduction in residual voltage, so that overall the xerographic performance of the photoreceptor is improved. For a fixed corotron voltage, the acceptance voltage is also reduced with added chlorine but the reduction only becomes important at higher concentration. The dark decay rate was found to be, for the most part, independent of acceptance voltage, at least for low chlorine concentrations. This is consistent with the independence of dV/dt on the initial voltage V_1 in time zone 1.

In the present work, a simple incandescent lamp, rather than a special short wavelength lamp, was used to illuminate the sample surface after charging and dark decay. Hence, the Warter relation (equation 2.27) may not be valid in such circumstances to calculate the $\mu\tau_c$ products as given in Table 5-1. However, the values may be helpful to see changes and, in this case, indicate that $\mu\tau_c$ is much affected by the presence of the chlorine in increasing in its value by an order of magnitude. This change, presumably corresponds to an increase in the free time τ_c of the holes, and is consistent with the reduction in the trap concentration N_t with increased chlorine as calculated from the cycled-up values of residual voltage. The observed increase in voltage from V_r to $V_{r\infty}$ was smaller in the present results than increases previously reported [1] on amorphous selenium but the reason for this is not known. The strong increase

of V_r with acceptance voltage for the doped samples is surprising, since it implies, from the Warter relation, that $\mu\tau_c$ greatly decreases with increase of surface voltage.

The analysis of the dV/dt versus t plots shows that the simple power law function for the increase of space charge density with time $\rho(t)$, as used by Abkowitz et al [3][11], is not accurate enough to account sufficiently for the results. Application of a modified form for $\rho(t)$, that takes into account the ultimate charge density ρ_0 which is reached at a time longer than the release time of the holes from the deep centres, is found to explain the form of the results much more satisfactorily.

By applying this modified form for $\rho(t)$ to two of the dV/dt versus t plots, the parameters p , V_x and τ were obtained for the 6 ppm and 65 ppm doped samples, yielding practically the same average values of p of 0.96 and V_x of 965 volts but τ -values of 51 seconds for the 6 ppm sample and 25 seconds for the 65 ppm sample. Somewhat different parameters were found from the t_d versus $2V_d$ plots, yielding $p=0.98$, $V_x=820$ volts and $\tau=69$ sec for the 6 ppm sample and $p=0.75$, $V_x=670$ volts and $\tau=20$ sec for the 65 ppm sample. The difference between the two sets of data is believed to be due to a small loss of surface charge with time. However, both sets show a reduction in τ with increasing chlorine content and the V_x -values give about the same ρ_0 value of approximately 2×10^{-5} coulomb/cm³, which corresponds to a deep centre concentration of $N_0 = \rho_0/e$ of about 1.3×10^{14} cm⁻³. The question now arises as to whether the deep centres controlling dark decay, with a concentration of the order

of 10^{14} cm^{-3} and essentially independent of chlorine content are different from the traps controlling V_{∞} , with a concentration of about 10^{12} cm^{-3} , which decreases with increase of chlorine. The N_c deep centres become negatively charged when losing their holes and are thus acceptor-like, whereas the N_t traps become positively charged as holes transit near them and are thus donor-like. The question of whether the traps and the hole-producing centres are the same or different is not resolved here. However, the fact that the chlorine increases the hole free time τ_c but decreases the time τ_r to ionize holes from the centres is not a conflict.

The fact that the undoped sample showed no clear kinks in its dV/dt versus t plots, suggests that the dark decay in this case was partly due to injection or charge loss in addition perhaps to some depletion discharge. It should be realized that a kink would not be observable if V_i is too high, since then the final negative space charge width z_{∞} would be greater than the sample thickness L . In the present case, the limiting initial voltage is calculated to be about 1000 volts. Kinks were also not observed in the dV/dt versus t plots at different V_i for a sample fabricated without an aluminum oxide film between the selenium and the base, even though the chlorine doping level was as high as 65 ppm. Hence, this is a clear demonstration of the blocking action of the aluminum oxide film and the effect of its absence.

The xerographic measurements reported in the present work were always carried out using dark-rested samples. The need for this was amply shown in experiments where the sample was first illuminated with strong light for a long time (24 hours). Recovery of the dark

decay rate following this took a few hours but recovery of the residual voltage took a few days.

For the most part, the aluminum oxide blocking layer was deposited by r.f. sputtering from a target of Al_2O_3 on to metal substrates of aluminum, nickel or gold. It was found that deposition of oxide by d.c. reactive sputtering on the last two metals was unsatisfactory for reasons unknown. However, it worked well for aluminum. Measurements of capacitance at a frequency of 1 kHz were carried out on specially prepared samples with indium contacts to determine oxide thickness. The variation of capacitance and incremental resistance with frequency could be explained, for the most part, by a simple circuit model, in which the resistance measured at low frequency gave the resistance through the oxide layer. In the case of aluminum substrates, it was found that this resistance was almost an order of magnitude higher in oxides deposited by r.f. sputtering than in those prepared by d.c. reactive sputtering. However, in samples prepared with oxide deposited separately by both of these methods, no significant difference could be detected between them in the xerographic characteristics of acceptance voltage, dark decay rate and residual voltage. Electrical breakdown was observed in the aluminum oxide films at a field of about 10^6 volt/cm. Sputtered oxides have the advantage over "glow discharge" produced oxides in that, in the former case, a high purity target of aluminum or Al_2O_3 can be used, whereas in the latter case the oxidation arises from the substrate aluminum, which is often less than pure. Finally, it is of interest to point out that, since r.f. sputtered and d.c. reactive sputtered oxides are equally effective xerographically, d.c. sputtering would

be economically favoured for industrial scale use because of its lower capital equipment cost.

8.2 Future Work

The studies carried out and presented in this thesis have only covered a part of the work needed in this area. Arising out of the studies done so far and keeping to chalcogenide photoreceptors, useful work in this laboratory for future investigations could be along the following lines.

- 1) The present xerographic measurement apparatus is semiautomatic but further improvements are needed, including the addition of some suitable lamps for short-wavelength illumination.
- 2) The present measurements on chlorine-doped selenium were done with positive charging. Results with negative charging are also needed.
- 3) Only six different chlorine levels in the selenium were used in the present study. More precision on the role of the chlorine could be obtained with measurements on samples with intermediate concentrations of 10,20,30 40 and 50 ppm.
- 4) Efforts need to be directed at attempting to measure the chlorine content in the selenium films themselves, rather than just in the source material.

5) Studies should be made on the decay of the residual voltage with time in selenium samples to determine the relevant release time of the traps involved.

6) Studies should be done on current-voltage characteristics of the selenium xerographic samples both with and without electrodes.

7) The effect of dopants in selenium other than chlorine should be studied such as phosphorus, sodium and oxygen.

8) The xerographic performance of selenium xerographic samples should be evaluated with r.f. sputtered aluminum oxide blocking layers on substrates other than aluminum, such as nickel, copper, gold and platinum.

9) Studies need to be made on photoreceptors, containing different amounts of arsenic and/or tellurium at the concentrations used industrially.

REFERENCES

- [1] S.O. Kasap, **Handbook of Imaging Materials** (A.S.Diamond), (Marcel Dekker, New York, 1991). p.329.
- [2] Q.H. Zhang, M.Eng.Thesis. McGill University, Montreal. 1990
- [3] M. Abkowitz, F. Jansen and A.R. Melnyk, **Phil. Mag.** **51(4)** p.2567 (1984)
- [4] J.H. Dessauer and H.E. Clark, **Xerography and Related Processes**, (Focal Press, New York, 1965). p.89.
- [5] R.M. Schaffert, **Electrophotography**, (Focal Press, London, 1974). p.397.
- [6] R.M. Schaffert, **Recent Problems in Electrophotography**,
- [7] K.I. Jacobson and R.E. Jacobson, **Imaging Systems**, John Wiley & Sons, New York, 1976). p.263
- [8] S.O. Kasap, **J. Phys. D: Appl. Phys.** **25** p.83. (1992)
- [9] P.J. Warter, **Appl. Opt. Suppl.** **3**, p.65 (1969)
- [10] S.O. Kasap, **J. Electrostatics** **22**. p.69 (1989)
- [11] M.Abkowitz and S.Maitra **J. Appl. Phys.** **61** (3) 1038-1046 (1987)
- [12] S.O.Kasap, M.Baxendale and C Juhasz, **IEEE Trans. Industrial Applications** **27(4)** 620-626 (1991)